Master's Thesis of Pharmacy

New flavanones isolated from root bark of *Morus alba*, and use of Molecular networking in Network pharmacology

상백피로부터 새로운 플라바논 분리와 Network pharmacology에서 Molecular networking 응용법 연구

February 2023

Graduate School of Pharmacy
Seoul National University
Pharmacognosy Major
WON Hongic

New flavanones isolated from root bark of *Morus alba*, and use of Molecular networking in Network pharmacology

Advisor CHIN Young-Won

Submitting a Master's thesis of Pharmacy
December 2022

Graduate School of Pharmacy
Seoul National University
Pharmacognosy Major

WON Hongic

Confirming the master's thesis written by
WON Hongic
January 2023

Chair _____ (Seal)
Vice Chair _____ (Seal)
Examiner _____ (Seal)

Abstract

Morus alba L. (Moraceae) also well known as White mulberry, is herb that is widely distributed among different parts of Asia including Korea, Japan, China, Thailand and Cambodia. Traditionally, extract of root bark of *Morus alba* has been used as for treatment of cardio-protection, analgesic, antioxidant, and hyperlipidemia. Research for compounds with cholesterol-lowering effect is promising due to increasing medical burden caused by cardiovascular disease worldwide, which contributed to highest death toll in 2019. One of renowned causes for cardiovascular diseases (CVD) is high serum level of low density lipoprotein cholesterol (LDL-C) which is controlled by low density lipoprotein receptor (LDLR), the receptor that is degraded by PCSK9. Hence, to overcome CVD, it is crucial to identify chemical constituents with PCSK9-inhibiting effects.

The first part covers structural determination of twenty compounds isolated from PCSK9-lowering fractions including six newly discovered flavanones. Various column chromatography methods have been applied to methanol extract of *M. alba* root barks to isolate the twenty compounds. A wide range of physicochemical and spectroscopic methods such as 1D and 2D NMR spectroscopy and HRESIMS were enforced to confirm chemical structures of all twenty compounds with past research papers actively used as reference for partial fragments of the compounds.

The second part evaluates the addition of molecular networking to network pharmacology to predict both cholesterol-related diseases and active fraction with optimal skeleton.

Identification of compounds by molecular mass was aided by molecular network process supported with GNPS, while compound–target–disease network was built based on various Network pharmacology–related databases.

Keyword : *Morus alba*, flavanone, network pharmacology, molecular network
Student Number : 2021–28287

Table of Contents

List of Schemes

List of Tables

List of Figures

List of Abbreviations

$[\alpha]_D^{20}$: specific rotation at 25 degrees Celsius

n−BuOH: *n*−butanol

CC: column chromatography

$CDCl_3$: deuterated chloroform

$CHCl_3$: chloroform

CH_3Cl: acetonitrile

COSY: correlation spectroscopy

CVD: cardiovascular disease

d: doublet

dd: doublet of doublet

ECD: electronic circular dichroism

FA: formic acid

H_2O: distilled water

HMBC: heteronuclear multiple−bond correlation

HPLC: high performance liquid chromatography

HRESIMS: high−resolution electrospray ionization mass spectrometry

HSQC: heteronuclear single quantum coherence

Hz: hertz

IR: infrared spectroscopy

LDL−C: low density lipoprotein cholesterol

LDLR: low density lipoprotein receptor

m: multiplet

MeOD−d_4: deuterated methanol

MeOH: methanol

min: minutes

MPLC: medium pressure liquid chromatography

mRNA: messenger RNA

m/z: mass to charge ratio

NMR: nuclear magnetic resonance

NOESY: nuclear overhauser effect spectroscopy

PCSK9: proprotein convertase subilisin/kexin type9

RP: reverse phase

s: singlet

t: triplet

TLC: thin−layer chromatography

t_R: retention time

UPLC; ultra−high performance liquid chromatography

UV: ultraviolet absorption spectroscopy

Part 1

Isolation of twenty compounds from *Morus alba* including six new flavanones

Chapter 1. Introduction

1.1. Study Background

1.1.1. Relationship between cholesterol and CVD

Cholesterol is essential substance for humans that act as precursor for the synthesis of bile acids and steroid hormones (Choi et al., 2020). Most of cholesterol is produced by liver before delivery to other organs, packed inside low-density lipoprotein (LDL) particles (Choi et al., 2020). However, American Heart Association (AHA) and Centers for Disease Control and Prevention (CDC) highlighted that build-up of LDL-C in plasma, the condition that is also known as hypercholesterolemia, could form plaque on the walls of blood vessels. Such blockage is significant risk factor for cardiovascular disease (CVD) (Wouters, et al., 2005), and is regarded as one of disease groups with high prevalence and global mortality as of 2019 (Roth et al., 2020). Therefore, minimization of fat and lipid deposition in blood vessel is crucial to minimize current increase of medical burden caused by CVD. Hence, lowering serum LDL-C has always been therapeutic target for treatment of CVD (Choi et al., 2022).

By far, it is known that low density lipoprotein receptor (LDLR) is ligand that is responsible for utilization of the LDL-C within cells (Go, 2012). The LDLR pathway is negative feedback system that regulates plasma and intracellular cholesterol homeostasis (Zhang Y et al., 2016). Expression of LDLR is regulated at two stages; sterol regulatory element-binding protein-2 (SREBP-2) and SREBP cleavage-activating protein (SCAP) at transcriptional level, and proprotein convertase subtilisin/kexin type 9 (PCSK9) at post-transcriptional level (Zhang Y et al., 2016). Therefore, activation of PCSK9 dysregulates LDLR expression, causing abnormal lipid accumulation in cells and tissues (Zhang Y et al., 2016). To overcome this issue, PCSK9 has become major drug target for CVD which could result in reduction of LDL-C (Lagace, 2014).

1.1.2. PCSK9 inhibitory effect of root bark of *Morus alba*

Morus alba L., also commonly known as White mulberry, is traditional medicinal plant classified under Moraceae family (Stone, 2009). The plant reaches up to 15 meters in height and bears black, purple or white fruits (Stone, 2009) which are used for consumable products such as wine, juice, ice cream and jam (Pel, 2017). The species is distributed broadly among different parts of Asia including Cambodia, China, Japan, Korea, and Thailand (Pel, 2017).

400 years old Korean medical book "Donguibogam" stated that *Morus alba* was used to treat fever, constipation, diabetes and arthritis since ancient times (Lee and Yoon, 2005). Recently, more clinical effects of *Morus alba* are under investigation, and other discovered benefits include not only for common symptoms such as

liver and kidney protection, reduction of blood pressure, diuretic, anti-cough, analgesic and anti-cancer (Eo et al., 2014), but also hypolipidemic effects from extract of root bark (El-Beshbishy, 2006).

Three of known compounds with PCSK9 inhibitory effects (Masagalli et al., 2021) isolated from root bark of *Morus alba* include Moracin C (Pel, 2017; Li M, 2018) and S (Seong, 2018), and Morusalfuran D (Ha and Shrestha, 2020). Supported by above literatures, root bark of *Morus alba* should be considered for investigation of PCSK9 inhibitor candidates.

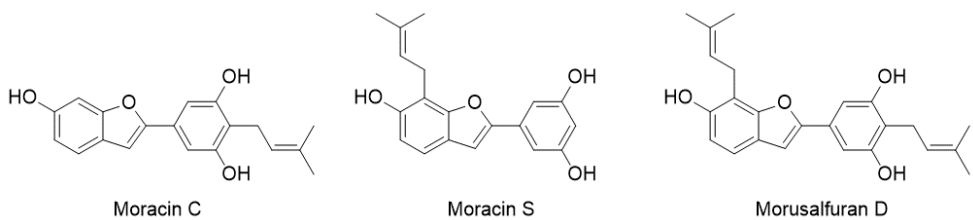

Figure 1. Chemical structures of key compounds of *Morus alba* root bark with PCSK9 inhibiting activity

1.2. Purpose of Research

The aim of part 1 of this study is to identify PCSK9 inhibitor candidates available from fractions with low PCSK9 expression activity *in-vitro*. Methanol extract of dried root bark of *Morus alba* was isolated using various column chromatography methods to obtain twenty single compounds including six newly discovered flavanones. Structures of the chemical compounds were determined by various physicochemical and spectroscopic methods such as 1D and 2D NMR spectroscopy and HRESIMS.

Chapter 2. Experimental section

2.1. Materials

2.1.1. Plant material

The dried barks of root of *Morus alba*, originated from China, were purchased from a Korean market NAUM in March 2021 and were identified by Dr. H.-S. Chae. A voucher specimen (Voucher No.: CYWSNU-KP0023) was deposited at the College of Pharmacy, Seoul National University, Republic of Korea.

Figure 2. Dried root bark of *Morus alba*

2.1.2. Reagents and apparatus

- Anisaldehyde-H_2SO_4 (TLC plate spraying with solvent)
- Biotage SNAP HP-Sil cartridge (Biotage, Uppsala, Sweden)
- Chloroform-*d* HPLC (D, 99.8%) +0.05% v/v TMS +Silver foil (Cambridge(CIL), Inc., USA)
- Column Chromatography (CC) silica gel (particle size: 40-60 μm, 230-400 mesh, Merck, Darmstadt, Germany)

- Cosmosil 140C18 RP silica gel, MPLC column (Cosmosil, Kyoto, Japan)
- Dimethyl sulfoxide-d_6 (D, 99.9%), +0.05% v/v TMS (Cambridge (CIL), Inc., USA)
- Formic acid (Sigma, St. Louis, MO, USA)
- HPLC grade acetonitrile & methanol (SK chemical, Korea)
- J' sphere ODS-M80, HPLC column (S-4 ㎛, 250 x 4.6 mm, YMC Co., Ltd., Japan)
- Luna, C18 (S-5 ㎛, 250 x 100 mm, Phenomenex, CA, USA)
- Methanol-d_4 (D, 99.8%) +0.05% v/v TMS (Cambridge(CIL), Inc., USA)
- Sephadex LH-20 (GE Healthcare, Uppsala, Sweden)
- TLC Silica gel 60 F_{254} plates (Merck, Darmstadt, Germany)
- TLC Silica gel 60 RP-18 $F_{254}S$ plates (Merck, Darmstadt, Germany)
- Waters BEH C18, HRESI-QTOF-MS column (2.1 x 150 mm, 1.7 μm, Waters USA)

2.1.3. Analytical equipment

- A Biotage Isolera One, medium-pressure liquid chromatography (MPLC) (Biotage, Uppsala, Sweden)
- ASCO P-2000 digital polarimeter (JASCO, Tokyo, Japan/JASCO, Easton, MD, USA)
- Bruker AVANCE 500 MHz spectrometer (Bruker, USA)
- Bruker AVANCE 800 MHz spectrometer (Bruker, Karlsruhe, Germany)
- Convection oven CO-81, Autoclave (Hanyang Scientific Equipment Co., Ltd)

- Chirascan-Plus Electronic circular dichroism (Applied Photophysics Ltd, Japan)
- EYELA CA-1112CE, Low temperature circulator (Eyela., USA)
- EYELA N-1200AS-W, Evaporator (Eyela., Japan)
- FT-IR (JASCO, FT/IR-4200)
- Gilson 321 pump and Gilson 172 diode array detector, Semipreparative high-pressure liquid chromatography (HPLC) (Gilson, Madison, WI, USA)
- JNM-ECA AVANCE 400 MHz spectrometer (JEOL Ltd., Japan)
- JNM-ECA AVANCE 600 MHz spectrometer (JEOL Ltd., Japan)
- Milli-Q system (Waters Corporation, Milford, MA, USA)
- POWER SOMIC 520, Ultrasonic Bath Sonicator (HWASHIN TECH Co, Korea)
- TOF-MS (Agilent, Q-TOF 6530 MS / Agilent, 1290 Infinity) - (No.068) (USA)
- UV Hand Lamp VL-4.LC (Vilber Lourmat, France)
- UV/vis spectrophotometer (Beckman Coulter GmbH, North Rhine-Westphalia, Germany).
- Waters Xevo G2 Q-TOF mass spectrometer, UHPLC-ESI-QTOF-MS (Waters, Medford, MA, USA)

2.1.4. Software

Measurement and analysis of mass spectra were performed using MassLynx 4.0 software (Waters Co., USA) and MassHunter software (Agilent Co., USA). Drawing of chemical structures and

analysis of obtained NMR spectrum were achieved using ChemDraw 20.0 (ChemOffice, PerkinElmer) and MestReNova software (Mastrelab Research, Escondido, CA, USA) respectively.

2.2. Method

2.2.1. Extraction, separation and purification

The dried root barks of *Morus alba* L. (5.4 Kg) were extracted with methanol (100%, 3 x 13 L) per day at room temperature. The extract was then evaporated under vacuum at 40 degrees Celsius to yield a residue (349.60 g). The residue was then suspended in distilled water (2 L), then successively partitioned with hexane, chloroform, ethyl acetate, and *n*-butanol (3 x 2 L each). Based on cell assay (Figure 3-4), chloroform fraction (87.52 g) was fractionated using silica gel column chromatography (CC, 6 x 40 cm) starting with a gradient of hexane-ethyl acetate (20:1 to 1:1), followed by chloroform-methanol (5:1) to obtain 22 fractions (MAC-1 to MAC-22). As shown in Figure 5-6, MAC-6, 7, 8, 9, 14, 15 and 16 showed both increase and decrease in LDLR and PCSK9 mRNA expression respectively. Based on TLC and UPLC results, MAC-15 and MAC-16 were considered to be almost equal and hence they were merged. As a result, MAC-6, 7, 8, 9, 14 and newly merged MAC-15 were decided to be separated.

MAC-6 (3.2120 g) was separated by RP-MPLC with solvent gradient MeOH-H_2O (40:60 to 100:0) to obtain 2 single compounds (methyl 2,4-dihydroxybenzoate and β-sitosterol), predicted from ^{1}H NMR, as well as 4 sub-fractions (MAC-6A to MAC-6D). MAC-6C (97.4 mg) was further separated by

preparative HPLC (Luna 5 μm C18(2), 250 x 10 mm, CH_3CN (0.1% FA) 85% isocratic, 3 mL/min, 254 nm) to yield 8 sub-fractions (MAC-6C.1 to MAC-6C.8). MAC-6C.8 (7.3 mg) was purified using HPLC (J'sphere ODS-M80, 250 x 4.6 mm, CH_3CN (0.1% FA) 80% isocratic, 1 mL/min, 274 nm) to give morusalnol E (**3**) (2.0 mg, t_R = 31 min).

MAC-7 (1.3267 g) was chromatographed by RP-MPLC and eluted with MeOH-H_2O (10:90 to 100:0) to afford 6 sub-fractions (MAC-7A to MAC-7F). MAC-7F (973.6 mg) was divided using silica gel column chromatography (CC, 3 x 19 cm) starting with a gradient of hexane-ethyl acetate (1:0 to 1:1), then increased to chloroform-methanol (5:1), then washed with 100% methanol to obtain 9 sub-fractions (MAC-7A to MAC-7I). MAC-7FD (528.9 mg) was separated by sephadex LH-20 column (2 x 47 cm, CH_3Cl:MeOH 1:1) to obtain 5 sub-fractions (MAC-7FD.sep1 to MAC-7FD.sep5). Finally, MAC-7FD.sep4 (40.8 mg) was purified with HPLC (Luna 5 μm C18(2), 250 x 10 mm, MeOH (0.1% FA) 85% isocratic, 3 mL/min, 280 nm) to obtain sanggenol O (**8**) (6.0 mg, t_R = 18 min), sanggenol W (**1**) (2.5 mg, t_R = 22 min) and morusalnol F (**4**) (3.5 mg, t_R = 36 min).

MAC-8 (3.0391 g) was purified on a silica gel column (CC, 3 x 19 cm) starting with a gradient of hexane-ethyl acetate (20:1 to 1:1), then changed to chloroform-methanol (5:1) for washing to obtain 3 sub-fractions (MAC-8A to MAC-8C). MAC-8B (1.1388 g) was further separated using HPLC (Luna 5 μm C18(2), 250 x 10 mm, MeOH (0.1% FA) 70%→90%, 3 mL/min, 280 nm) to yield cycloaltilisin 7 (**10**) (4.5 mg, t_R = 56 min) and 8 other peaks. MAC-8B.9 (15.6 mg) was purified using HPLC (Luna 5 μm C18(2), 250 x 10 mm, MeOH (0.1% FA) 90% isocratic, 3 mL/min, 210 nm) to

yield betulinic acid (**13**) (1.7 mg, t_R = 19 min) and cyclomorusin (**9**) (2.6 mg, t_R = 20 min).

MAC-9 (4.3474 g) was separated by RP-MPLC eluting with MeOH-H_2O (10:90 to 100:0) to achieve 4 sub-fractions (MAC-9A to MAC-9D). MAC-9B (23.1 mg) was re-separated using HPLC (Luna 5 μm C18(2), 250 x 10 mm, CH_3CN (0.1% FA) 65% isocratic (25 min) followed by 90% isocratic (13 min) and 100% isocratic (10 min), 3 mL/min, 210 nm) to yield morusalfuran E (**16**) (1.2 mg, t_R = 25 min), sanggenofuran B (**17**) (1.9 mg, t_R = 34 min) and abyssinoflavanone V (**7**) (2.8 mg, t_R = 39 min). Small proportion (236.2 mg) of MAC-9C (2.2522 g) was separated using HPLC (Luna 5 μm C18(2), 250 x 10 mm, MeOH (0.1% FA) 65% isocratic, 3 mL/min, 280 nm) to obtain neovanone A (**5**) (4.0mg, t_R = 40 min) and neovanone B (**6**) (3.1mg, t_R = 42 min), morusalnol D (**2**) (1.4 mg, t_R = 50 min), and sanggenol P (**11**) (11.6 mg, t_R = 53 min).

MAC-14 (5.3125 g) was separated by RP-MPLC eluting with MeOH-H_2O (1:99 to 100:0) to obtain 17 sub-fractions (MAC-14A to MAC-14P, and MAC-14R). All sub-fractions that were subjected to purification were aided by HPLC (Luna 5 μm C18(2), 250 x 10 mm, isocratic CH_3CN (0.1% FA), 3 mL/min) at different concentration of acetonitrile. MAC-14C (7.6 mg) was purified (15% CH_3CN, 280 nm) to obtain umbelliferone (**15**) (1.8 mg, t_R = 35 min). MAC-14E (11.0 mg) was purified (25% CH_3CN, 254 nm) to isolate moracin M (**18**) (1.7 mg, t_R = 38 min). MAC-14G (40.4 mg) was refined (35% CH_3CN, 280 nm) to gain moracin B (**19**) (8.8 mg, t_R = 39 min). Finally, MAC-14H (18.2 mg) was purified (37% CH_3CN, 283 nm) to attain moracin S (**20**) (5.1 mg, t_R = 46 min).

MAC-15 (2.2146 g) was separated by RP-MPLC eluting with MeOH-H_2O (10:90 to 100:0) to obtain 13 sub-fractions (MAC-15A to MAC-15O). MAC-15B (36.1 mg) was purified using HPLC (Luna 5 μm C18(2), 250 x 10 mm, MeOH 35% isocratic, 3 mL/min, 254 nm) to obtain scopoletin (**14**) (4.1 mg, t_R = 20 min). MAC-15M (940.8 mg) was subjected to separation by sephadex LH-20 column (2 x 47 cm, CH_3Cl:MeOH 1:1) to obtain 4 sub-fractions (MAC-15M.sep1 to MAC-15M.sep4). MAC-15M.sep4 (6.1 mg) was purified using HPLC (Luna 5 μm C18(2), 250 x 10 mm, MeOH 50% isocratic, 3 mL/min, 200 nm) to obtain morachalcone A (**12**) (2.5 mg, t_R = 28 min).

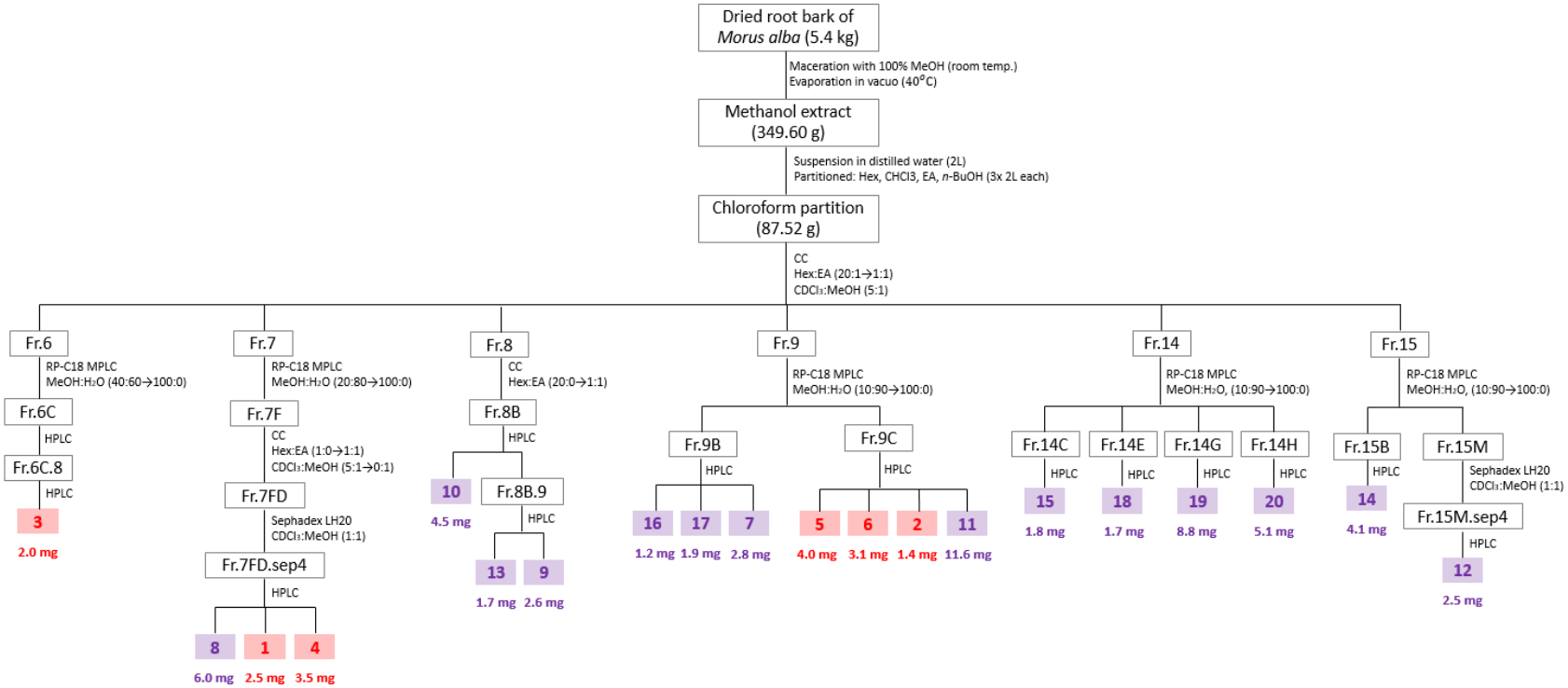

Scheme 1. Isolation scheme of compounds from *Morus alba*

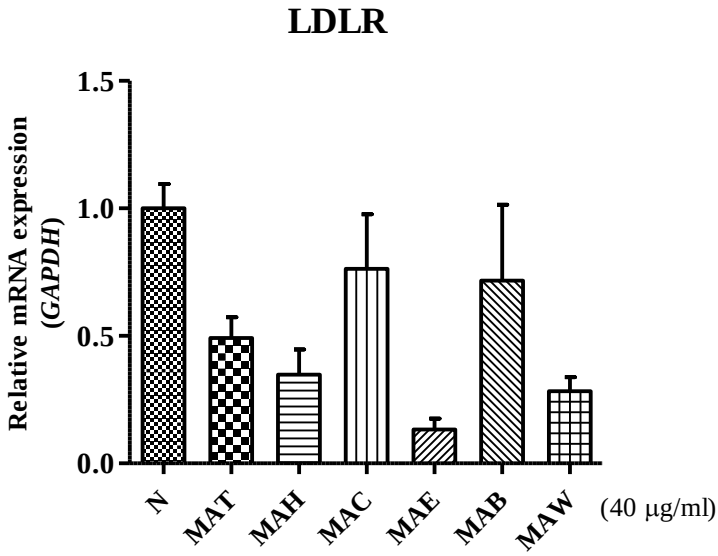

Figure 3. LDLR mRNA expression after partition

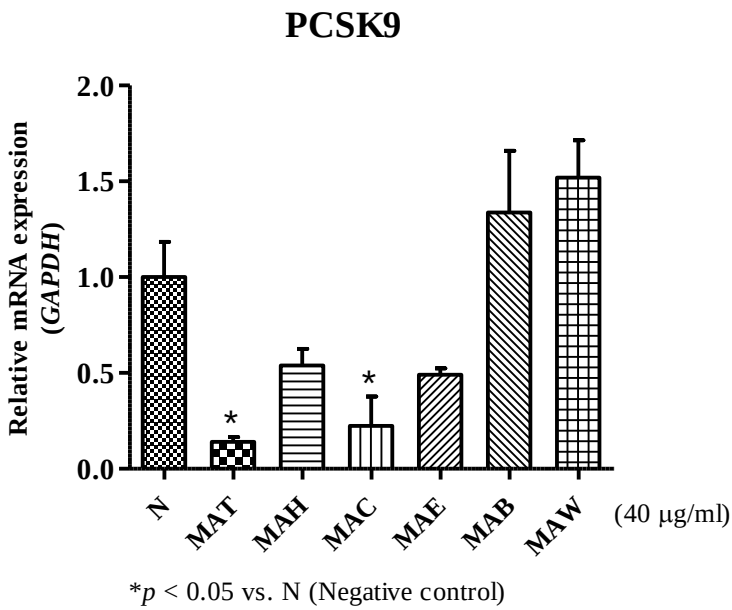

Figure 4. PCSK9 mRNA expression after partition

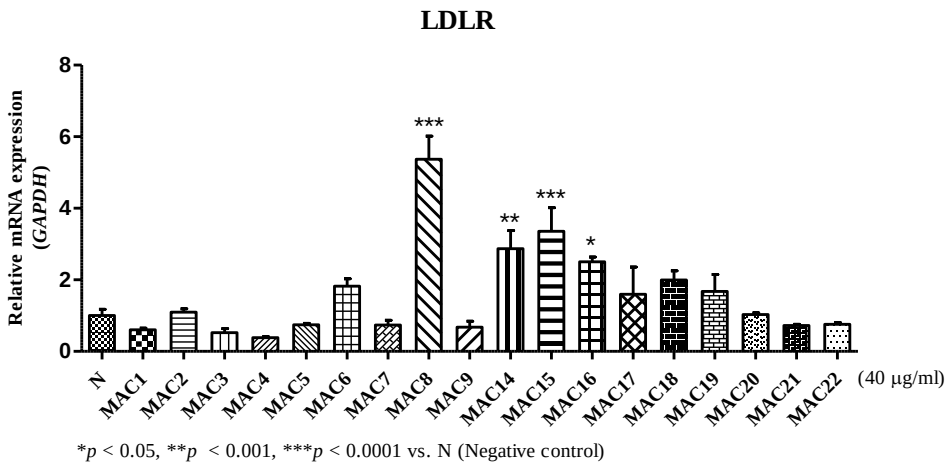

Figure 5. LDLR mRNA expression after fractionation using silica gel column chromatography

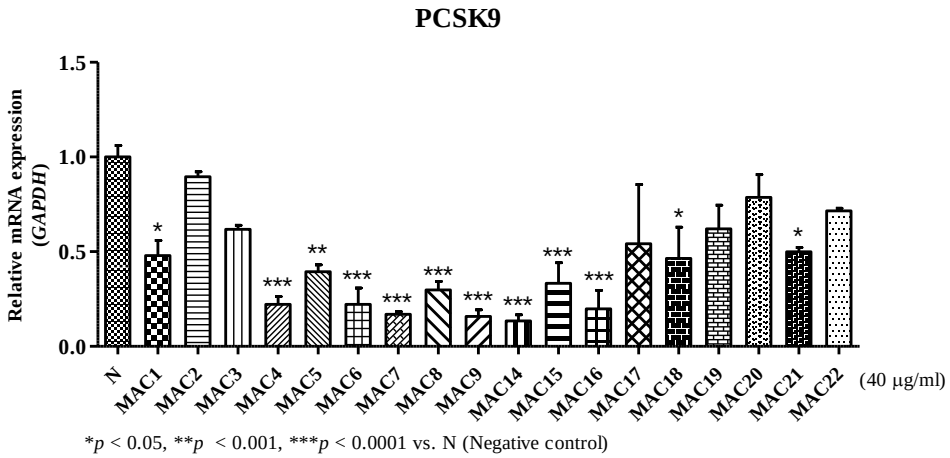

Figure 6. PCSK9 mRNA expression after fractionation using silica gel column chromatography

2.2.2. Chemical and spectral properties of isolated chemical compound

Compound 1

Yellow oil

$C_{25}H_{24}O_6$

$[\alpha]_D^{20}$ −40.73 (*c* 0.12, MeOH)

ECD (MeOH) λ_{max} ($\Delta\varepsilon$) 196 (−0.84), 217 (+0.78), 270 (−0.46) nm

UV (MeOH) λ_{max} (log ε) 228 (4.69), 271 (4.80) nm

IR (neat) ν_{max} 3300, 2973, 1754, 1639, 1453, 1350, 1298, 1158, 1119, 1044, 892, 817, 679 cm^{-1}

HRESIMS *m/z* 419.1476 $[M - H]^-$ (calcd for $C_{25}H_{23}O_6$, 419.1495)

^1H NMR data (400 MHz, $CDCl_3$) see Table 1

^{13}C NMR data (100 MHz, $CDCl_3$) see Table 1

Compound 2

Colorless amorphous solid

$C_{30}H_{34}O_6$

$[\alpha]_D^{20}$ −20.01 (*c* 0.14, MeOH)

ECD (MeOH) λ_{max} ($\Delta\varepsilon$) 196 (−0.57), 222 (+0.98) nm

UV (MeOH) λ_{max} (log ε) 229 (4.43), 287 (4.46) nm

IR (neat) ν_{max} 3361, 2924, 1638, 1464, 1350, 1278, 1163, 1096, 834 cm^{-1}

HRESIMS *m/z* 489.2296 $[M - H]^-$ (calcd for $C_{30}H_{33}O_6$, 489.2283)

^1H NMR data (400 MHz, $CDCl_3$) see Table 1

^{13}C NMR data (100 MHz, $CDCl_3$) see Table 1

Compound 3

White amorphous solid

$C_{30}H_{34}O_5$

$[\alpha]_D^{20}$ +64.70 (*c* 0.10, MeOH)

ECD (MeOH) λ_{max} ($\Delta\varepsilon$) 230 (+3.15), 295 (–2.32) nm

UV (MeOH) λ_{max} (log ε) 272 (4.63) nm

IR (neat) ν_{max} 3354, 2917, 1637, 1450, 1350, 1294, 1159, 1103, 825 cm^{-1}

HRESIMS *m/z* 473.2351 $[M - H]^-$ (calcd for $C_{30}H_{33}O_5$, 473.2333)

^1H NMR data (400 MHz, MeOD–d_4) see Table 1

^{13}C NMR data (100 MHz, MeOD–d_4) see Table 1

Compound **4**

Yellow amorphous solid

$C_{30}H_{34}O_6$

$[\alpha]_D^{20}$ –3.84 (*c* 0.31, MeOH)

ECD (MeOH) λ_{max} ($\Delta\varepsilon$) 195 (–0.76), 219 (+1.12) nm

UV (MeOH) λ_{max} (log ε) 207 (4.51), 227 (4.28), 272 (4.56) nm

IR (neat) ν_{max} 3411, 2973, 2925, 2279, 1753, 1638, 1456, 1380, 1301, 1162, 1102, 1037, 896, 817, 661 cm^{-1}

HRESIMS *m/z* 489.2304 $[M - H]^-$ (calcd for $C_{30}H_{33}O_6$, 489.2283)

^1H NMR data (400 MHz, $CDCl_3$) see Table 1

^{13}C NMR data (100 MHz, $CDCl_3$) see Table 1

Compound **5**

Brown amorphous solid

$C_{25}H_{26}O_7$

$[\alpha]_D^{20}$ –32.15 (*c* 0.17, MeOH)

ECD (MeOH) λ_{max} ($\Delta\varepsilon$) 232 (+7.88), 287 (–0.85), 312 (+1.80) nm

UV (MeOH) λ_{max} (log ε) 285 (4.47) nm

IR (neat) ν_{max} 3219, 2925, 1751, 1638, 1462, 1353, 1290, 1166, 1064, 828, 679 cm^{-1}

HRESIMS *m/z* 437.1617 $[M - H]^-$ (calcd for $C_{25}H_{25}O_7$, 437.1606)

^1H NMR data (400 MHz, MeOD−d_4) see Table 2

^{13}C NMR data (200 MHz, MeOD−d_4) see Table 2

Compound **6**

Brown amorphous solid

$C_{25}H_{26}O_7$

$[\alpha]_D^{20}$ +10.21 (*c* 0.31, MeOH)

ECD (MeOH) λ_{max} ($\Delta\varepsilon$) 237 (+1.40), 290 (−1.75), 312 (+2.29), 354 (+1.61) nm

UV (MeOH) λ_{max} (log ε) 284 (4.47) nm

IR (neat) ν_{max} 2927, 1753, 1637, 1518, 1350, 1187, 679 cm^{-1}

HRESIMS *m/z* 437.1616 $[M - H]^-$ (calcd for $C_{25}H_{25}O_7$, 437.1606)

^1H NMR data (400 MHz, MeOD−d_4) see Table 2

^{13}C NMR data (150 MHz, MeOD−d_4) see Table 2

Compound **7**

Colorless amorphous solid

$C_{20}H_{18}O_5$

ECD (MeOH) λ_{max} ($\Delta\varepsilon$) 286 (−15.4), 332 (+3.76) nm

HRESIMS *m/z* 337.1063 $[M - H]^-$ (calcd for $C_{20}H_{17}O_5$, 337.1076)

^1H NMR data (400 MHz, $CDCl_3$) see Table 2

^{13}C NMR data (100 MHz, $CDCl_3$) see Table 2

Compound **8**

Yellow oil

$C_{25}H_{24}O_6$

ECD (MeOH) λ_{max} ($\Delta\varepsilon$) 215 (+18.6), 241 (−3.30), 257 (+3.44), 285 (−12.4) nm

HRESIMS *m/z* 419.1498 $[M - H]^-$ (calcd for $C_{25}H_{23}O_6$, 419.1495)

^{1}H NMR data (400 MHz, $CDCl_3$) see Table 2

^{13}C NMR data (100 MHz, $CDCl_3$) see Table 2

Compound **9**

Yellow amorphous powder

$C_{25}H_{22}O_6$

HRESIMS *m/z* 417.1328 $[M - H]^-$ (calcd for $C_{25}H_{21}O_6$, 417.1338)

^{1}H NMR data (400 MHz, MeOD−d_4) see Table 3

^{13}C NMR data (100 MHz, MeOD−d_4) see Table 3

Compound **10**

Yellow amorphous solid

$C_{25}H_{26}O_5$

ECD (MeOH) λ_{max} ($\Delta\varepsilon$) 238 (+3.61), 293 (−3.55) nm

HRESIMS *m/z* 405.1708 $[M - H]^-$ (calcd for $C_{25}H_{25}O_5$, 405.1702)

^{1}H NMR data (400 MHz, $CDCl_3$) see Table 3

^{13}C NMR data (100 MHz, $CDCl_3$) see Table 3

Compound **11**

Brown amorphous solid

$C_{30}H_{36}O_6$

ECD (MeOH) λ_{max} ($\Delta\varepsilon$) 289 (−2.13) nm

HRESIMS *m/z* 491.2441 $[M - H]^-$ (calcd for $C_{30}H_{35}O_6$, 491.2439)

^{1}H NMR data (400 MHz, MeOD−d_4) see Table 3

^{13}C NMR data (100 MHz, MeOD−d_4) see Table 3

Compound **12**

Golden powder

$C_{20}H_{20}O_5$

HRESIMS *m/z* 339.1237 $[M - H]^-$ (calcd for $C_{20}H_{19}O_5$, 339.1232)

^{1}H NMR data (400 MHz, MeOD−d_4) see Table 3

^{13}C NMR data (100 MHz, MeOD−d_4) see Table 3

Compound **13**

White amorphous powder

$C_{30}H_{48}O_3$

HRESIMS *m/z* 455.3542 $[M - H]^-$ (calcd for $C_{30}H_{47}O_3$, 455.3531)

^{1}H NMR data (400 MHz, $CDCl_3$) see Table 4

^{13}C NMR data (100 MHz, $CDCl_3$) see Table 4

Compound **14**

Yellow powder

$C_{10}H_8O_4$

HRESIMS *m/z* 191.0344 $[M - H]^-$ (calcd for $C_{10}H_7O_4$, 191.0344)

^{1}H NMR data (400 MHz, MeOD−d_4) see Table 5

^{13}C NMR data (100 MHz, MeOD−d_4) see Table 5

Compound **15**

White amorphous solid

$C_9H_6O_3$

HRESIMS *m/z* 161.0239 $[M - H]^-$ (calcd for $C_9H_5O_3$, 161.0244)

^{1}H NMR data (400 MHz, MeOD−d_4) see Table 5

^{13}C NMR data (150 MHz, MeOD−d_4) see Table 5

Compound **16**

White amorphous solid

$C_{16}H_{14}O_4$

HRESIMS *m/z* 269.0808 $[M - H]^-$ (calcd for $C_{16}H_{13}O_4$, 269.0814)

^{1}H NMR data (400 MHz, $CDCl_3$) see Table 5

^{13}C NMR data (100 MHz, $CDCl_3$) see Table 5

Compound **17**

Light brown amorphous solid

$C_{20}H_{20}O_4$

HRESIMS *m/z* 323.1280 $[M - H]^-$ (calcd for $C_{20}H_{19}O_4$, 323.1283)

^1H NMR data (400 MHz, $CDCl_3$) see Table 6

^{13}C NMR data (100 MHz, $CDCl_3$) see Table 6

Compound **18**

White amorphous solid

$C_{14}H_{10}O_4$

HRESIMS *m/z* 241.0513 $[M - H]^-$ (calcd for $C_{14}H_9O_4$, 241.0506)

^1H NMR data (400 MHz, MeOD−d_4) see Table 6

^{13}C NMR data (100 MHz, MeOD−d_4) see Table 6

Compound **19**

Light brown amorphous solid

$C_{16}H_{14}O_5$

HRESIMS *m/z* 285.0758 $[M - H]^-$ (calcd for $C_{16}H_{13}O_4$, 285.0768)

^1H NMR data (400 MHz, MeOD−d_4) see Table 6

^{13}C NMR data (100 MHz, MeOD−d_4) see Table 6

Compound **20**

Colorless amorphous solid

$C_{19}H_{18}O_4$

HRESIMS *m/z* 309.1123 $[M - H]^-$ (calcd for $C_{19}H_{17}O_4$, 309.1132)

^1H NMR data (400 MHz, MeOD−d_4) see Table 6

^{13}C NMR data (100 MHz, MeOD−d_4) see Table 6

Table 1. ^{1}H and ^{13}C NMR spectroscopic data of compounds **1** – **4**

No.	**1**		**2**		**3**		**4**	
	δ_C	δ_H (J in Hz)	δ_C	δ_H (J in Hz)	δ_C	δ_H (J in Hz)	δ_C	δ_H (J in Hz)
1	–	–	–	–	–	–	–	–
2	74.0	5.67, dd (3.2, 13.1)	74.1	5.67, dd (3.1, 13.2)	80.8	5.32, m, overlapped	77.2	5.58, dd (3.2, 12.7)
3	42.5	2.97, dd (13.1, 17.2) 2.79, dd (3.2, 17.2)	42.5	3.02, dd (13.2, 17.0) 2.78, dd (3.1, 17.0)	44.1	3.12, dd (12.4, 17.3) 2.72, dd (3.0, 17.3)	41.7	3.12, dd (12.7, 17.3) 2.72, dd (3.2, 17.3)
4	196.8	–	196.9	–	198.3	–	196.1	–
5	151.4	–	164.4	–	159.4	–	158.5	–
6	96.2	5.96, s	96.4	5.99, s	103.8	–	103.3	–
7	162.0	–	163.9	–	163.7	–	162.4	–
8	102.9	–	95.3	5.98, s	96.8	5.88, s	96.1	5.96, s
9	163.0	–	164.3	–	164.3	–	161.6	–
10	102.9	–	103.3	–	103.7	–	102.8	–
1'	119.0	–	117.7	–	129.6	–	116.6	–
2'	150.7	–	149.3	–	129.1	7.15, d (2.3)	153.6	–
3'	109.4	–	109.6	–	130.8	–	114.7	–
4'	158.5	–	150.7	–	156.8	–	155.5	–
5'	107.7	6.38, d (8.4)	118.2	–	115.8	6.77, d (8.2)	108.0	6.43, d (8.4)
6'	126.3	7.21, d (8.4)	126.7	7.06, s	126.3	7.12, dd (2.3, 8.2)	125.2	6.98, d (8.4)
1''	–	–	–	–	–	–	–	–
2''	76.6	–	78.7	–	82.0	–	80.9	–
3''	129.5	5.62, d (10.0)	128.5	5.57, d (10.1)	126.3	5.51, d (10.1)	125.2	5.45, d (10.2)
4''	116.3	6.63, d (10.0)	117.0	6.67, d (10.1)	116.7	6.62, d (10.1)	115.7	6.66, d (10.2)
5''	28.4	1.45, s	–	–	–	–	–	–
6''	28.0	1.44, s	–	–	–	–	–	–
1'''	–	–	41.0	1.71−1.65, m	42.8	1.73−1.64, overlapped	41.7	1.75−1.63, m, overlapped
2'''	78.2	–	22.7	2.06, m	23.8	2.08, m	22.7	2.07, m
3'''	126.2	5.50, d (10.0)	124.0	5.06, m	125.1	5.09, m	123.7	5.08, m

4‴	115.4	6.63, d (10.0)	131.8	–	132.7	–	132.0	–
5‴	28.4	1.44, s	25.6	1.53, s	25.9	1.64, s	25.7	1.66, s
6‴	27.8	1.41, s	17.6	1.63, s	17.7	1.55, s	17.7	1.57, s
1⁗	–	–	30.4	3.32, d	29.3	3.29, overlapped	22.5	3.46, d, overlapped
2⁗	–	–	121.8	5.32, m	123.8	5.31, m	121.2	5.32, m
3⁗	–	–	136.1	–	133.3	–	135.9	–
4⁗	–	–	25.8	1.80, s	26.0	1.73, s	25.8	1.77, s
5⁗	–	–	17.9	1.82, s	17.9	1.57, s	17.9	1.84, s
5–OH	–	12.38, s	–	12.15, s	–	–	–	12.15, s
2'–OH	–	–	–	–	–	–	–	6.30, s
4'–OH	–	–	–	5.49, s	–	–	–	5.27, m
2''–CH_3	–	–	26.3	1.37, s	27.7	1.38, s	27.3	1.41, s

Table 2. ^{1}H and ^{13}C NMR spectroscopic data of compounds **5** – **8**

No.	**5**		**6**		**7**		**8**	
	δ_C	δ_H (J in Hz)	δ_C	δ_H (J in Hz)	δ_C	δ_H (J in Hz)	δ_C	δ_H (J in Hz)
1	–	–	–	–	–	–	–	–
2	74.6	5.67, dd (2.9, 13.0)	74.6	5.67, dd (2.9, 13.0)	79.1	5.31, dd (3.0, 13.1)	74.1	5.66, dd (3.2, 13.3)
3	42.7	3.07, dd (13.0, 17.2) 2.75, dd (2.9, 17.2)	42.7	3.07, dd (13.0, 17.1) 2.75, dd (2.9, 17.1)	43.2	3.09, dd (13.1, 17.2) 2.77, dd (3.0, 17.2)	42.5	2.99, dd (13.3, 17.3) 2.79, dd (3.2, 17.3)
4	197.7	–	197.6	–	196.1	–	197.0	–
5	168.7	–	165.6	–	103.2	–	163.9	–
6	97.3	5.91, s	97.3	5.89, d (2.0)	164.5	–	96.5	5.99, s, overlapped
7	165.0	–	168.8	–	96.7	5.99, s	164.5	–
8	96.4	5.89, s	96.3	5.91, d (2.0)	164.4	–	95.4	5.99, s, overlapped
9	165.6	–	165.0	–	95.5	5.99, s	164.4	–
10	103.3	–	103.2	–	163.3	–	103.3	–
1'	119.2	–	119.1	–	121.5	–	117.9	–
2'	159.6	–	159.5	–	124.4	7.06, d (2.2)	150.2	–
3'	108.3	–	108.2	–	130.3	–	110.0	–
4'	161.6	–	161.6	–	153.5	–	148.9	–
5'	109.3	6.49, d (8.1)	109.3	6.51, d (8.5)	116.6	6.81, d (8.3)	114.6	–
6'	137.1	7.68, d (8.1)	137.1	7.68, d (8.5)	127.2	7.17, dd (2.2, 8.3)	123.3	6.99, s
1''	–	–	–	–	–	–	116.6	6.67, d (10.0)
2''	82.5	–	82.5	–	77.2	–	129.2	5.59, d (10.0)
3''	47.6	2.91, d (17.0) 2.79, d (17.0)	47.6	2.91, d (17.2) 2.80, d (17.2)	131.5	5.66, d (9.8)	76.8	–
4''	200.6	–	200.6	–	121.9	6.33, d (9.8)	28.2	1.43, s
5''	–	–	–	–	28.1	1.45, s	28.0	1.43, s
6''	–	–	–	–	28.1	1.45, s	–	–
1'''	40.1	1.81−1.72, m	40.2	1.83−1.68, m	–	–	122.1	6.28, d (9.8)
2'''	23.3	2.14, m	23.3	2.14, m	–	–	128.3	5.51, d (9.8)
3'''	124.6	5.11, m	124.6	5.10, m	–	–	77.2	–

4‴	133.2	–	133.2	–	–	–	28.2	1.42, s
5‴	25.9	1.67, s	25.9	1.67, s	–	–	27.8	1.39, s
6‴	17.7	1.59, s	17.7	1.58, s	–	–	–	–
5-OH	–	–	–	–	–	12.06, s	–	12.13, s
2″-CH_3	24.1	1.43, s	24.1	1.44, s	–	–	–	–

Table 3. ^{1}H and ^{13}C NMR spectroscopic data of compounds 9 – 12

No.	9		10		11		12	
	δ_C	δ_H (J in Hz)	δ_C	δ_H (J in Hz)	δ_C	δ_H (J in Hz)	δ_C	δ_H (J in Hz)
α	–	–	–	–	–	–	141.8	8.08, d (15.5)
β	–	–	–	–	–	–	117.8	7.71, d (15.5)
1	–	–	–	–	–	–	115.7	–
2	159.7	–	78.9	5.33, dd (2.9, 13.0)	76.7	5.67, dd (3.0, 12.4)	160.8	–
3	106.4	–	43.2	3.07, dd (13.0, 17.1) 2.77, dd (2.9, 17.1)	43.2	3.06, dd (12.4, 17.2) 2.73, dd (3.0, 17.2)	103.6	6.34, d (2.4)
4	179.8	–	196.0	–	198.3	–	162.8	–
4a	102.8	–	–	–	–	–	–	–
5	157.3	–	162.6	–	165.5	–	109.1	6.35, dd (2.4, 8.3)
6	100.8	6.13, s	96.0	5.94, s	97.0	5.87, d (2.1)	132.3	7.51, d (8.3)
7	162.8	–	158.4	–	168.3	–	–	–
8	108.6	–	102.8	–	96.3	5.91, d (2.1)	–	–
8a	160.5	–	–	–	–	–	–	–
9	70.7	6.15, d (9.3)	162.5	–	165.2	–	–	–
10	122.4	5.41, d (9.3)	102.7	–	103.4	–	–	–
11	140.0	–	–	–	–	–	–	–
12	18.7	1.70, s	–	–	–	–	–	–
13	26.0	1.94, s	–	–	–	–	–	–
14	115.6	6.82, d (9.9)	–	–	–	–	–	–
15	129.1	5.72, d (9.9)	–	–	–	–	–	–
16	79.3	–	–	–	–	–	–	–
17	28.5	1.46, s	–	–	–	–	–	–
18	28.5	1.46, s	–	–	–	–	–	–
1'	110.4	–	130.6	–	119.6	–	114.7	–
2'	126.4	7.65, d (8.4)	127.0	7.32, d (7.4)	151.8	–	163.4	–
3'	111.3	6.54, dd (2.4, 8.4)	115.7	6.88, d (7.4)	118.7	–	116.6	–
4'	165.1	–	156.1	–	154.4	–	165.1	–

5'	105.1	6.31, d (2.4)	115.7	6.88, d (7.4)	122.1	–	108.1	6.40, d (8.8)
6'	152.5	–	128.0	7.32, d (7.4)	125.5	6.96, s	130.2	7.75, d (8.8)
1''	–	–	–	–	23.8	3.41, d (6.9)	22.6	Overlapped with MeOH
2''	–	–	80.9	–	124.0	5.19, t (6.9, 6.9)	123.8	5.22, t (7.3, 7.3)
3''	–	–	125.1	5.44, d (10.2)	136.5	–	131.8	–
4''	–	–	115.8	6.66, d (10.2)	16.4	1.79, s	26.0	1.78, s
5''	–	–	–	–	40.9	1.99, t (7.4, 7.4)	18.0	1.66, s
6''	–	–	–	–	27.7	2.07, m	–	–
7''	–	–	–	–	125.4	5.06, t (7.1, 7.1)	–	–
8''	–	–	–	–	132.3	–	–	–
9''	–	–	–	–	25.9	1.62, s	–	–
10''	–	–	–	–	17.8	1.57, s	–	–
1'''	–	–	41.7	1.75–1.62, m	29.3	3.25, d (7.1)	–	–
2'''	–	–	22.6	2.06, m	124.0	5.28, t (7.1, 7.1)	–	–
3'''	–	–	123.8	5.08, m	133.5	–	–	–
4'''	–	–	132.0	–	26.0	1.74, s	–	–
5'''	–	–	25.7	1.66, s	17.9	1.69, s	–	–
6'''	–	–	17.7	1.57, s	–	–	–	–
C=O	–	–	–	–	–	–	194.4	–
4'-OH	–	–	–	12.29, *br* s	–	–	–	–
2''-CH_3	–	–	–	1.40, d (2.2)	–	–	–	–

Table 4. ^{1}H and ^{13}C NMR spectroscopic data of compound **13**

No.	**13**	
	δ_C	δ_H (J in Hz)
1	38.9	–
2	29.7	–
3	79.0	3.19, dd (5.0, 11.2)
4	38.7	–
5	55.4	–
6	18.3	–
7	34.3	–
8	40.7	–
9	50.5	–
10	37.2	–
11	20.9	–
12	25.5	–
13	38.4	–
14	42.5	–
15	30.6	–
16	32.2	–
17	55.4	–
18	46.9	–
19	49.3	3.01, m
20	150.4	–
21	29.7	–
22	34.3	–
23	27.4	0.95, s
24	15.4	0.77, s
25	16.1	0.84, s
26	16.0	0.98, s
27	14.7	0.99, s
28	182.0	–
29	109.7	4.76, s
		4.63, s
30	19.4	1.70, s

Table 5. ^{1}H and ^{13}C NMR spectroscopic data of compounds **14** – **16**

No.	**14**		**15**		**16**	
	δ_C	δ_H (J in Hz)	δ_C	δ_H (J in Hz)	δ_C	δ_H (J in Hz)
1	–	–	–	–	–	–
2	164.2	–	163.8	–	156.9	–
3	112.5	6.20, d (9.4)	112.2	6.18, d (9.5)	101.9	6.93, s
3a					122.4	–
4	146.2	7.86, d (9.4)	146.1	7.85, d (9.5)	121.1	7.44, d (8.6)
5	109.9	7.10, s	130.7	7.45, d (8.5)	112.1	6.87, dd (2.2, 8.6)
6	147.2	–	114.6	6.79, dd (2.3, 8.5)	158.2	–
7	153.1	–	163.3	–	95.9	7.06, d (2.2)
7a	–	–	–	–	155.9	–
8	104.0	6.76, s	103.5	6.70, d (2.3)	–	–
9	151.6	–	157.3	–	–	–
10	112.5	–	113.2	–	–	–
1'	–	–	–	–	132.8	–
2'	–	–	–	–	101.6	6.39, t (2.0, 2.0)
3'	–	–	–	–	161.3	–
4'	–	–	–	–	102.7	6.96, t (2.0, 2.0)
5'	–	–	–	–	154.6	–
6'	–	–	–	–	104.1	6.90, t (2.0, 2.0)
6–OCH_3	–	–	–	–	55.5	3.88, s
3'–OCH_3	–	–	–	–	55.8	3.86, s
OCH_3	56.4	3.90, s	–	–	–	–

Table 6. ^{1}H and ^{13}C NMR spectroscopic data of compounds **17** – **20**

No.	17		18		19		20	
	δ_C	δ_H (J in Hz)	δ_C	δ_H (J in Hz)	δ_C	δ_H (J in Hz)	δ_C	δ_H (J in Hz)
1	–	–	–	–	–	–	–	–
2	154.6	–	156.2	–	156.3	–	156.0	–
3	101.2	6.86, s	102.2	6.91, *br* s	102.1	6.95, s	102.6	6.89, s
3a	122.5	–	123.1	–	123.0	–	123.0	–
4	121.0	7.42, d (8.5)	122.1	7.35, d (8.4)	106.2	7.14, s	119.0	7.16, d (8.3)
5	112.0	6.87, dd (2.5, 8.5)	113.3	6.73, dd (2.1, 8.4)	148.3	–	113.2	6.72, d (8.3)
6	158.1	–	156.9	–	144.8	–	155.9	–
7	95.9	7.04, d (2.5)	98.5	6.89, d (2.1)	95.9	6.92, s	112.7	–
7a	155.8	–	157.3	–	150.6	–	153.9	–
1'	129.9	–	133.9	–	133.9	–	134.1	–
2'	104.5	6.88, s	104.0	6.75, d (2.2)	104.9	6.85, d, overlapped	104.0	6.78, d (2.2)
3'	155.3	–	160.0	–	162.7	–	160.0	–
4'	113.7	–	103.6	6.24, t (2.2, 2.2)	102.3	6.33, t (2.2, 2.2)	103.5	6.24, t (2.2, 2.2)
5'	155.3	–	160.0	–	160.0	–	160.0	–
6'	104.5	6.88, s	104.0	6.75, d (2.2)	102.5	6.85, d, overlapped	104.0	6.78, d (2.2)
1''	22.6	3.45, d (7.1)	–	–	–	–	23.7	3.59, d (7.3)
2''	121.2	5.29, t (7.1, 7.1)	–	–	–	–	123.6	5.41, t (7.3, 7.3)
3''	135.8	–	–	–	–	–	132.4	–
4''	25.8	1.85, s	–	–	–	–	26.0	1.89, s
5''	18.0	1.78, s	–	–	–	–	18.2	1.69, s
6–OCH_3	55.8	3.87, s	–	–	56.7	3.92, s	–	–
3'–OCH_3	–	–	–	–	55.7	3.81, s	–	–

Chapter 3. Results

3.1. Structural elucidation of isolated compounds

3.3.1. Compound 1

Compound **1** was isolated as yellow oil. Its molecular formula $C_{25}H_{24}O_6$ was deduced based on HRESIMS ion peak observed at *m/z* 419.1476 $[M - H]^-$ (calcd for $C_{25}H_{23}O_6$, 419.1495), showing fourteen degrees of unsaturation. From the infrared (IR) spectrum, absorption bands indicated presence of hydroxyl group (3300 cm^{-1}) and carbonyl group (1639 cm^{-1}). The maximum UV absorption at 287 nm indicated that main structure is flavonoid.

The ABX−type spin system observed at δ_H 5.67 (1H, dd, *J* = 3.2, 13.1 Hz, H–2), δ_H 2.97 (1H, dd, *J* = 13.1, 17.2 Hz, H–3_{ax}), and δ_H 2.79 (1H, dd, *J* = 3.2, 17.2 Hz, H–3_{eq}) in the ^{1}H NMR spectrum, conjugated with oxygenated carbon resonance at δ_C 74.0 (C–2), methylene resonance at δ_C 42.5 (C–3), and carbonyl resonance at δ_C 196.8 (C–4) in the ^{13}C NMR spectrum indicated the presence of flavanone skeleton (Ichimaru et al., 1996). In addition, four methyl groups [δ_H 1.45 (3H, s, H–4''), 1.44 (3H, s, H–5''), 1.44 (3H, s, H–4'''), and δ_H 1.41 (3H, s, H–5''')] and two pairs of olefin proton doublets sharing *cis* coupling [δ_H 6.63 (1H, d, *J* = 10.0 Hz, H–3''), 5.62 (1H, d, *J* = 10.0 Hz, H–2''), 6.63 (1H, d, *J* = 10.0 Hz, H–1'''), and 5.50 (1H, d, *J* = 10.0 Hz, H–2''')] indicated that oxygen atoms at C–4' and C–7 position cyclized onto C–2''' and C–2'' of prenyl group respectively, forming two pyran rings (Patil et al., 2002), and thereby showing similar ^{1}H NMR pattern to sanggenol O (**8**) (Jung et al., 2015).

The HMBC correlations from δ_H 5.67 (H–2) to δ_C 163.0 (C–9), from δ_H 2.97 (H–3a) to δ_C 102.9 (C–10), and from δ_H 5.96 (H–6) to δ_C 102.9 (C–10), δ_C 162.0 (C–7) and δ_C 102.9 (C–8) confirmed the structures of ring A and C of flavanone. Also, the HMBC correlations from δ_H 6.38 (H–5') to δ_C 119.0 (C–1') and δ_C 109.4 (C–3'), from δ_H 7.21 (H–6') to δ_C 150.7 (C–2'), and from δ_H 5.67 (H–2) to δ_C 119.0 (C–1') and δ_C 150.7 (C–2') confirmed structure of ring B and its connection to C–2 of ring C.

Further HMBC correlations δ_H 1.45 (H–5'')/δ_C 76.6 (C–2''), δ_H 1.44 (H–6'')/δ_C 129.5 (C–3''), δ_H 5.62 (H–3'')/δ_C 109.4 (C–3'), and δ_H 6.63 (H–4'')/δ_C 76.6 (C–2'') and δ_C 158.5 (C–4') confirmed that one of two identified dihydropyran rings is attached to C–4' and C–3' of ring B, while δ_H 1.44 (H–5''')/δ_C 78.2 (C–2'''), δ_H 1.41 (H–6''')/δ_C 126.2 (C–3'''), δ_H 5.50 (H–3''')/δ_C 102.9 (C–8), and δ_H 6.63 (H–4''')/δ_C 162.0 (C–7) confirmed the other dihydropyran ring at C–7 and C–8 of ring A.

Negative Cotton effect observed at 270 nm directed that compound **1** is 2*S*−flavanone (Slade et al., 2005). Based on the result, final structure for compound **1** was decided as (2*S*)−5,2'−dihydroxyl−3',4'−(2'',2''−dimethylpyrane)−7,8−(2''',2'''−dimethylpyrane)−flavanone, simply named as sanggenol W. It is the first time that sanggenol W was discovered and reported from natural product.

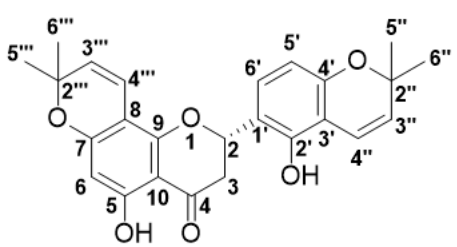

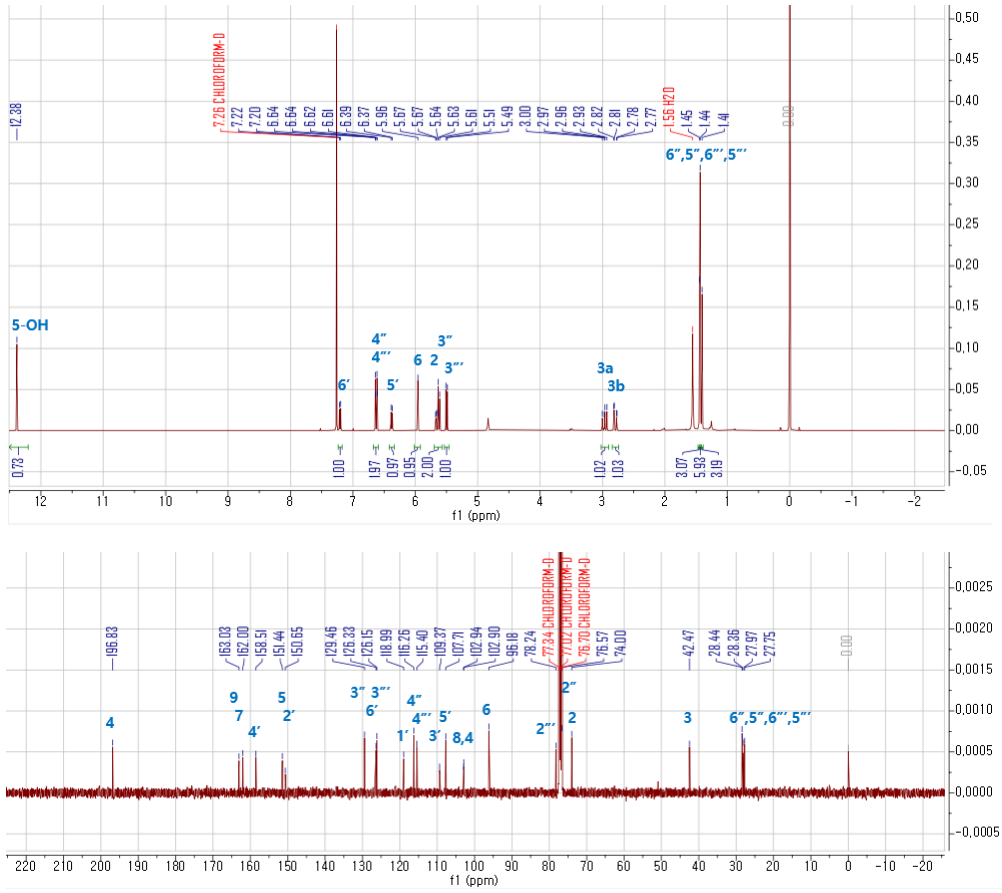

Figure 7. ^{1}H NMR and ^{13}C NMR spectra of compound **1** (recorded at 400/100 MHz, $CDCl_3$)

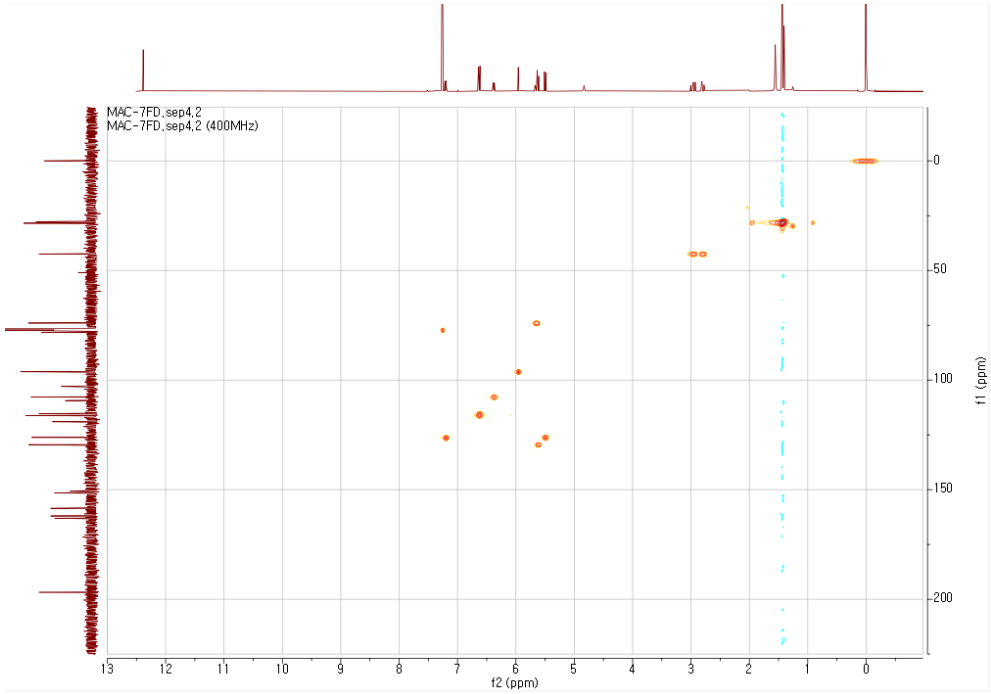

Figure 8. HSQC spectrum of compound **1** in $CDCl_3$

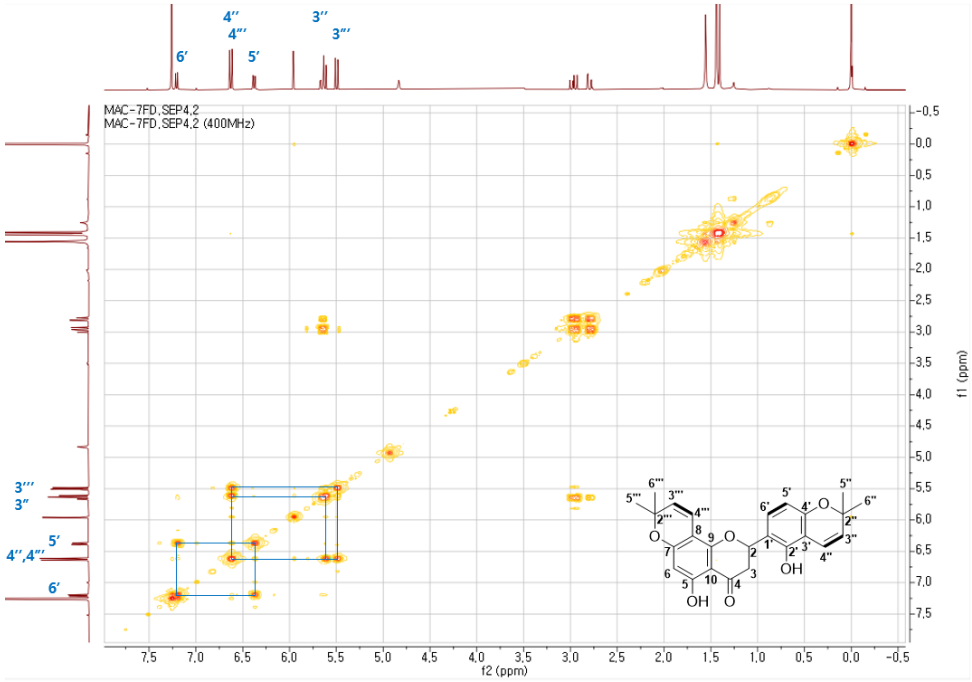

Figure 9. Key COSY correlation of compound **1** in $CDCl_3$

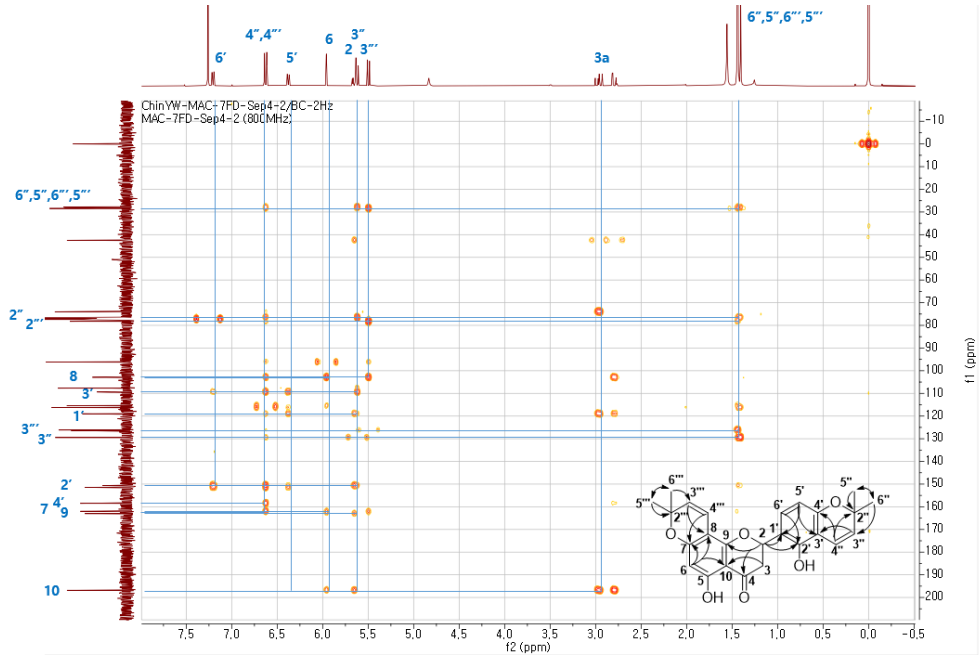

Figure 10. Key HMBC correlation of compound **1** in $CDCl_3$

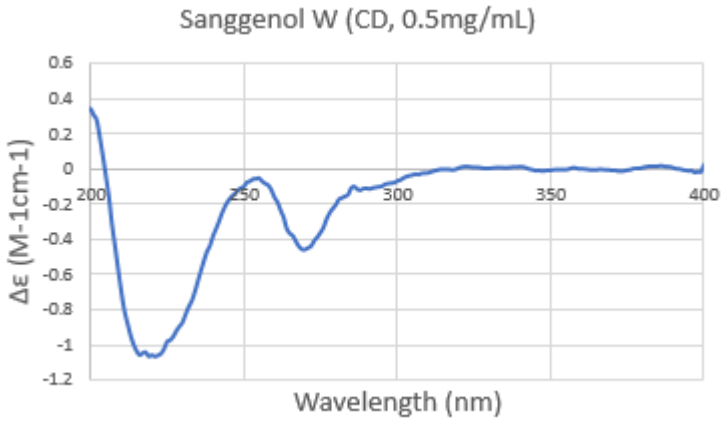

Figure 11. Experimental ECD spectra of compound **1**

3.3.2. Compound **2**

The molecular formula of compound **2**, isolated as colorless amorphous solid, was determined as $C_{30}H_{34}O_6$ based on HRESIMS results (*m/z* 489.2296 $[M - H]^-$ (calcd for $C_{30}H_{33}O_6$, 489.2296)). Not only ABX-type spin system [δ_H 5.67 (1H, dd, H-2), δ_H 3.12 (1H, dd, J = 12.4, 17.3 Hz, H-3_{ax}), and δ_H 2.72 (1H, dd, J = 3.0, 17.3 Hz, H-3_{eq})] was observed from ^{1}H NMR data of compound **2** like compound **1**, but also prenyl group [δ_H 5.32 (1H, m, H-2''''), 1.80 (3H, s, H-4''''), and 1.82 (3H, s, H-5'''')]. Prenyl-like structure [δ_H 1.71-1.65 (2H, m, H-1'''), 2.06 (2H, m, H-2'''), 5.06 (1H, m, H-3'''), 1.53 (3H, s, H-5'''), 1.63 (3H, s, H-6''')], named as 2-methylhex-2-ene, was also identified after comparison with ^{1}H NMR pattern of dimethylpyran ring from cycloaltilisin 7 (**10**).

The HMBC correlations within 2-methylhex-2-ene, displayed by δ_H 1.53 (H-5''')/δ_C 131.8 (C-4'''), δ_H 1.63 (H-6''')/δ_C 124.0 (C-3'''), and δ_H 2.06 (H-2''')/δ_C 131.8 (C-4'''), δ_C 124.0 (C-3'''), δ_C 41.0 (C-1''') and δ_C 78.7 (C-2''), confirmed its internal substructure. Its position was fixed at C-2'' from HMBC correlation at δ_H 1.71-1.65 (H-1''')/δ_C 78.7 (C-2''). Position of the independent fifth methyl group was also decided to be at C-2'' from δ_H 5.57 (H-3'')/δ_C 26.3 (2''-CH_3). The prenyl group was located at C-5' based on HMBC correlations from δ_H 3.31 (H-1'''') to δ_C 118.2 (C-5'), δ_C 150.7 (C-4') and δ_C 126.7 (C-6'),

From the CD spectrum, negative and positive Cotton effects were clearly observed at around 295 nm and 334 nm respectively, indicating that configuration at C-2 is (*S*) (Slade et al., 2005). Hence, final structure for novel compound, morusalnol D, was decided as (2*S*)-5,7,4'-trihydroxyl-2',3'-(2'',2''-dimethylpyrane)

−1‴,5'−diprenylflavanone. It is the first time that morusalnol D was discovered and reported from natural product.

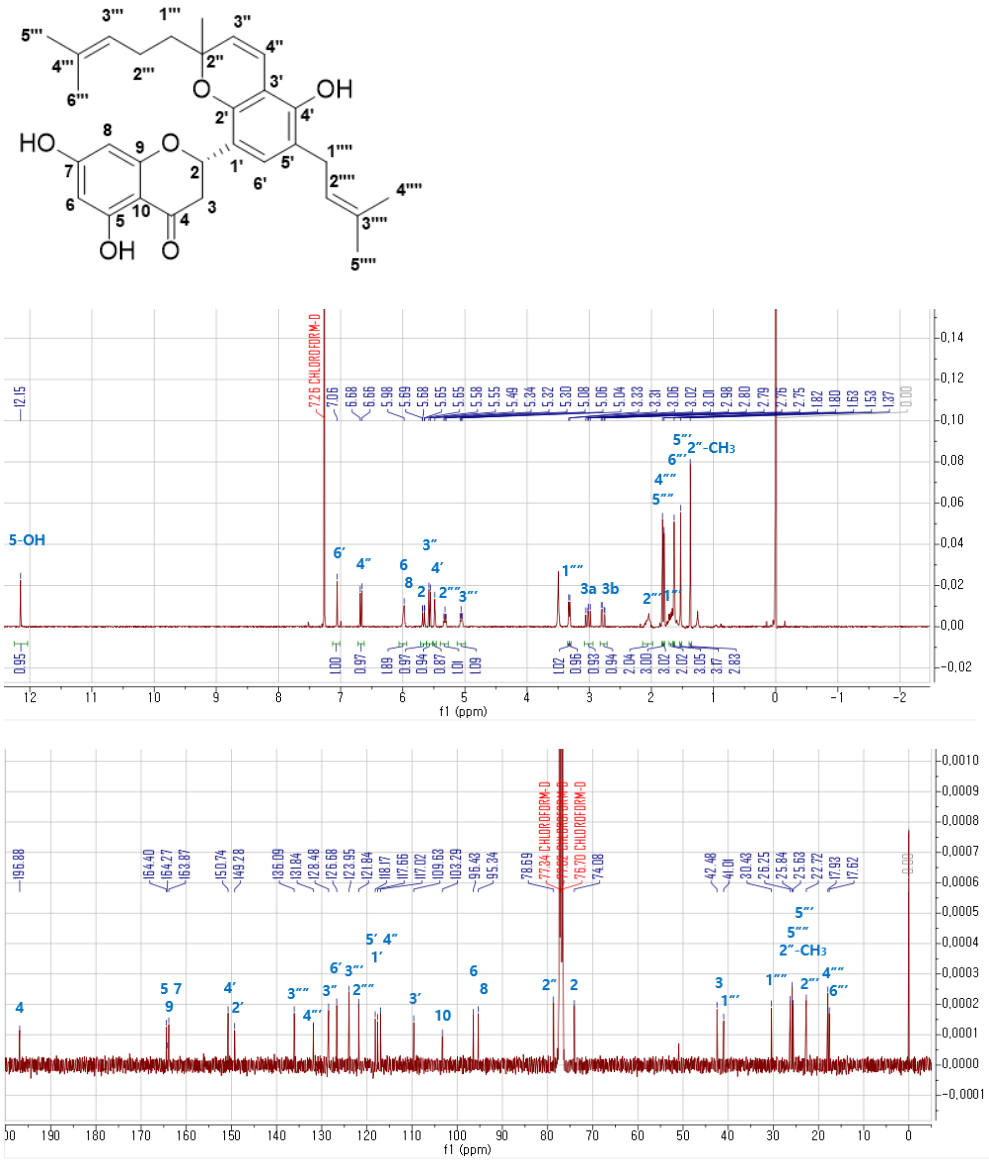

Figure 12. ^{1}H and ^{13}C NMR spectra of compound **2** (recorded at 400/100 MHz, $CDCl_3$)

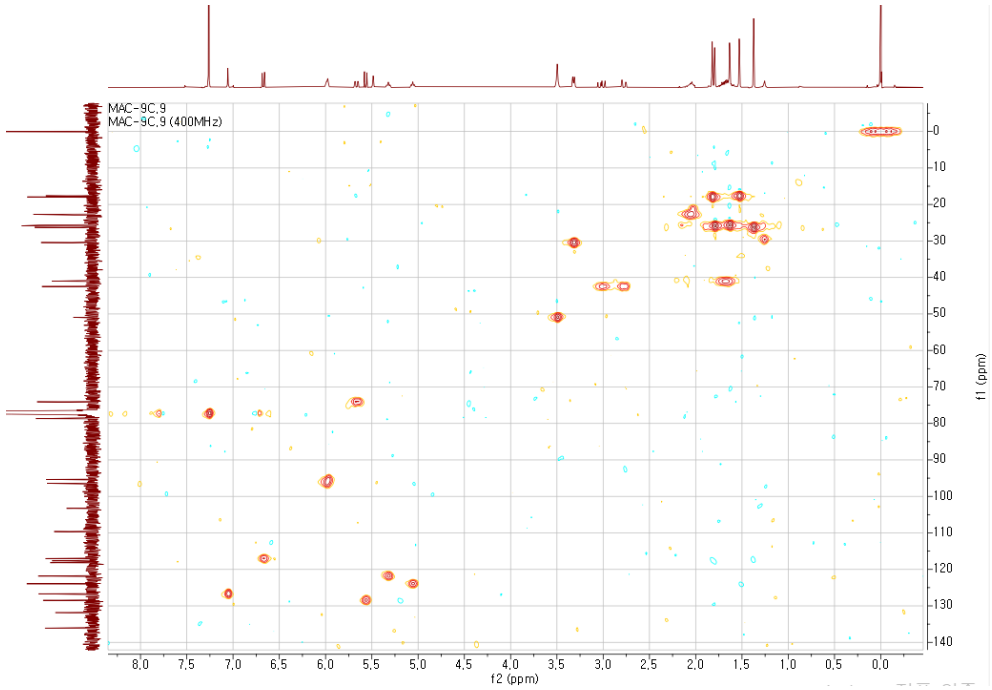

Figure 13. HSQC spectrum of compound **2** in $CDCl_3$

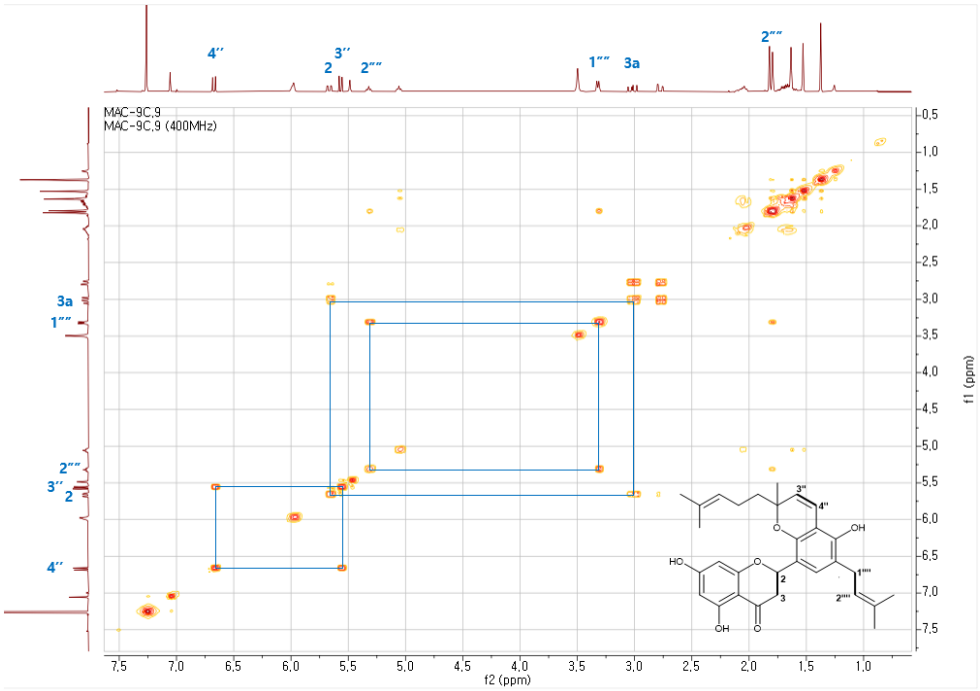

Figure 14. Key COSY correlation of compound **2** in $CDCl_3$

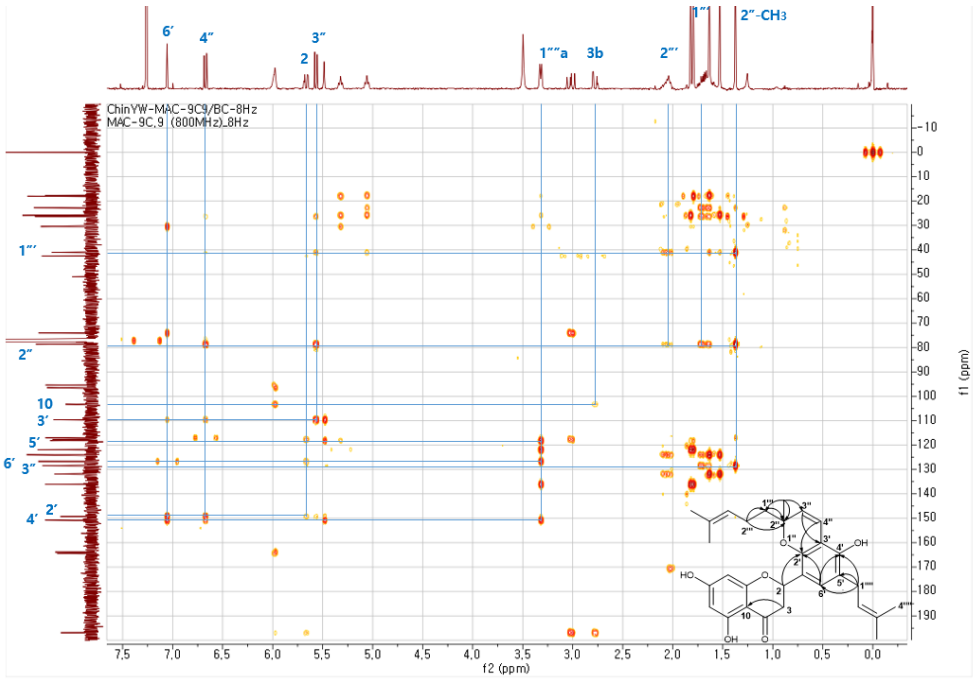

Figure 15. Key HMBC correlation of compound 2 in $CDCl_3$

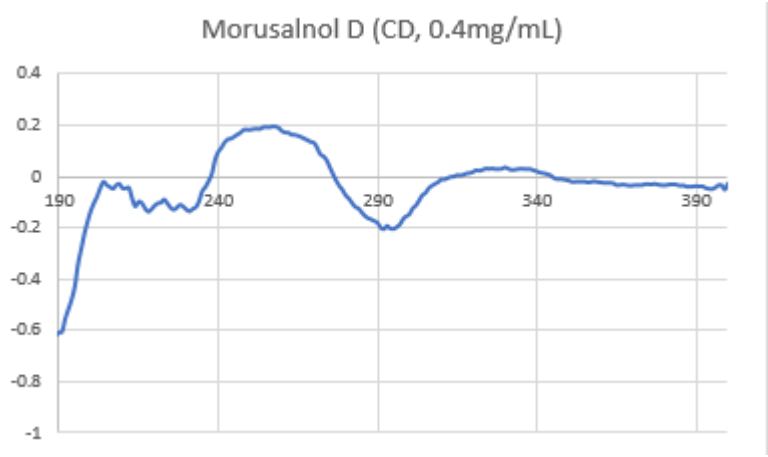

Figure 16. Experimental ECD spectra of compound 2

3.3.3. Compound **3**

Compound **3** was isolated as white amorphous solid with its molecular formula assigned as $C_{30}H_{34}O_5$ after analysis of HRESIMS (*m/z* 473.2351 $[M - H]^-$ (calcd for $C_{30}H_{33}O_5$, 473.2333)). From the ^1H NMR spectrum, characteristic for flavanone was detected like **1** and **2** from the ABX−type spin system [δ_H 5.32 (1H, m, H–2), 3.12 (1H, dd, J = 12.4, 17.3 Hz, H–3_{ax}), and 2.72 (1H, dd, J = 3.0, 17.3 Hz, H–3_{eq})], as well as 1,3,4−trisubstituted aromatic ring [δ_H 7.15 (1H, d, J = 2.3 Hz, H–2'), 6.77 (1H, d, J = 8.2 Hz, H–5'), and 7.12 (1H, dd, J = 2.3, 8.2 Hz, H–6')]. Likewise, one prenyl group [δ_H 5.31 (1H, m, H–2''''), 1.73 (3H, s, H–4''''), and 1.57 (3H, s, H–5'''')] and 2−methylhex−2−ene [δ_H 1.73−1.64 (2H, m, overlaid, H–1'''), 2.08 (2H, m, H–2'''), 5.09 (1H, m, H–3'''), 1.64 (3H, s, H–5'''), and 1.55 (3H, s, H–6''')] was also identified.

A COSY correlation between δ_H 6.77 (H–5') and δ_H 7.12 (H–2') was observed, and the HMBC correlation from both δ_H 7.12 (H–6') and δ_H 3.29 (H–1'''') to δ_C 156.8 (C–4') and δ_C 129.1 (C–2') aided by extra HMBC correlation δ_H 3.29 (H–1'''')/δ_C 130.8 (C–3') established both presence of the 1,3,4−trisubstituted ring and position of prenyl group at δ_C 130.8 (C–3').

Furthermore, HMBC correlations δ_H 6.62 (H–4'')/δ_C 163.72 (C–7), δ_H 5.51 (H–3'')/δ_C 103.82 (C–6), and from δ_H 1.38 (2''–CH_3) to δ_C 126.26 (C–3'') and δ_C 81.98 (C–2'') fixed the pyran ring at C–6 and C–7 of ring A. Extra HMBC correlations δ_H 2.08 (H–2''')/δ_C 42.8 (C–1''') and δ_H 1.38 (2''–CH_3)/δ_C 42.8 (C–1''') confirmed that 2−methylhex−2−ene is bound to C–2''.

Supported by negative and positive Cotton effects observed at 290 nm and 334 nm respectively, final structure for compound **3**

was decided as (2*S*)−5,4'−dihydroxyl−6,7−(2'',2''−dimethylpyrane)−1''',3'−diprenylflavanone, namely morusalnol E. It is the first time that morusalnol E was discovered and reported from natural product.

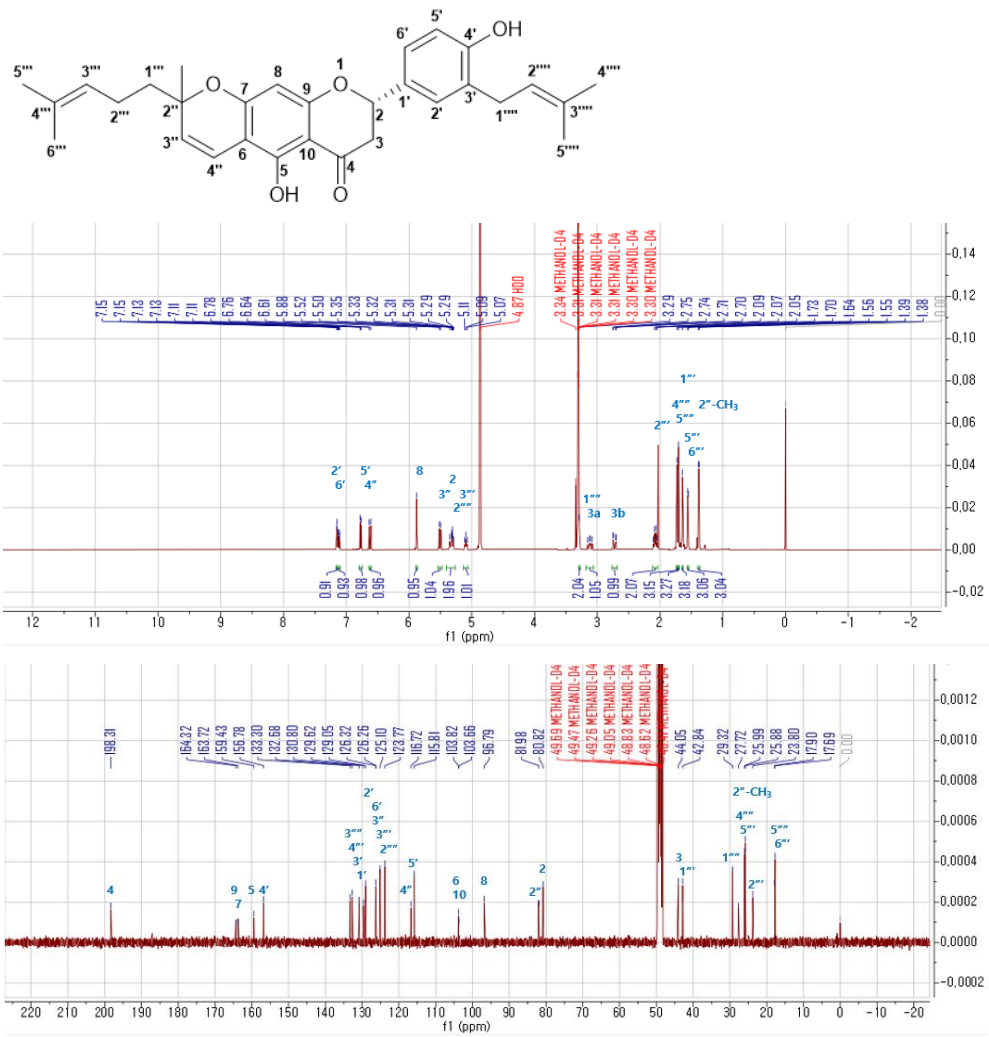

Figure 17. ^{1}H and ^{13}C NMR spectra of compound **3** (recorded at 400/100 MHz, MeOD−d_4)

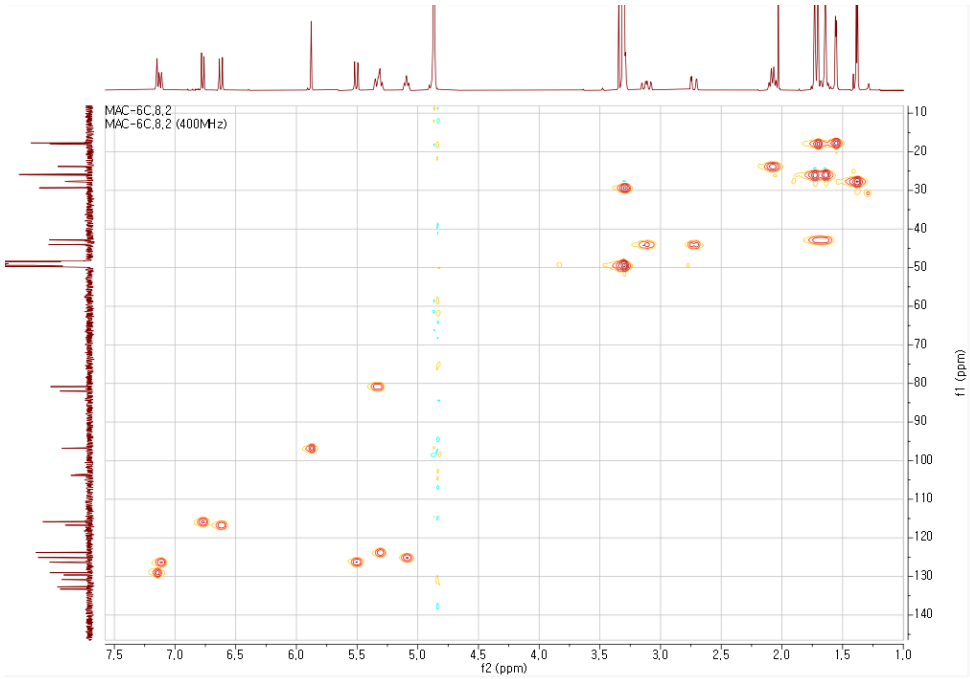

Figure 18. HSQC spectrum of compound **3** in MeOD−d_4

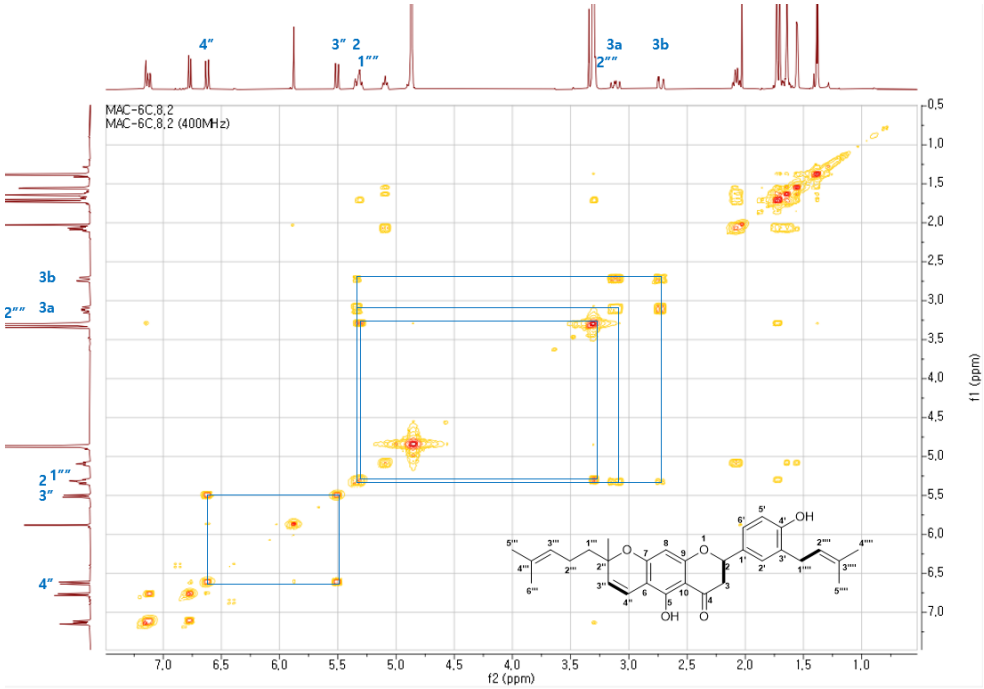

Figure 19. Key COSY correlation of compound **3** in MeOD−d_4

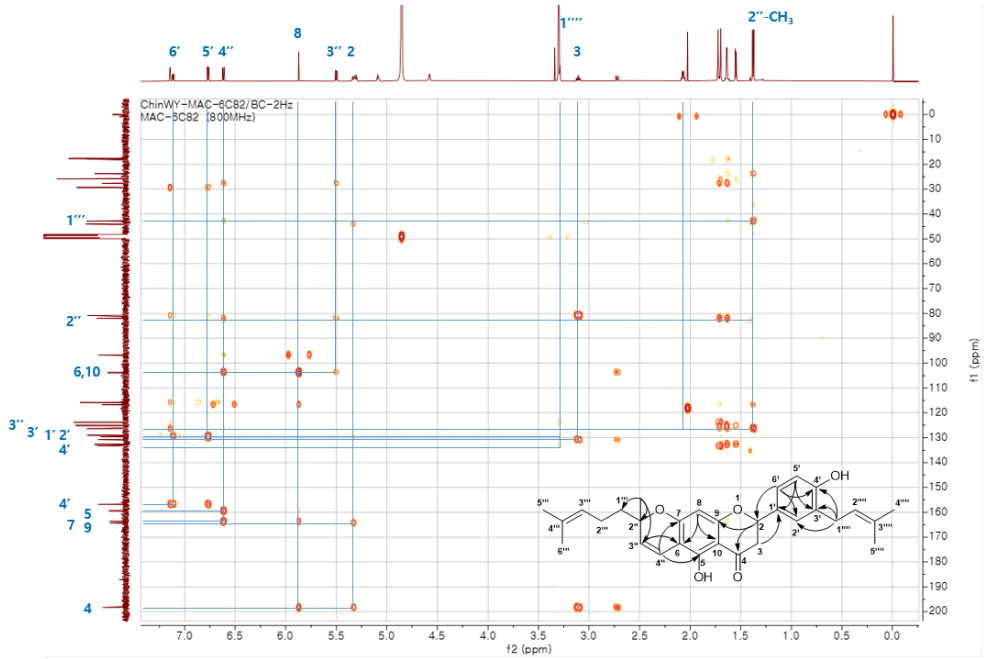

Figure 20. Key HMBC correlation of compound **3** in MeOD−d_4

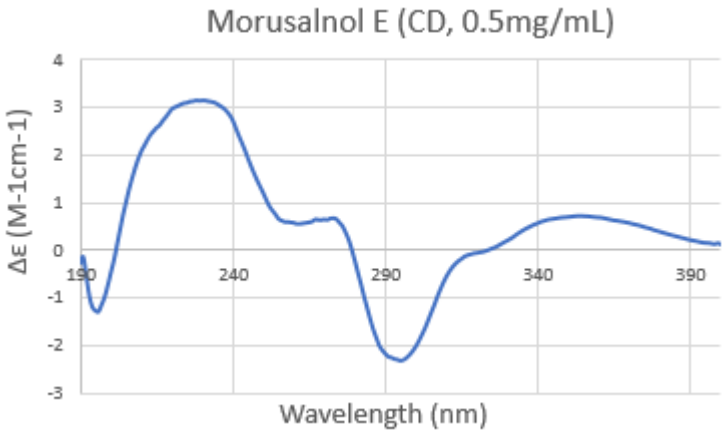

Figure 21. Experimental ECD spectra of compound **3**

3.3.4. Compound **4**

Compound **4** was gained as yellow amorphous solid with a molecular formula of $C_{30}H_{34}O_6$ on the basis of HRESIMS (*m/z* 489.2304 $[M-H]^-$ (calcd for $C_{30}H_{33}O_6$, 489.2283)), showing an increase of one oxygen compared to compound **3**. The ^1H NMR demonstrated similarity to **3**, exhibiting flavanone skeleton [δ_H 5.58 (1H, dd, *J* = 3.2, 12.7 Hz, H–2), 3.12 (1H, dd, *J* = 12.7, 17.3 Hz, H–3_{ax}), and 2.72 (1H, dd, *J* = 3.2, 17.3 Hz, H–3_{eq})], prenyl moiety [δ_H 3.46 (2H, d, H–1'''', overlaid), 5.32 (1H, m, H–2''''), 1.77 (3H, s, H–4''''), and δ_H 1.41 (3H, s, H–5'''')] and 2–methylhex–2–ene [δ_H 1.75–1.63 (2H, m, overlaid, H–1'''), δ_H 2.07 (2H, m, H–2'''), δ_H 5.08 (1H, m, H–3'''), δ_H 1.66 (3H, s, H–5'''), and δ_H 1.57 (3H, s, H–6''')]. Nevertheless, 1,3,4–trisubstituted ring of **3** was replaced by *ortho*–positioned aromatic protons [δ_H 6.43 (1H, d, *J* = 8.4 Hz, H–5') and 6.98 (1H, d, *J* = 8.4 Hz, H–6')].

While COSY correlation between δ_H 6.43 (H–5') and δ_H 6.98 (H–6') reinforced the above statement, HMBC correlations from δ_H 6.43 (H–5') to δ_C 116.6 (C–1') and δ_C 114.7 (C–3'), from δ_H 6.98 (H–6') to δ_C 155.5 (C–4') and δ_C 153.6 (C–2'), and from prenyl protein δ_H 3.46 (H–1'''') to δ_C 153.6 (C–2'), δ_C 114.7 (C–3') and δ_C 155.5 (C–4') confirmed ring B and position of prenyl moiety at C–3'.

Moreover, HMBC correlations δ_H 6.66 (H–4'')/δ_C 162.36 (C–7), δ_H 5.45 (H–3'')/δ_C 103.27 (C–6), from δ_H 1.41 (2''–CH_3) to δ_C 125.20 (C–3''), δ_C 80.94 (C–2'') and δ_C 41.70 (C–1'''), and from δ_H 2.07 (H–2''') to δ_C 41.70 (C–1''') confirmed the structure of rings A and D plus position of 2–methylhex–2–ene at C–2''.

The experimental CD spectrum presented the pattern of 2*S*–configuration of flavanone (Slade et al., 2005), and hence final

structure for compound **4** was decided as (2*S*)−5,2',4'−trihydroxyl−6,7−(2'',2''−dimethylpyrane)−1''',3'−diprenylflavanone, namely morusalnol F. It is the first time that morusalnol F was discovered and reported from natural product.

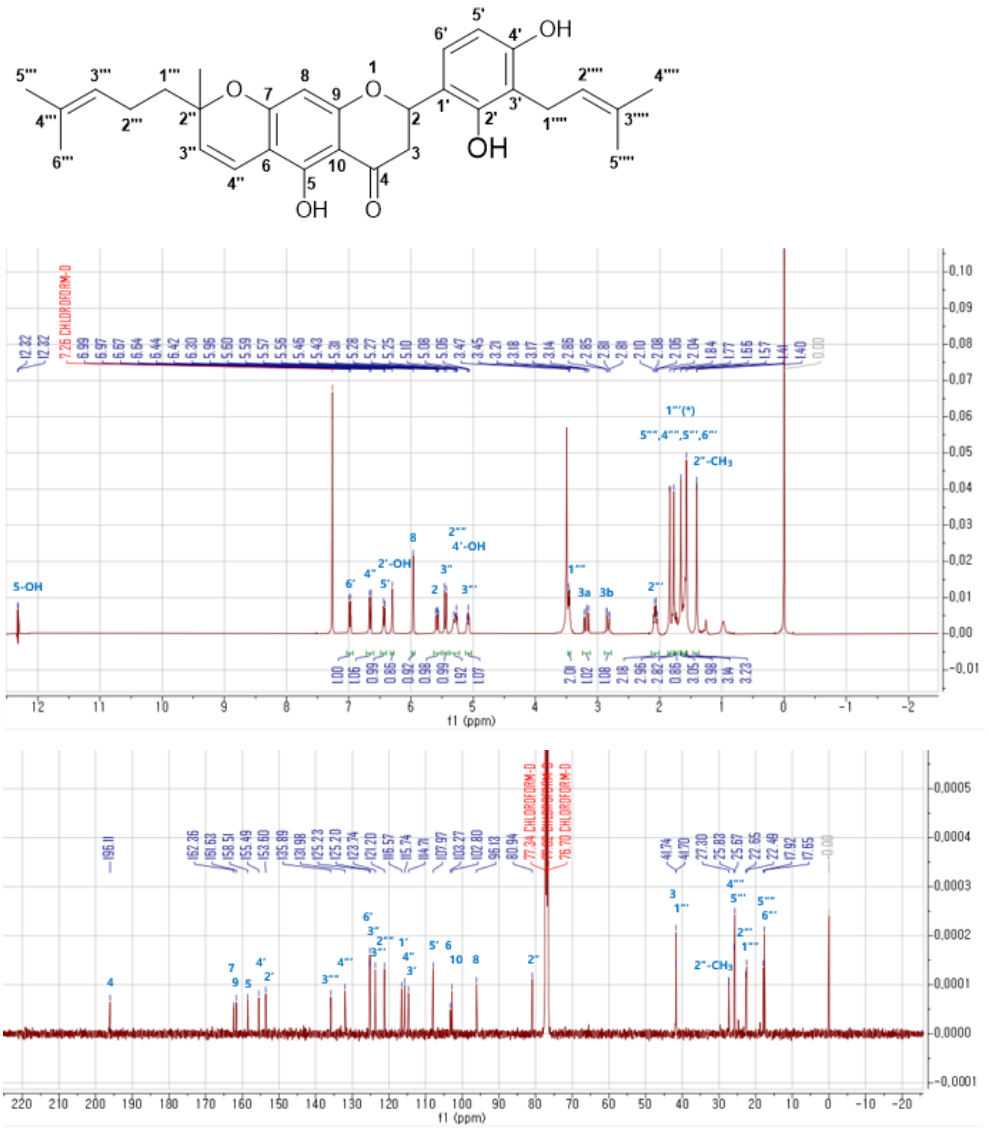

Figure 22. ^{1}H and ^{13}C NMR spectra of compound **4** (recorded at 400/100 MHz, $CDCl_3$)

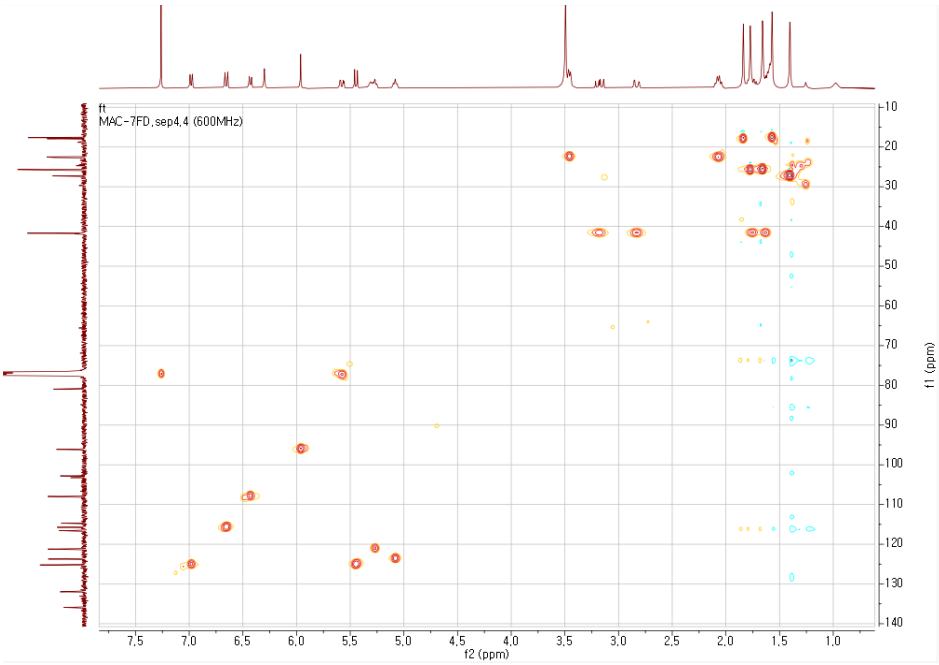

Figure 23. HSQC spectrum of compound **4** in $CDCl_3$

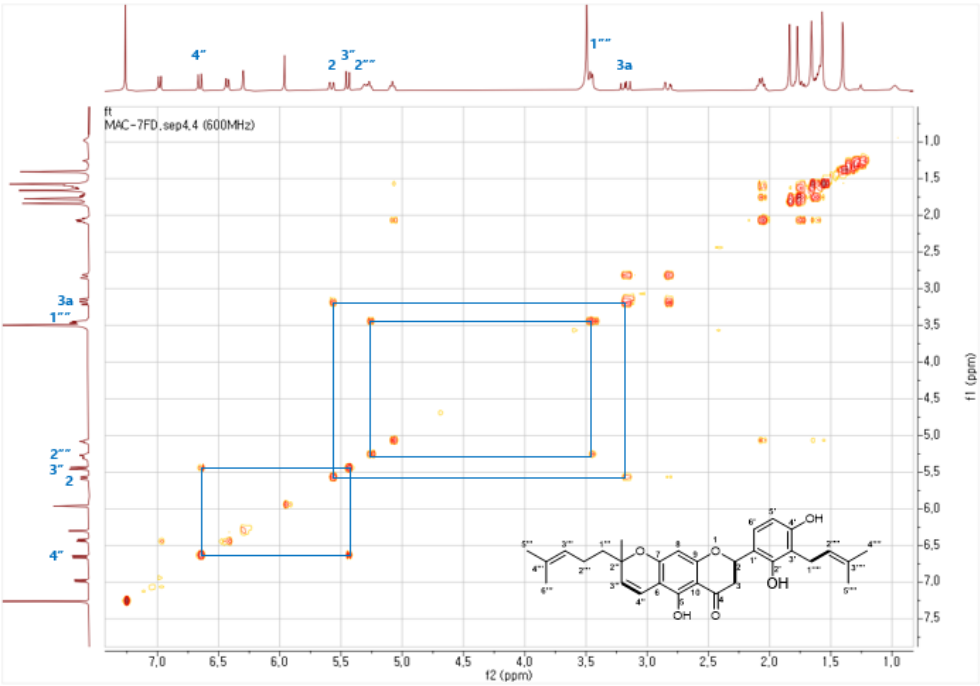

Figure 24. Key COSY correlation of compound **4** in $CDCl_3$

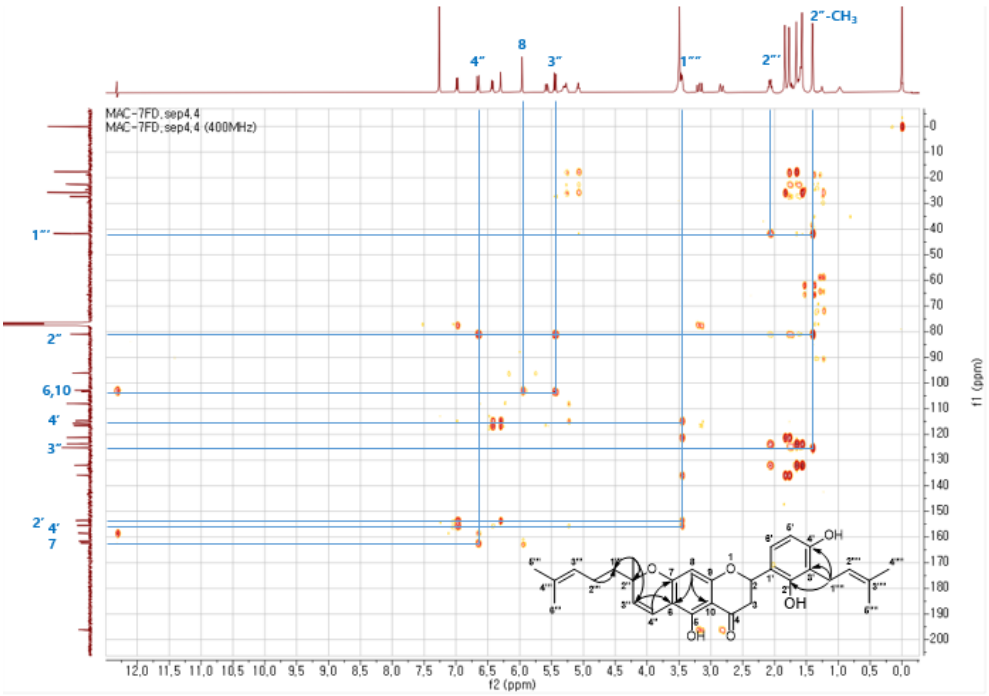

Figure 25. Key HMBC correlation of compound **4** in $CDCl_3$

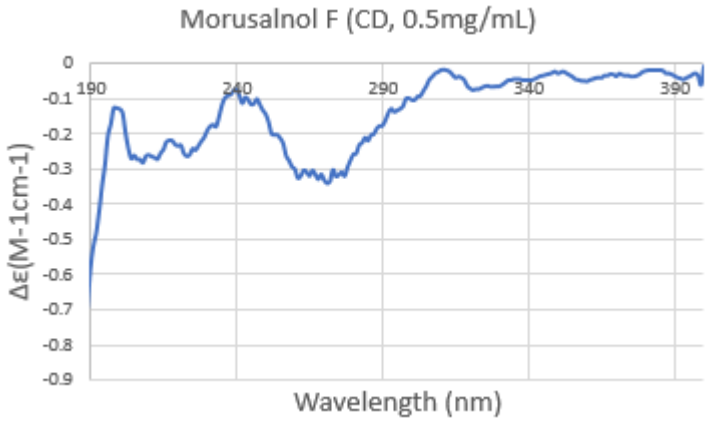

Figure 26. Experimental ECD spectra of compound **4**

3.3.5. Compound **5**

Compound **5**, obtained as brown amorphous solid, was found to have molecular formula of $C_{25}H_{26}O_7$ based on HRESIMS peak observed at *m/z* 437.1617 $[M - H]^-$ (calcd for $C_{25}H_{25}O_7$, 437.1606). Alongside observed ABX-type spin system [δ_H 5.67 (1H, dd, *J* = 2.9, 13.0 Hz, H–2), δ_H 3.07 (1H, dd, *J* = 13.0, 17.2 Hz, H–3_{ax}), and δ_H 2.75 (1H, dd, *J* = 2.9, 17.2 Hz, H–3_{eq})] in the ^{1}H NMR spectrum, another set of flavanone-like structure was proposed from proton signals [δ_H 2.91 (1H, d, *J* = 17.0 Hz, H–3''a) and δ_H 2.79 (1H, d, *J* = 17.0 Hz, H–3''b)] which partially overlapped with H–3_{ax} and H–3_{eq}. The carbon resonances unveiled at δ_C 82.5 (C–2''), δ_C 47.6 (C–3''), and δ_C 200.6 (C–4'') from ^{13}C NMR spectrum and HSQC spectrum speculated the existence of the second flavanone-like skeleton, which was conjectured to be pyran-4-one ring (ring D). The presence of 2-methylhex-2-ene [δ_H 1.81-1.72 (2H, m, H–1'''), 2.14 (2H, m, H–2'''), 5.11 (1H, m, H–3'''), 1.67 (3H, s, H–5'''), and 1.59 (3H, s, H–6''')] was also identified from 1D NMR.

The HMBC correlations from δ_H 3.07 (H–3_{eq}) to δ_C 197.7 (C–4) and δ_C 103.3 (C–10), from δ_H 5.89 (H–8) to δ_C 165.6 (C–9), δ_C 103.3 (C–10) and δ_C 97.3 (C–6), and from δ_H 5.91 (H–6) to δ_C 165.0 (C–7) and δ_C 168.7 (C–5) completed rings A and C of flavanone.

Likewise, the HMBC correlations from δ_H 6.49 (H–5') to δ_C 161.6 (C–4'), δ_C 108.3 (C–3') and δ_C 119.2 (C–1'), from δ_H 7.68 (H–6') to δ_C 161.6 (C–4'), δ_C 159.6 (C–2') and δ_C 74.6 (C–2), and from δ_H 5.67 (H–2) to δ_C 119.2 (C–1') and δ_C 159.6 (C–2') confirmed ring B and binding between rings B and C.

Moreover, the HMBC correlations from δ_H 2.91 (H–3''a) to δ_C 200.6 (C–4''), δ_C 82.5 (C–2'') and δ_C 24.1 (2''–CH_3), from δ_H 1.43

(2''–CH_3) to δ_C 82.5 (C–2'') and δ_C 40.1 (C–1'''), from δ_H 1.67 (H–5''') and δ_H 1.59 (H–6''') to both δ_C 133.2 (C–4''') and δ_C 124.6 (C–3'''), and from δ_H 2.14 (H–2''') to δ_C 124.6 (C–3''') and δ_C 40.1 (C–1''') concluded structure of ring D and position of 2−methylhex−2−ene. Vivid correlation between δ_H 6.49 (H–5') and δ_C 200.6 (C–4'') further support that rings B and D are connected at C–3' and C–4'.

Reinforced by negative and positive Cotton effects at 287 and 312 nm respectively in CD spectra, absolute configuration at C–2 for compound **5** was decided as 2*S*. However, (2''*R*) and (2''*S*) showed almost no difference from calculated CD spectra, and therefore stereochemistry at remaining chiral centre, C–2'', is yet to be determined. Final structure for compound **5**, namely neovanone A, is illustrated with compound **6** due to identical planar structure but difficulty in determining absolute configuration.

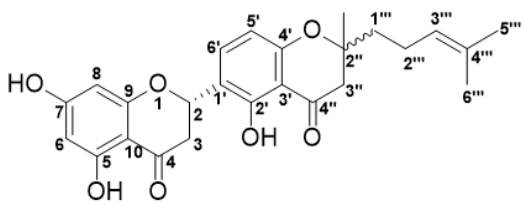

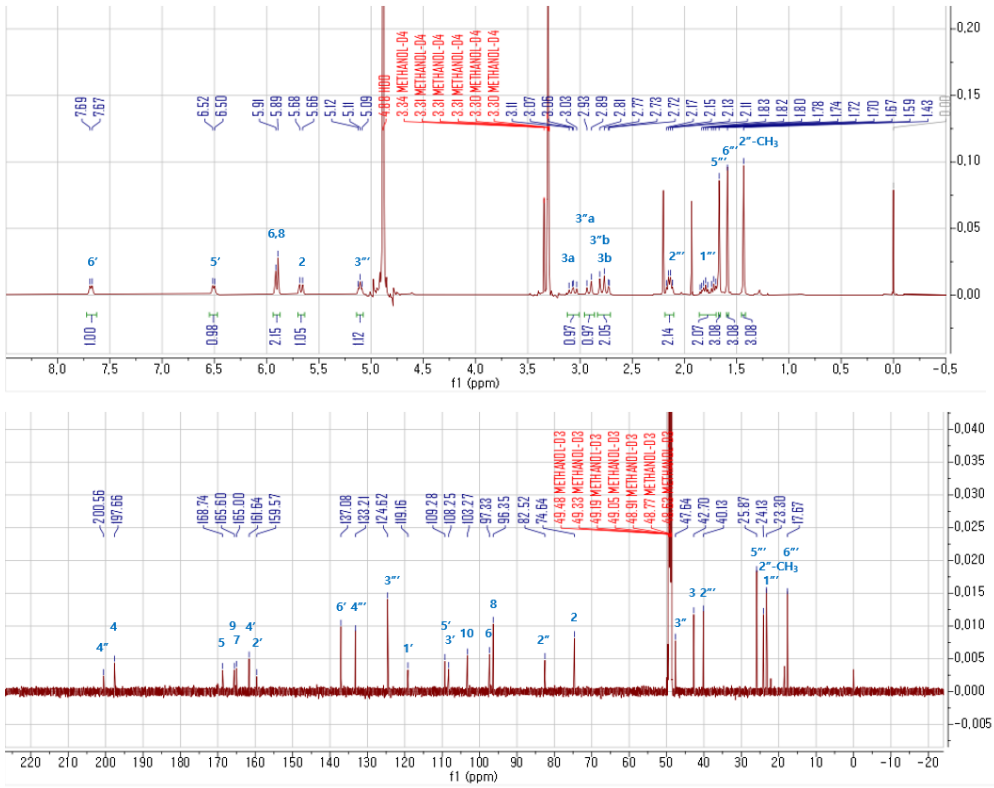

Figure 27. ^{1}H and ^{13}C NMR spectra of compound **5** (recorded at 400/150 MHz, MeOD−d_4)

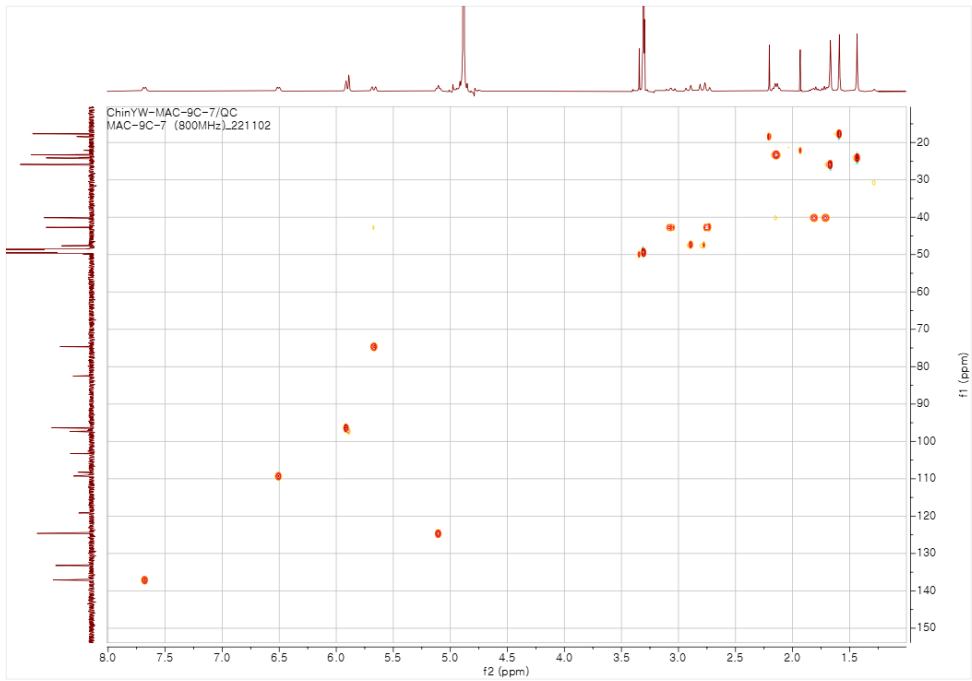

Figure 28. HSQC spectrum of compound **5** in MeOD−d_4

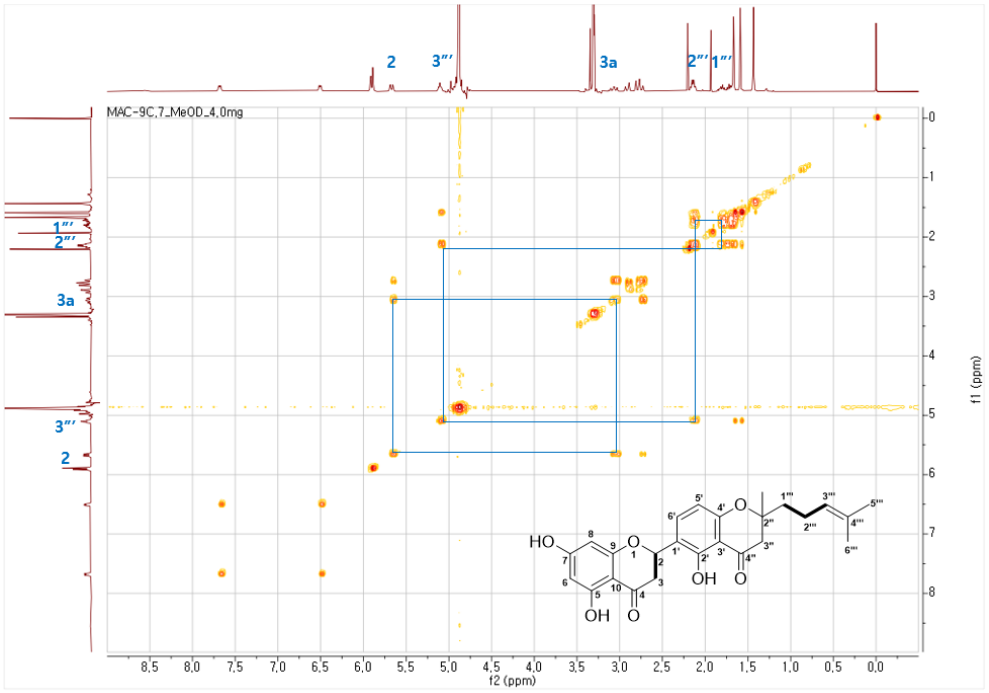

Figure 29. Key COSY correlations of compound **5** in MeOD−d_4

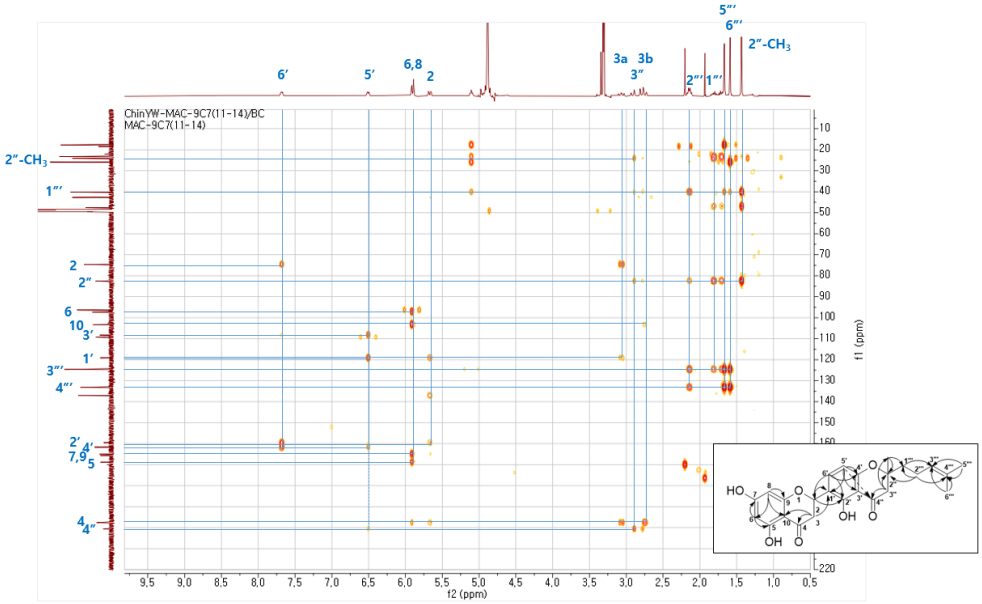

Figure 30. Key HMBC correlations of compound **5** in MeOD−d_4

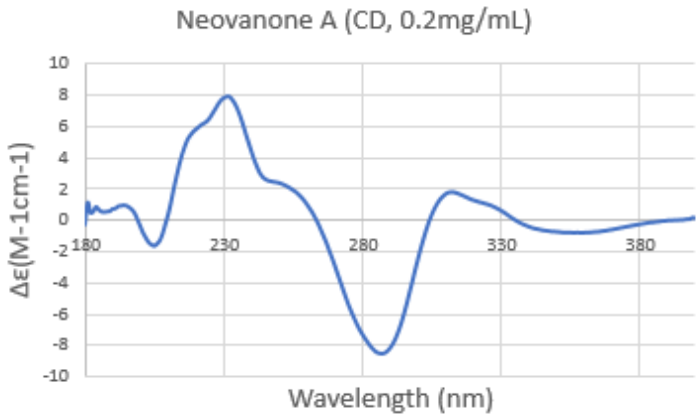

Figure 31. Experimental ECD spectra of compound 5

3.3.6. Compound **6**

HRESIMS analysis of compound **6**, brown amorphous solid, established equivalent molecular formula of $C_{25}H_{26}O_7$ to **5** based on HRESIMS negative ion peak at *m/z* 437.1616 $[M - H]^-$ (calcd for $C_{25}H_{25}O_7$, 437.1606). It was also noticeable that both ^1H and ^{13}C NMR of compound **6** were almost identical to that of Neovanone A (**5**). The HSQC spectra, again, confirmed that compounds **5** and **6** were identical in planar structure despite having been separated by HPLC (Figure 37), and thus compound **6** was named neovanone B.

The above claim was supported by HMBC correlations from δ_H 2.75 (H–3_{eq}) to δ_C 197.6 (C–4) and δ_C 103.2 (C–10), from δ_H 5.91 (H–8) to δ_C 103.2 (C–10) and δ_C 97.3 (C–6) within rings A and C, as well as from δ_H 5.67 (H–2) to δ_C 119.1 (C–1'), from δ_H 6.51 (H–5') to δ_C 119.1 (C–1') and δ_C 108.2 (C–3'), from δ_H 2.91 (H–3''a) to δ_C 108.2 (C–3') and δ_C 24.1 (2''–CH_3), and from δ_H 1.44 (2''–CH_3) to δ_C 40.2 (C–1''') within rings B and D and 2 methylhex−2−ene.

Finally, CD spectrum for compound **6** displayed 2*S*–flavanone pattern based on negative and positive Cotton effects at 290 and 312 nm respectively. However, a difference was acknowledged at 354 nm of the experimental CD curve as shown in Figure 38 where **5** showed negative Cotton effect while **6** showed positive Cotton effect. As with compound **5**, calculated CD curve was to be acquired to decide absolute configuration at C–2'', the only remaining chiral center for compounds **5** and **6**, but (2''*R*) and (2''*S*) showed almost no difference.

Overall, final structure for both compounds **5** and **6** were temporarily decided as (2*S*,2''*R**)−5,7,2'−trihydroxy−2'−methyl−2'−(4−methylpent−3−en−1−yl)−[2,1'−bichromane]−4,4''−dione

and (2*S*,2''*S**)−5,7,2'−trihydroxy−2'−methyl−2'−(4−methylpent−3−en−1−yl)−[2,1'−bichromane]−4,4''−dione until absolute configuration at C–2'' is fully established. It is the first time that compounds **5** and **6** were discovered and reported from natural product.

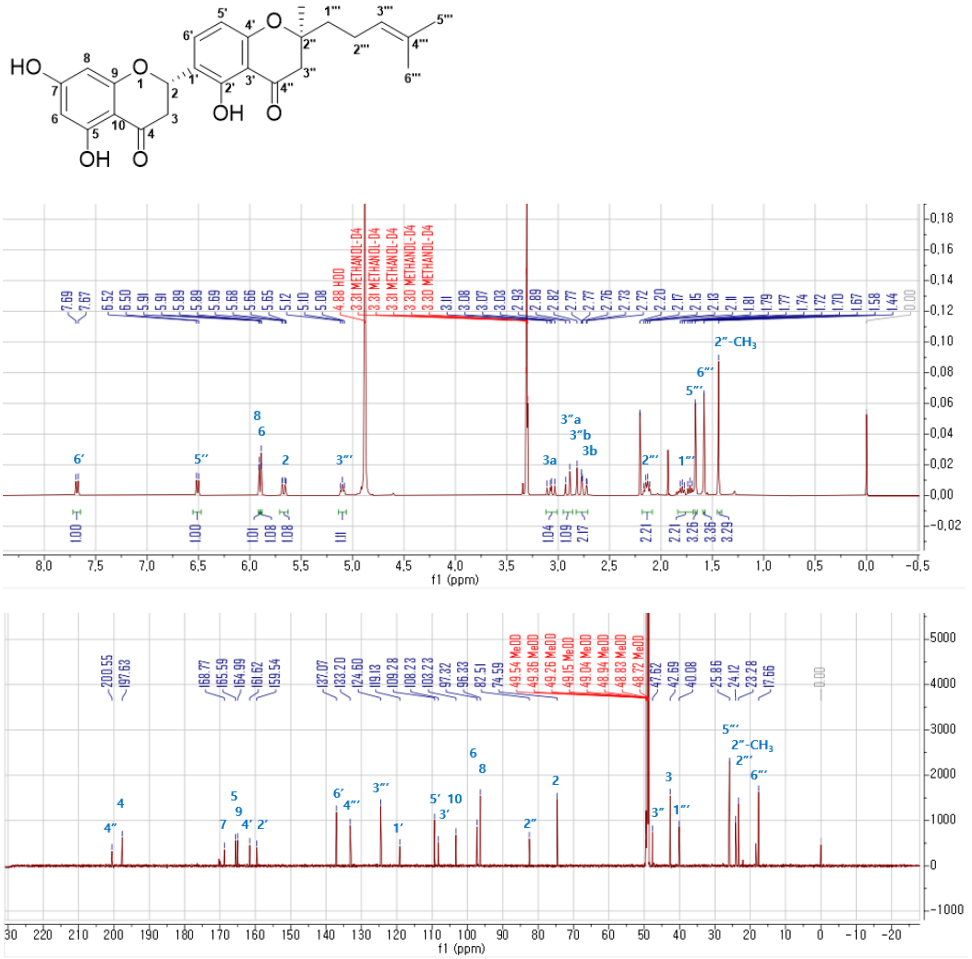

Figure 32. ^{1}H and ^{13}C NMR spectra of compound **6** (recorded at 400/200 MHz, MeOD−d_4)

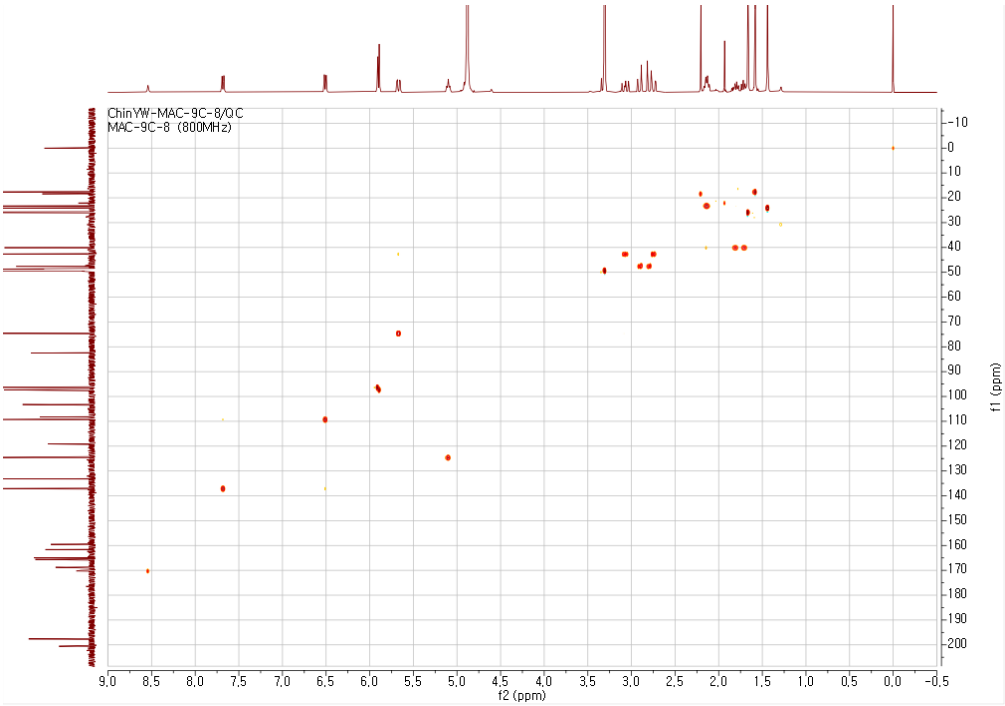

Figure 33. HSQC spectrum of compound **6** in MeOD−d_4

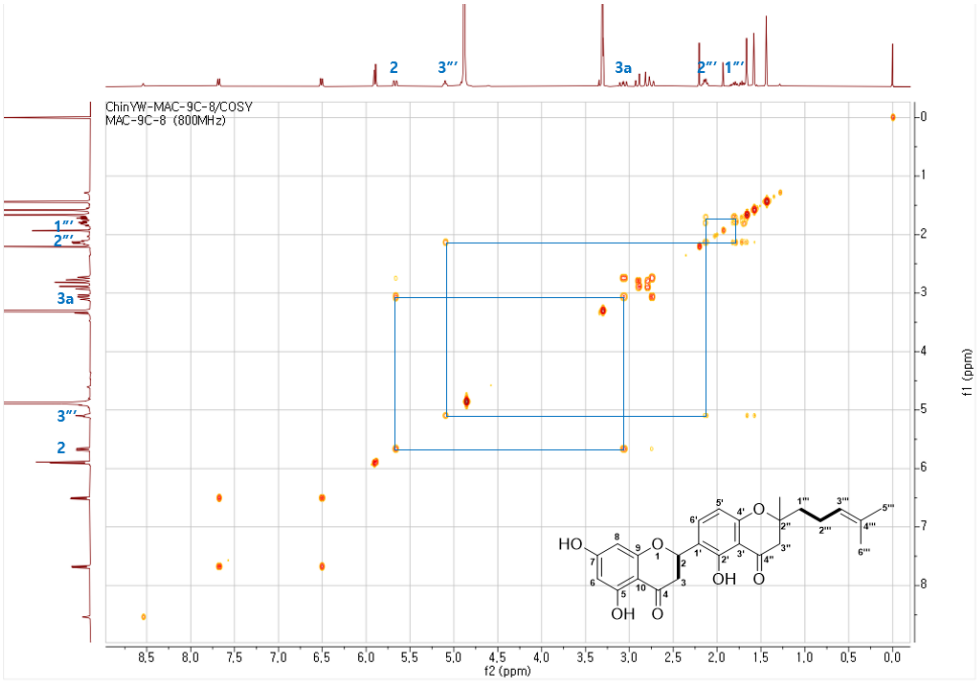

Figure 34. Key COSY correlation of compound **6** in MeOD−d_4

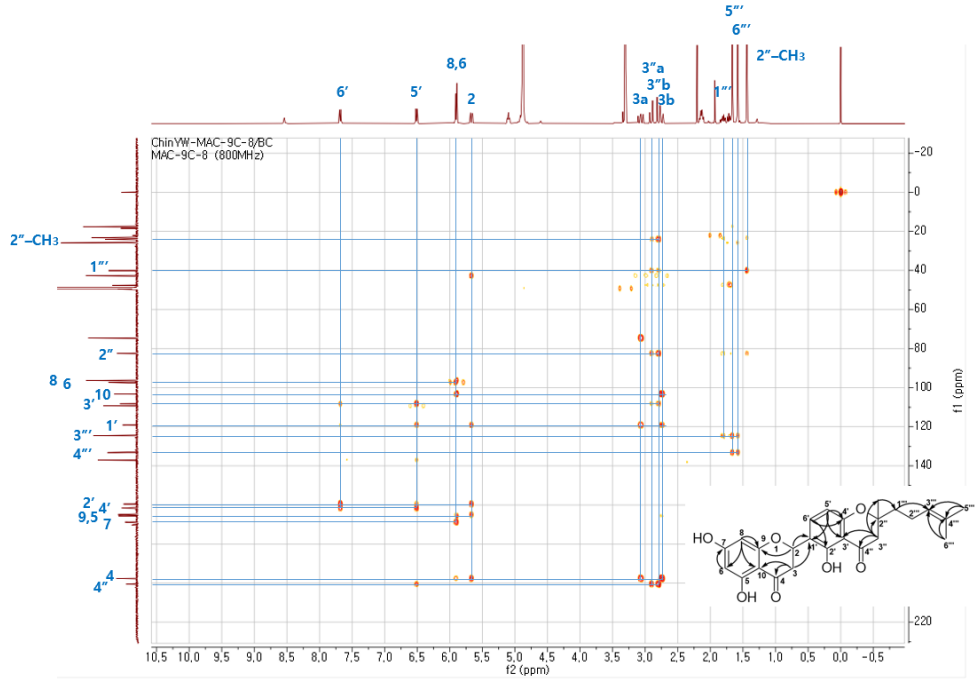

Figure 35. Key HMBC correlation of compound 6 in MeOD−d_4

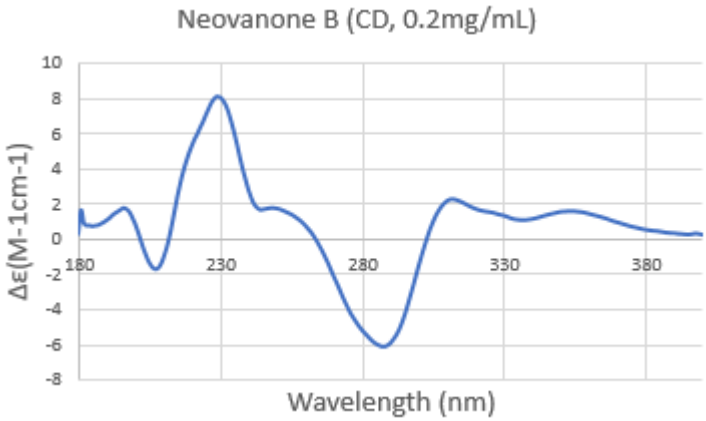

Figure 36. Experimental ECD spectra of compound 6

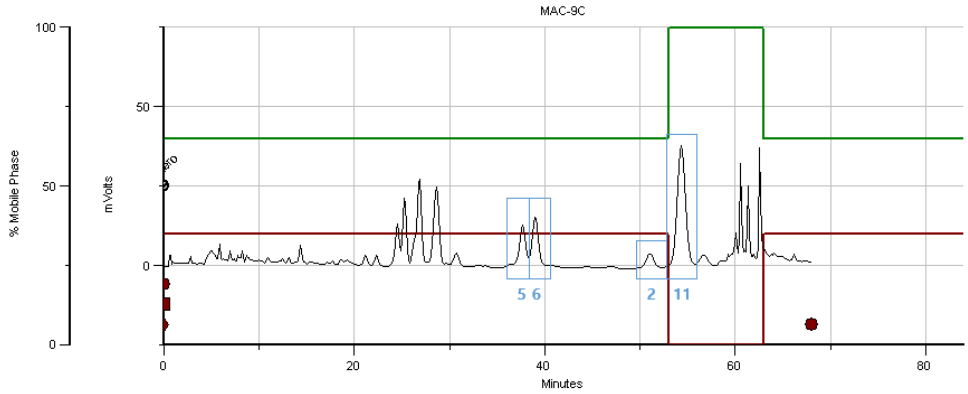

Figure 37. HPLC chromatogram of injected MAC−9C sample to obtain **5**, **6**, **2**, and **11**

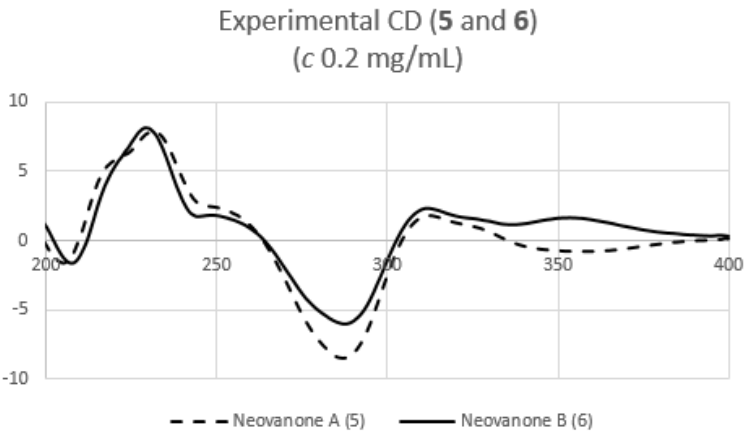

Figure 38. Comparison of experimental CD spectra of **5** and **6**

3.3.7. Compound **7**

Compound **7** was isolated as colorless amorphous solid with molecular formula of $C_{20}H_{18}O_5$ based on HRESIMS spectra showing deprotonated ion at *m/z* 337.1063 $[M - H]^-$ (calcd for $C_{20}H_{17}O_5$, 337.1076). From the ^1H NMR spectrum, the ABX−type spin system [δ_H 5.31 (1H, dd, *J* = 3.0, 13.1 Hz, H–2), 3.09 (1H, dd, *J* = 13.1, 17.2 Hz, H–3_{ax}), and 2.77 (1H, dd, *J* = 3.0, 17.2 Hz, H–3_{eq})], 1,3,4−trisubstituted aromatic ring [δ_H 7.06 (1H, d, *J* = 2.2 Hz, H–2'), 7.17 (1H, dd, *J* = 2.2, 8.3 Hz, H–6'), and 6.81 (1H, d, *J* = 8.6 Hz, H–5')], and dimethylpyran ring through gem−dimethyl resonance [δ_H 5.66 (1H, d, *J* = 9.8 Hz, H–3''), 6.33 (1H, d, *J* = 9.8 Hz, H–4''), and 1.45 (6H, s, H–5'' and H–6'')].

The HMBC correlations from δ_H 7.06 (H–2') to δ_C 127.20 (C–6') and δ_C 153.54 (C–4'), from δ_H 6.33 (H–4'') to δ_C 153.5 (C–4') and δ_C 77.2 (C–2''), δ_H 5.66 (H–3'')/δ_C 77.2 (C–2''), and from δ_H 1.45 (H–5'' and H–6'')/δ_C 131.5 (C–3'') completed the binding of 1,3,4−trisubstituted aromatic ring with 2,2−dimethylpyran ring. Additional HMBC correlation from δ_H 7.17 (H–6') to δ_C 79.13 (C–2) was identified to confirm the binding of rings B and C.

From CD spectra, negative and positive Cotton effects were observed at 286 nm and 332 nm respectively, indicating that configuration at C–2 is (*S*) (Slade et al., 2005). Along with ^1H and ^{13}C NMR data from another resource, finalized the structure of compound **7** as abbyssinoflavanone V (Cui et al., 2007).

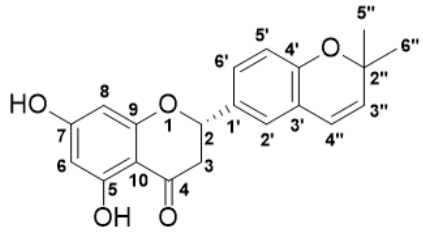

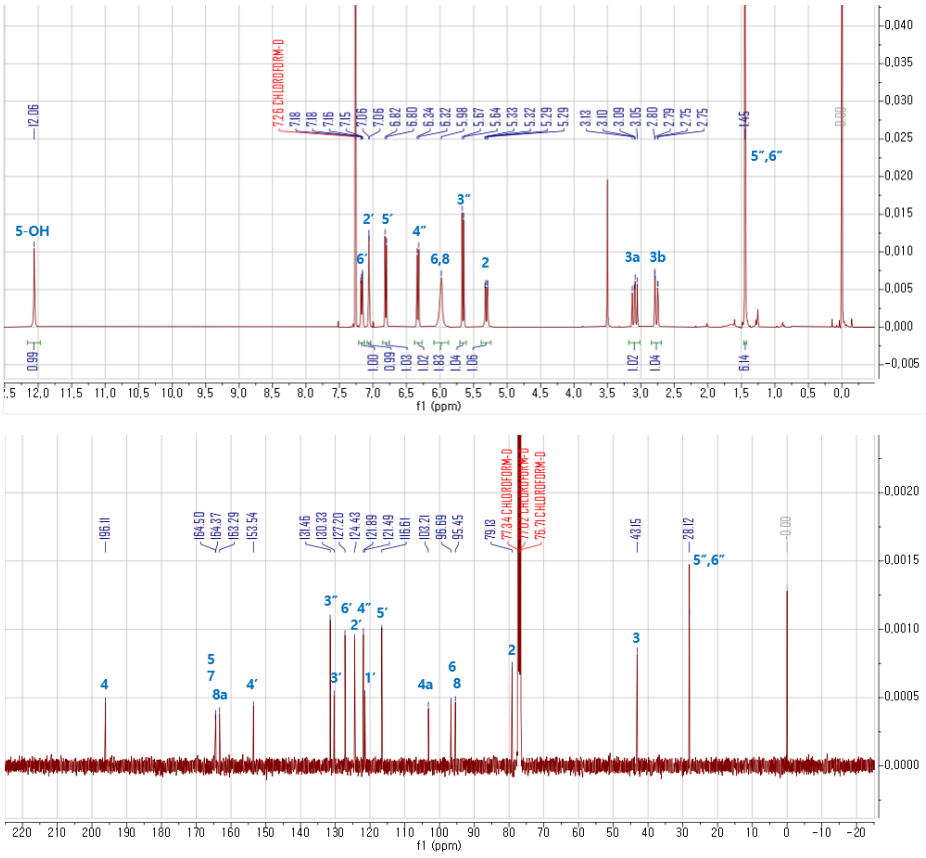

Figure 39. ^{1}H and ^{13}C NMR spectra of compound **7** (recorded at 400/100 MHz, $CDCl_3$)

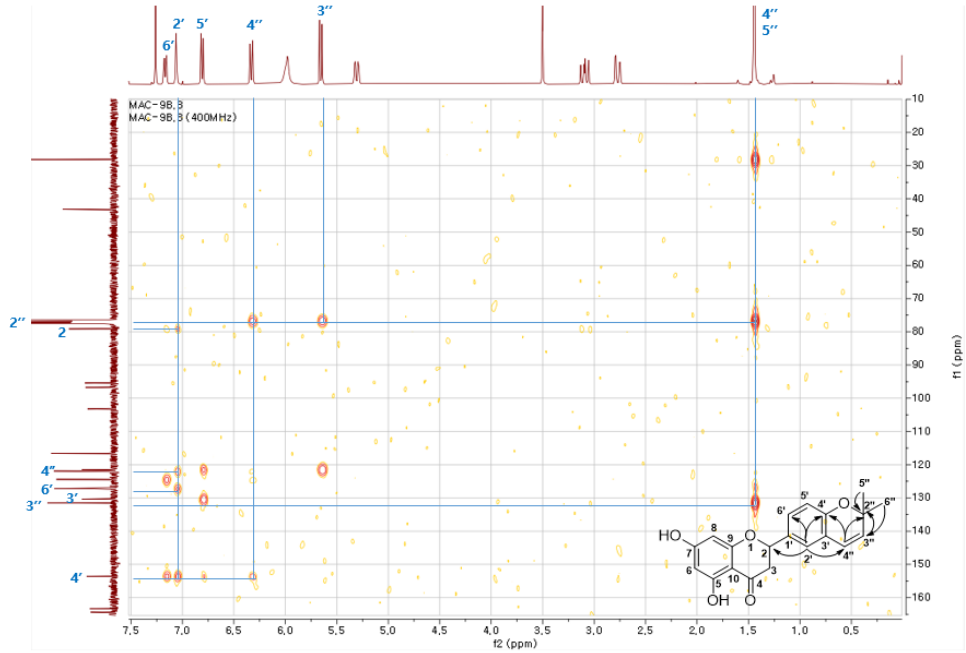

Figure 40. Key HMBC correlation of compound **7** in $CDCl_3$

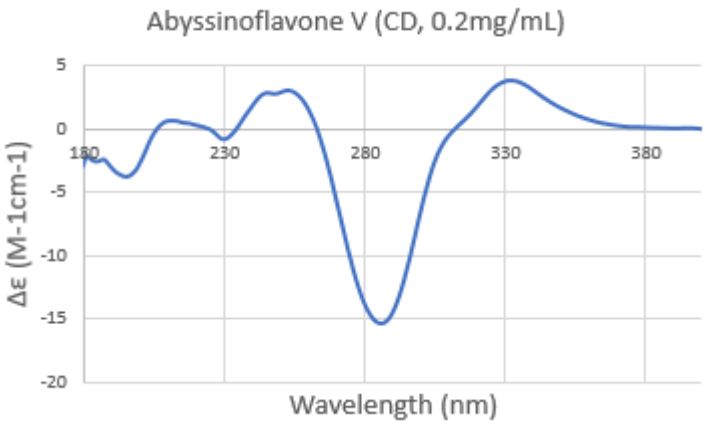

Figure 41. Experimental ECD spectra of compound **7**

3.3.8. Compound **8**

Compound **8** was isolated as yellow oil, and HRESIMS demonstrated deprotonated ion at *m/z* 419.1498 $[M - H]^-$ (calcd for $C_{25}H_{23}O_6$, 419.1495), indicating molecular formula of $C_{25}H_{24}O_6$. In ^1H NMR spectrum, presence of the flavanone [δ_H 5.66 (1H, dd, J = 3.0, 13.3 Hz, H–2), 2.99 (1H, dd, J = 13.3, 17.3 Hz, H–3_{ax}), and 2.79 (1H, dd, J = 3.0, 17.3 Hz, H–3_{eq})], and two dihydropyran rings [δ_H 6.67 (1H, d, J = 10.0 Hz, H–1''), 5.59 (1H, d, J = 10.0 Hz, H–2''), 6.28 (1H, d, J = 9.8 Hz, H–1'''), and 5.51 (1H, d, J = 9.8 Hz, H–2''')] as with **1**.

The HMBC correlations from δ_H 5.99 (H–6, H−8) to δ_C 163.9 (C–5), and from δ_H 6.99 (H–6') to δ_C 74.1 (C–2), δ_C 122.1 (C–1'''), δ_C 148.9 (C–4') and δ_C 150.2 (C–2') completed rings A and B of main flavanone respectively. The HMBC correlations δ_H 5.59 (H–2'')/δ_C 110.0 (C–3'), δ_H 6.67 (H–1'')/δ_C 150.2 (C–2'), δ_H 6.28 (H–1''')/δ_C 148.9 (C–4') and δ_H 5.51 (H–2''')/δ_C 114.6 (C–5') successively connected two dihydropyran groups to ring B.

The CD spectrum showed negative Cotton effect near 285 nm and positive Cotton effect, although at minimum, at 325 nm, indicating that configuration at C–2 is (*S*) (Slade et al., 2005). Overall, compared with ^1H and ^{13}C NMR data from another resource, compound **8** was identified as (2*S*)−5,7−dihydroxyl−2',3'−(3'',3''−dimethylpyrane)−4',5'−(3''',3'''−dimethylpyrane)−flavanone, which is also well known as sanggenol O (Jung et al., 2015).

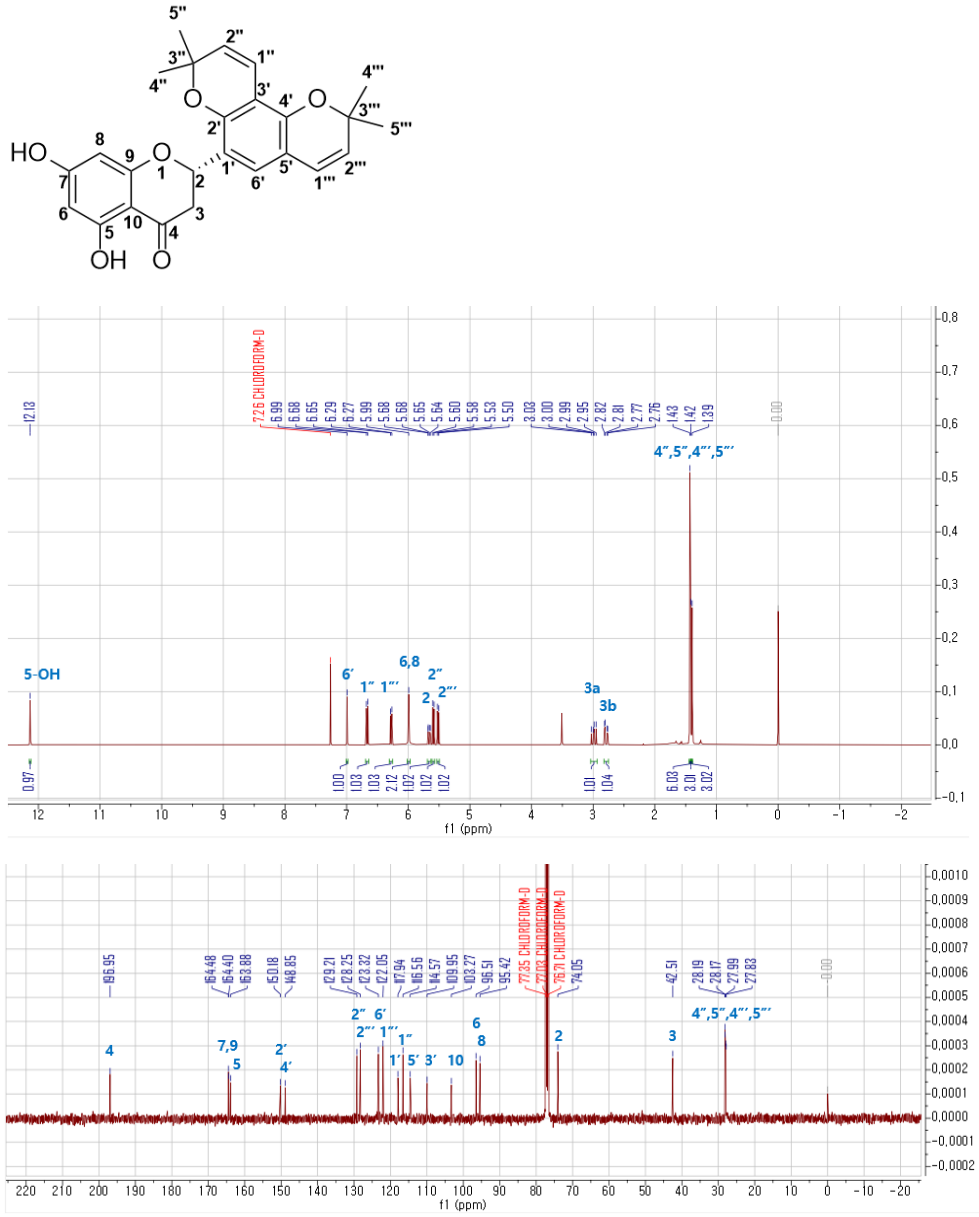

Figure 42. ^{1}H and ^{13}C NMR spectra of compound **8** (recorded at 400/100 MHz, $CDCl_3$)

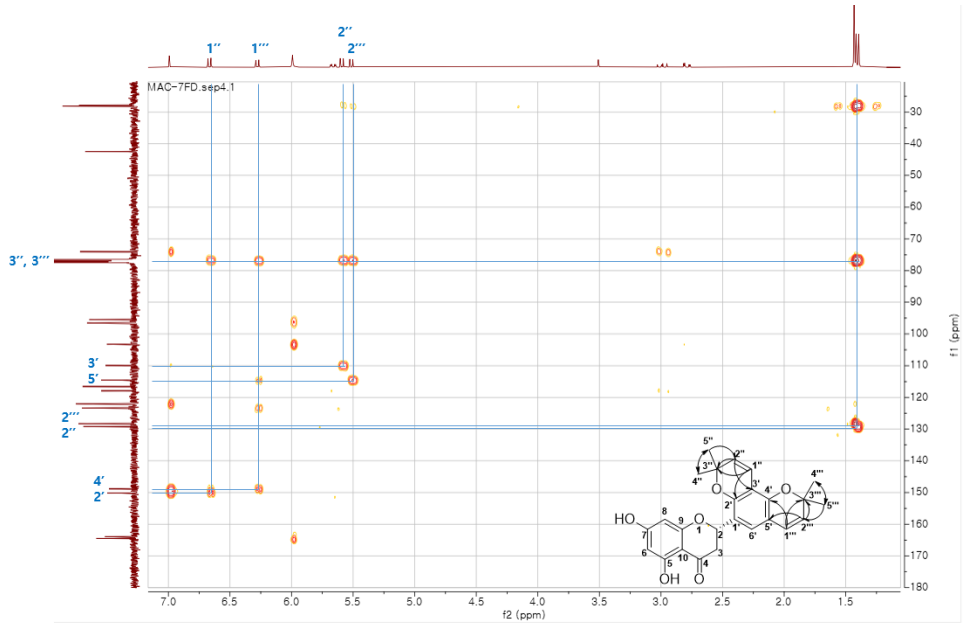

Figure 43. Key HMBC correlations of compound **8** in $CDCl_3$

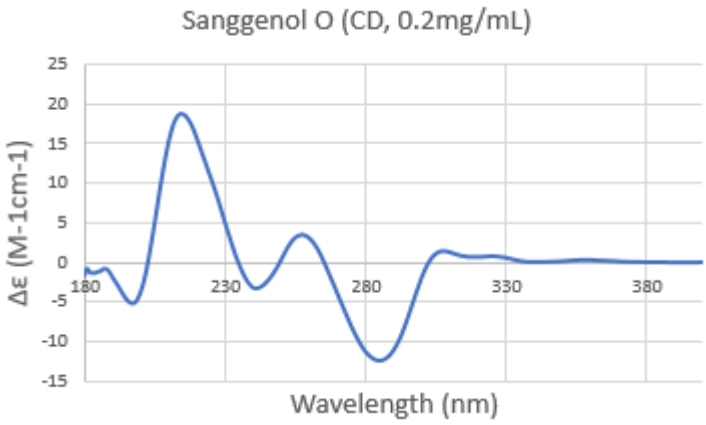

Figure 44. Experimental ECD spectra of compound **8**

3.3.9. Compound **9**

Compound **9** was isolated as yellow amorphous powder. Based on the HRESIMS results, the molecular formula was determined as $C_{25}H_{22}O_6$ from its deprotonated molecular ion at *m/z* 417.1328 [M – H]$^-$ (calcd for $C_{25}H_{21}O_6$, 417.1338). In ^{1}H NMR spectrum, 1,2,4–trisubstituted aromatic ring [δ_H 6.31 (1H, br d, *J* = 2.4 Hz, H–5'), 6.54 (1H, br d, *J* = 2.4, 8.4 Hz, H–3'), and 7.65 (1H, d, *J* = 8.4 Hz, H–2')] and dimethylpyran ring [δ_H 1.46 (6H, s, H–17, H–18, overlapped), 6.82 (1H, d, *J* = 9.9 Hz, H–14), and 5.72 (1H, d, *J* = 9.9 Hz, H–15)] as **1**. Compared with ^{1}H NMR data from another literature, compound **9** was identified as cyclomorusin (Wei et al., 2005). This was also supported by 25 peaks from the ^{13}C NMR which matched with the reference except C–2'. The difference was confirmed with a HSQC correlation δ_H 7.65 (H–2')/δ_C 126.4 (C–2').

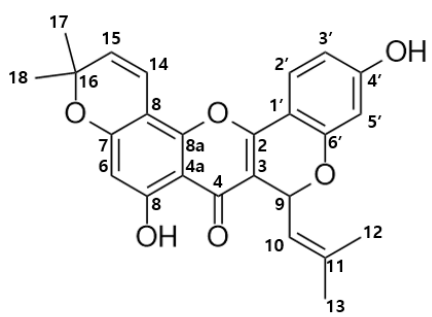

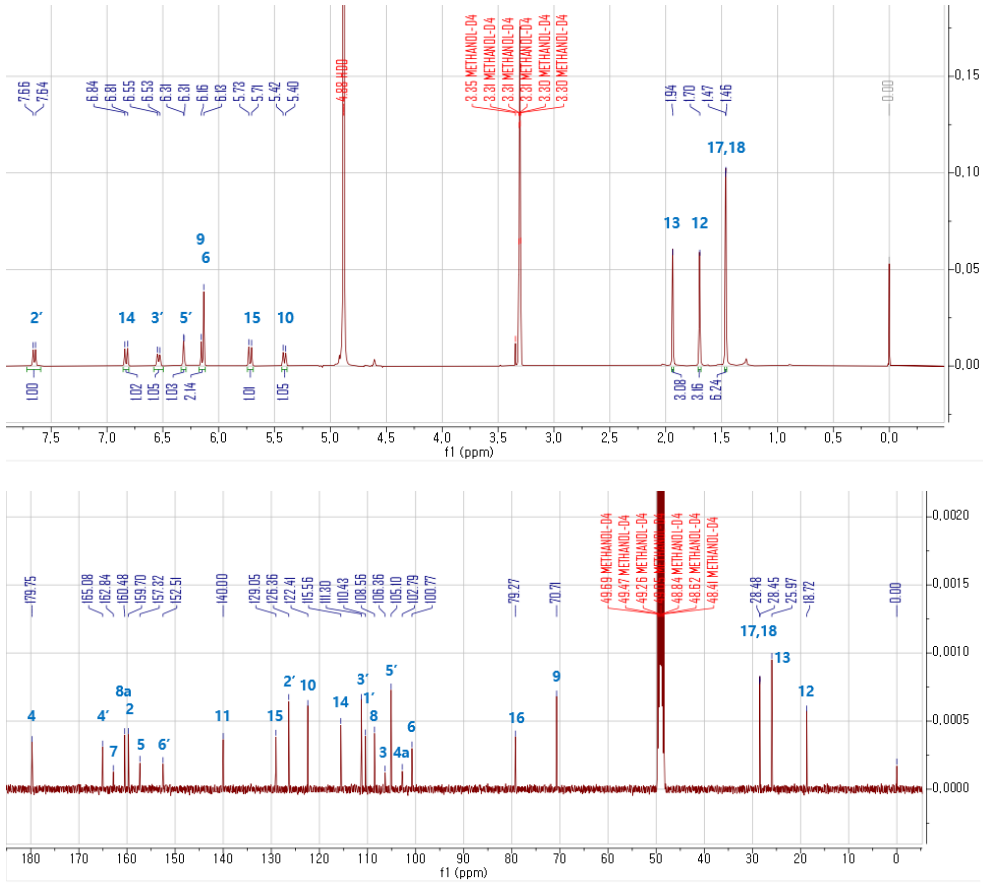

Figure 45. ^{1}H and ^{13}C NMR spectra of compound **9** (recorded at 400/100 MHz, $CDCl_3$)

3.3.10. Compound **10**

Compound **10** was isolated as yellow amorphous solid. Its molecular formula was decided to be $C_{25}H_{26}O_5$ based on HRESIMS results showing deprotonated ion at *m/z* 405.1708 $[M - H]^-$ (calcd for $C_{25}H_{25}O_5$, 405.1702). From the ^1H NMR spectrum not only the ABX-type spin system [δ_H 5.33 (1H, dd, J = 2.9, 13.0 Hz, H-2), 3.07 (1H, dd, J = 13.0, 17.1 Hz, H-3_{ax}) and 2.77 (1H, dd, J = 2.9, 17.1 Hz, H-3_{eq})] was detected for flavanone skeleton but also A_2B_2 spin system which represented 1,4-disubstituted ring [δ_H 7.32 (2H, d, J = 7.4 Hz, H-2', H-6') and 6.88 (2H, d, J = 7.4 Hz, H-3', H-5')] (Patil et al., 2002).

From ECD spectrum, negative Cotton effect was observed at 293 nm while positive Cotton effect was present at 353 nm, indicating that main structure of Compound **10** is (2*S*)-flavanone (Slade et al., 2005).

Overall, the absolute chemical structure was decided as cycloaltilisin 7 after comparison with ^1H and ^{13}C NMR data of another literature (Patil et al., 2002). It is first time that cycloaltilisin 7 was isolated from *Morus alba*.

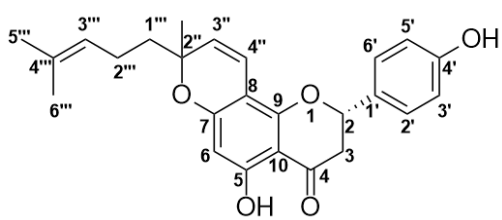

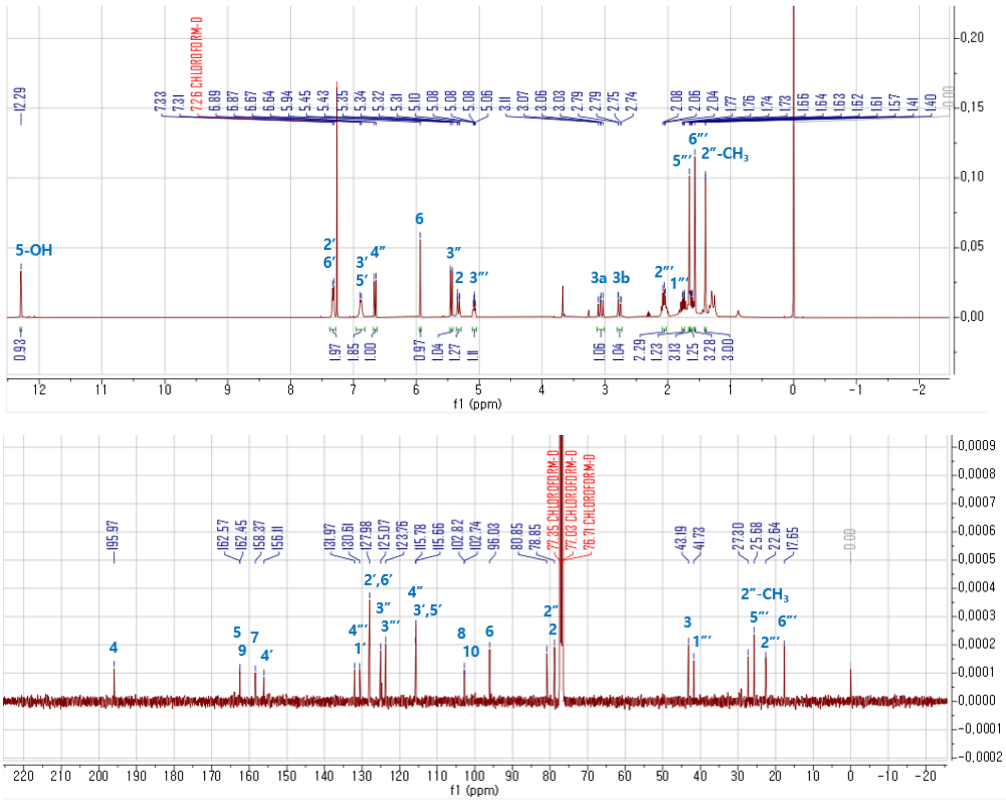

Figure 46. ^{1}H and ^{13}C NMR spectra of compound **10** (recorded at 400/100 MHz, $CDCl_3$)

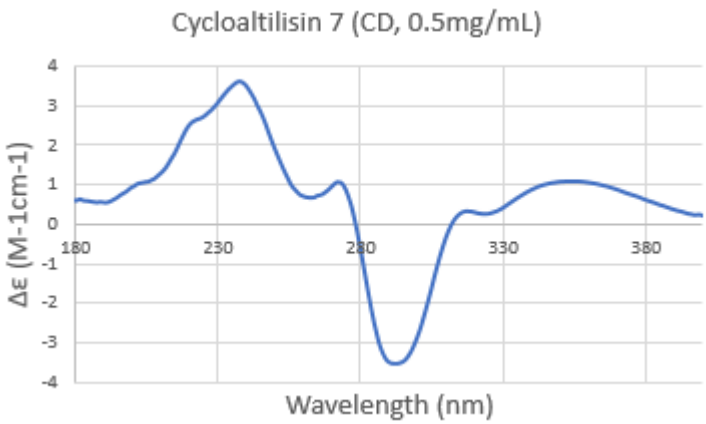

Figure 47. Experimental ECD spectra of compound **10**

3.3.11. Compound **11**

Compound **11** was isolated as colorless amorphous solid with molecular formula of $C_{30}H_{36}O_6$ based on HRESIMS spectra showing deprotonated ion at *m/z* 491.2441 $[M - H]^-$ (calcd for $C_{30}H_{35}O_6$, 491.2439). The ABX-type spin system [δ_H 5.67 (1H, dd, *J* = 3.0, 12.4 Hz, H–2), 3.06 (1H, dd, *J* = 12.4, 17.2 Hz, H–3_{ax}), and 2.73 (1H, dd, *J* = 3.0, 17.2 Hz, H–3_{eq})], *meta*-oriented aromatic protons [δ_H 5.87 (1H, d, *J* = 2.1 Hz, H–6) and 5.91 (1H, d, *J* = 2.1 Hz, H–8)], and presence of both prenyl and geranyl group, conjectured by five methyl groups and three alkene protons [δ_H 5.28 (1H, t, *J* = 7.1, 7.1 Hz, H–8'''), 5.19 (1H, t, *J* = 6.9, 6.9 Hz, H–2''), and 5.06 (1H, t, *J* =7.1, 7.1 Hz, H–7'')], were viewed from ^{1}H NMR spectrum. Thirty peaks identified from ^{13}C NMR spectrum confirmed that compound **11** contains thirty carbons.

Configured from negative Cotton effect observed at 289 nm, the absolute configuration of compound **11** was decided as (2*S*)-5,7,2',4'-tetrahydroxyl-3'-geranyl-5'-prenylflavanone, also known as sanggenol P from another literature (Guo et al., 2018).

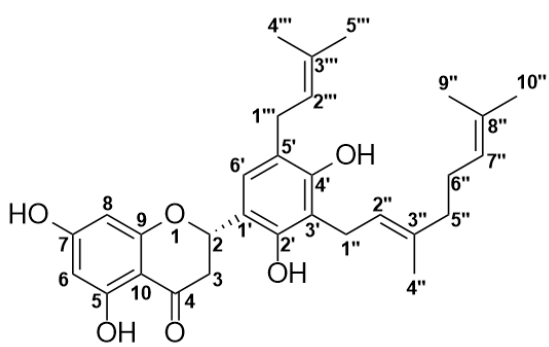

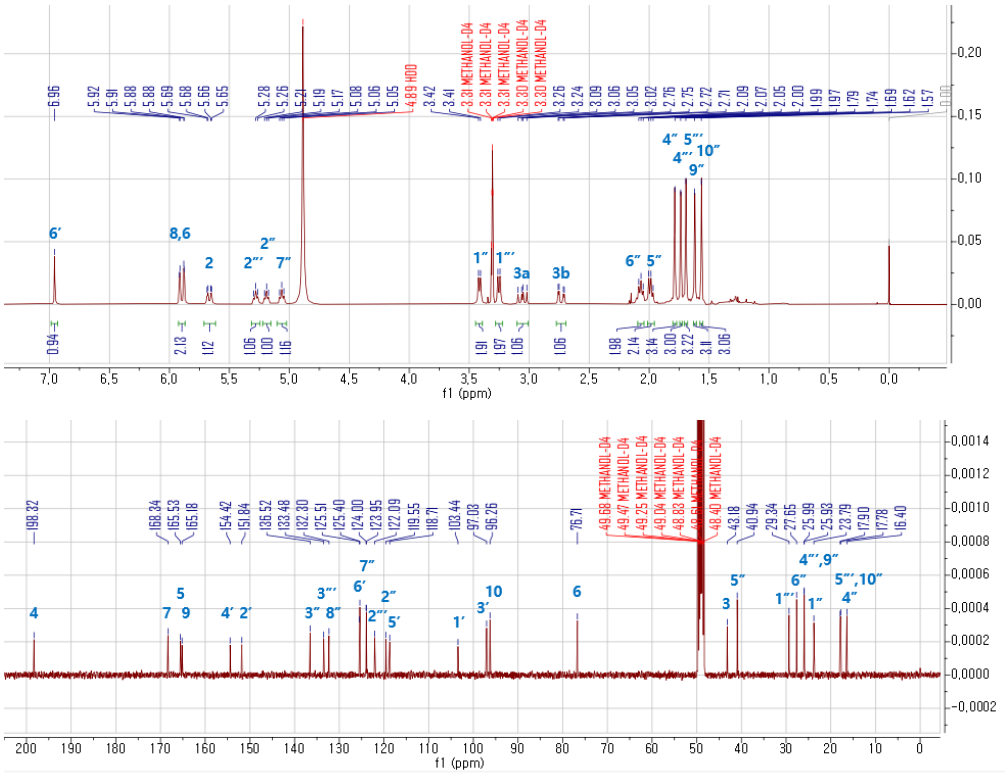

Figure 48. ^{1}H and ^{13}C NMR spectra of compound **11** (recorded at 400/100 MHz, MeOD−d_4)

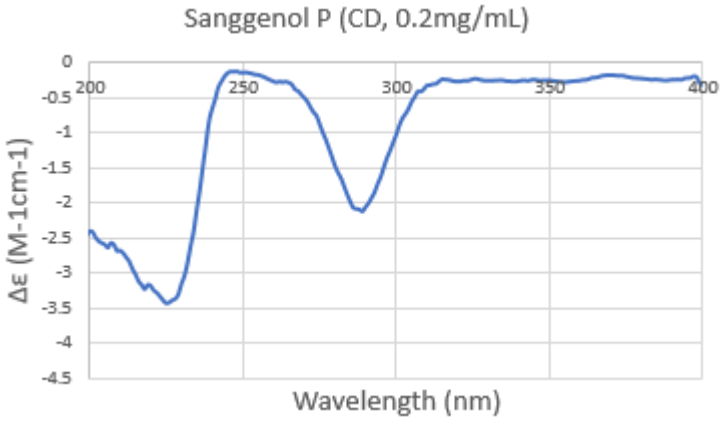

Figure 49. Experimental ECD spectra of compound **11**

3.3.12. Compound **12**

Compound **12** was isolated as golden powder. Based on the HRESIMS interpretation, $C_{20}H_{20}O_5$ was chosen as molecular formula (*m/z* 339.1237 $[M - H]^-$ (calcd for $C_{20}H_{19}O_5$, 339.1232)). The ^1H NMR spectrum showed various proton signals such as 1,2,4−trisubstituted aromatic ring [δ_H 6.34 (1H, d, *J* = 2.4 Hz, H–3), 6.35 (1H, dd, *J* = 2.4, 8.3 Hz, H–5), and 7.51 (1H, d, *J* = 8.3 Hz, H–6)], a pair of *ortho* aromatic protons [δ_H 6.40 (1H, d, *J* = 8.8 Hz, H–5') and 7.75 (1H, d, *J* = 8.8 Hz, H–6')], and characteristic of prenyl moiety [δ_H 1.78 (3H, s, H–4''), 1.66 (3H, s, H–5''), and 5.22 (1H, t, *J* = 7.3, 7.3 Hz, H–2'')]. Furthermore, proton signals at δ_H 8.08 (1H, d, *J* = 15.5 Hz, H–α) and δ_H 7.71 (1H, d, *J* = 15.5 Hz, H–β) coupled with a carbon peak at δ_C 194.4 (C=O) specified that the structure is chalcone−based. Compared with ^1H and ^{13}C NMR spectra provided by other resources, compound **12** was confirmed to be (*2E*)−1−[2,4−Dihydroxy−3−(3−methylbut−2−en−1−yl)phenyl]−3−(2,4−dihydroxyphenyl)prop−2−en−1−one, also known as morachalcone A (Romano, 2005; Sichaem, et al., 2022). Overlapped proton signal at H–1'' hidden behind methanol peak was confirmed with its HSQC correlation to δ_C 22.6 (C–1'') (Figure 51).

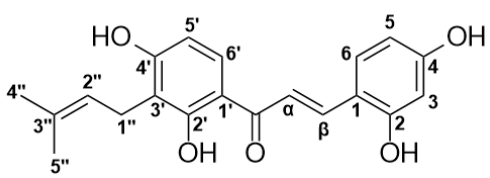

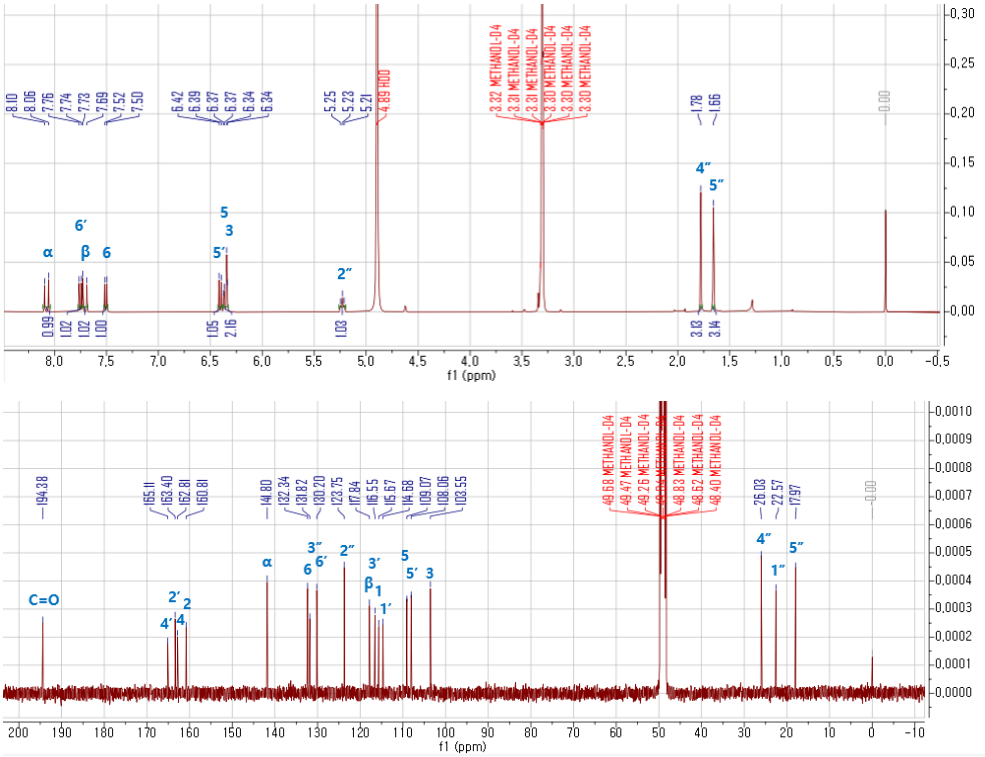

Figure 50. ^{1}H and ^{13}C NMR spectra of compound **12** (recorded at 400/100 MHz, MeOD−d_4)

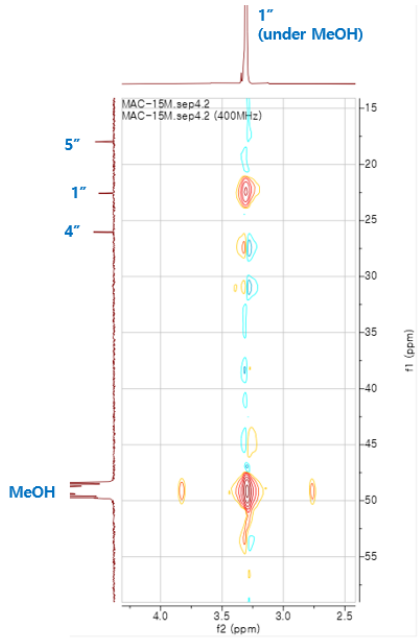

Figure 51. Key HSQC spectrum of compound **12** in MeOD−d_4

3.3.13. Compound **13**

Compound **13** was isolated as white amorphous powder with molecular formula of $C_{30}H_{48}O_3$ identified based on HRESIMS spectra (*m/z* 455.3542 $[M - H]^-$ (calcd for $C_{30}H_{47}O_3$, 455.3531)). In the ^1H NMR spectrum, five tertiary methyl groups [δ_H [0.99 (3H, s, H–27), 0.98 (3H, s, H–26), 0.95 (3H, s, H–23), 0.84 (3H, s, H–25) and 0.77 (3H, s, H–24)] and vinyl methyl [δ_H 1.70 (3H, s, H–30)] were identified. In addition, other proton NMR characteristics including secondary carbinol at δ_H 3.19 (1H, dd, J = 5.0, 11.2 Hz, H–3), methane at δ_H 3.01 (3H, m, H–19), and exomethylene group at δ_H 4.76 (1H, *br* s, H–29a) and δ_H 4.63 (1H, *br* s, H–29b) were also spotted. The ^{13}C NMR spectrum appealed presence of thirty carbon resonances. The NMR findings were compared with other literatures (Lin et al., 2015; Wu et al., 2018) that were in agreement with the obtained spectral data, indicating that compound **13** is betulinic acid.

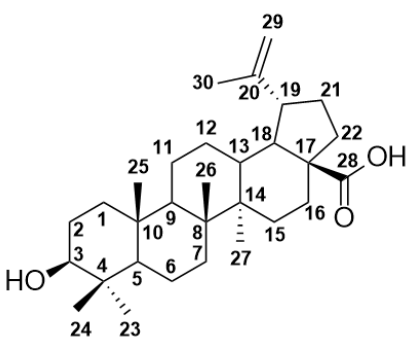

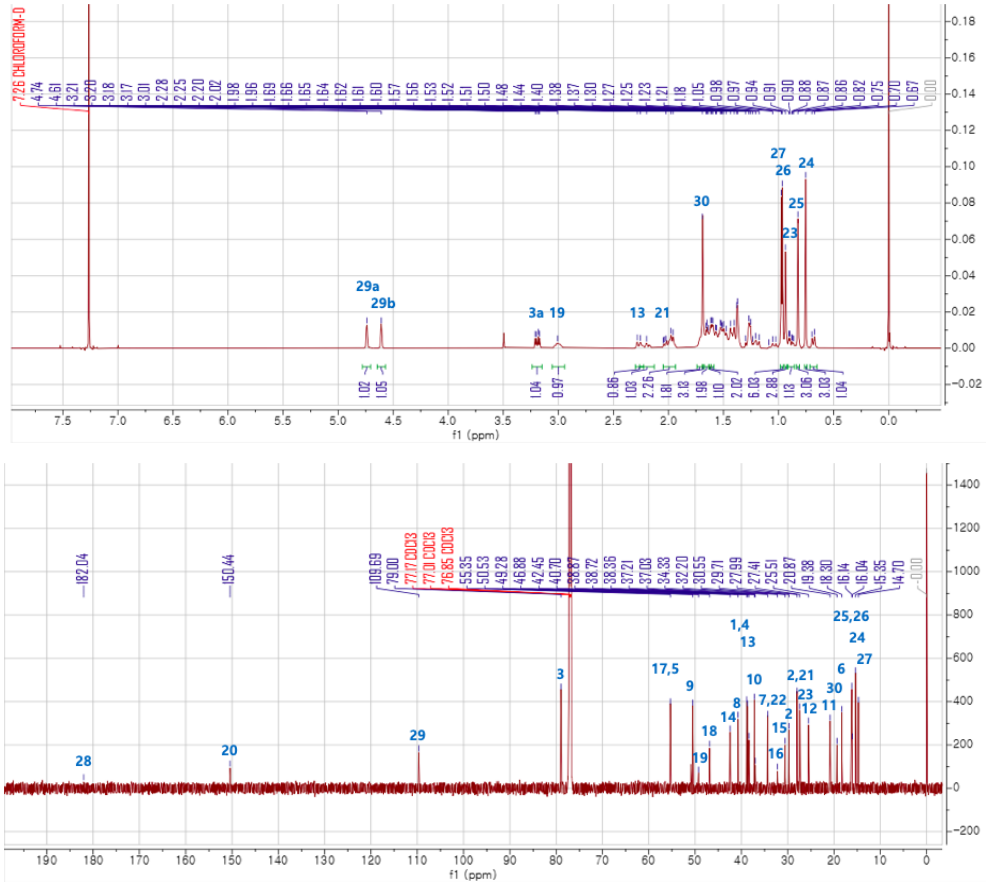

Figure 52. ^{1}H and ^{13}C NMR spectra of compound **13** (recorded at 400/100 MHz, $CDCl_3$)

3.3.14. Compound **14**

Compound **14** was isolated as yellow powder with its molecular formula approved as $C_{10}H_8O_4$ based on HRESIMS analysis (*m/z* 191.0344 $[M - H]^-$ (calcd for $C_{10}H_7O_4$, 191.0344)). In ^1H NMR spectrum, four protons [δ_H 7.86 (1H, d, J = 9.4 Hz, H–4), 7.10 (1H, s, H–5), 6.76 (1H, s, H–8), and 6.20 (1H, d, J = 9.4 Hz, H–3)] represented characteristic of aromatic protons of benzofuran–derivatives. Ten carbons were identified from ^{13}C NMR spectrum. Compared with 1D NMR spectra of other sources, compound **14** was confirmed to be 7–hydroxy–6–methoxy–2H–chromen–2–one, also known scopoletin (Barberá et al., 1986). The HMBC correlation from δ_H 3.90 (3H, s, 6–OCH_3) to δ_C 146.21 (C–6) confirmed the overall structure (Figure 54).

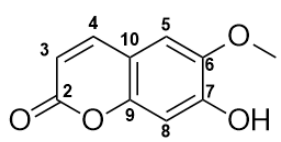

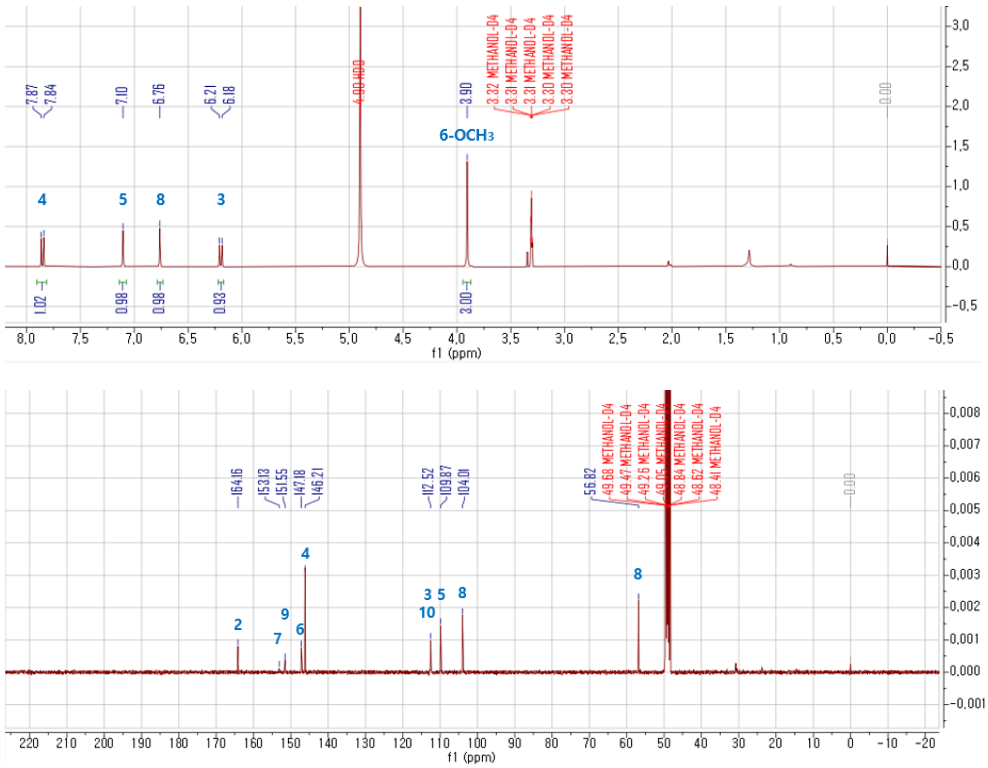

Figure 53. ^{1}H and ^{13}C NMR spectra of compound **14** (recorded at 400/100 MHz, MeOD−d_4)

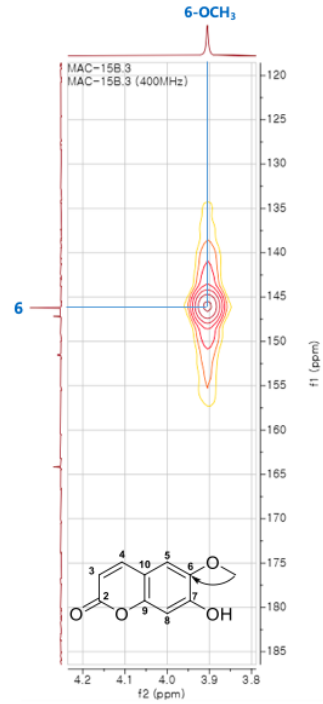

Figure 54. Key HMBC correlations of compound **14** in MeOD−d_4

3.3.15. Compound **15**

Compound **15** was obtained as white amorphous solid with its molecular formula $C_9H_6O_3$ proven based on HRESIMS deprotonated ion peak at *m/z* 161.0239 $[M - H]^-$ (calcd for $C_9H_5O_3$, 161.0244). In ^1H NMR spectrum, three proton signals at δ_H 6.79 (1H, dd, *J* = 2.3, 8.5 Hz, H–6), δ_H 7.45 (1H, d, *J* = 8.5 Hz, H–5) and δ_H 6.70 (1H, d, *J* = 2.3 Hz, H–8) directed to presence of 1,3,4–trisubstituted aromatic ring, while two proton signals at δ_H 7.85 (1H, d, *J* = 9.5 Hz, H–4) and δ_H 6.18 (1H, d, *J* = 9.5 Hz, H–3) approached to attendance by *ortho*–positioned aromatic ring. High coupling constant values indicated increased electronegativity of the nearby substituent, and hence it was predicted that C–2 is near electronegative atom. The ^{13}C NMR spectrum exposed that there are 9 carbons. Compared with 1D NMR data from another resource, compound **15** was identified as 7–hydroxy–2H–chromen–2–one, also known as umbelliferone (Seong et al., 2009).

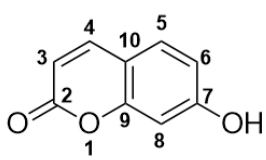

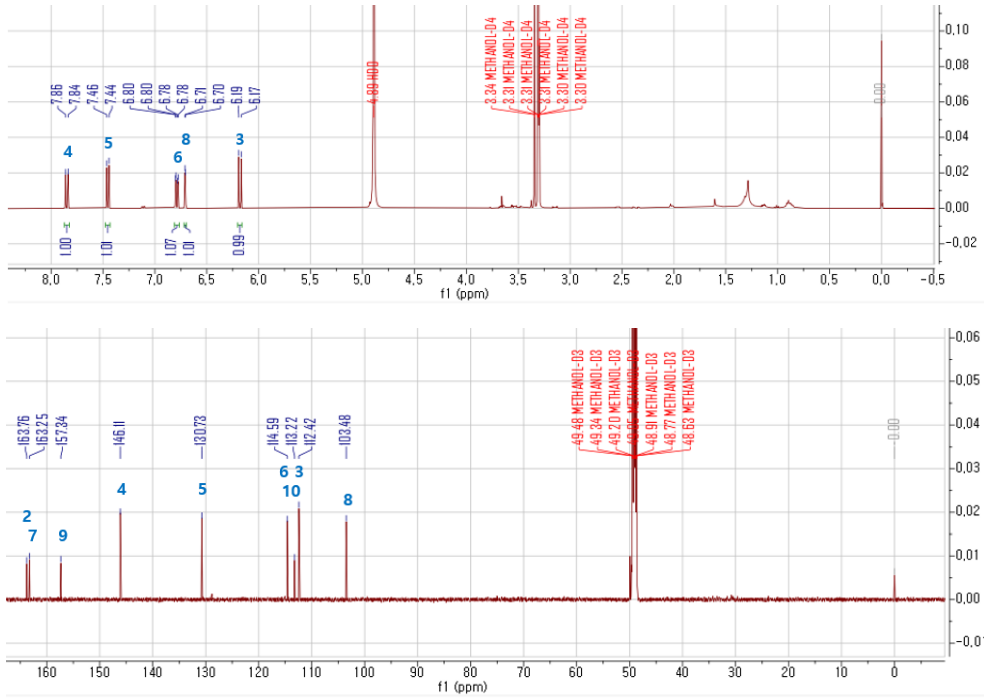

Figure 55. ^{1}H and ^{13}C NMR spectra of compound **15** (recorded at 400/150 MHz, MeOD−d_4)

3.3.16. Compound **16**

Molecular formula of compound **16**, white amorphous solid, was decided as $C_{16}H_{14}O_4$ based on HRESIMS results (*m/z* 269.0808 [M – H]$^-$ (calcd for $C_{16}H_{13}O_4$, 269.0814)). 1,2,4−trisubstituted aromatic ring [δ_H 7.44 (1H, d, *J* = 8.6 Hz, H–4), 7.06 (1H, d, *J* = 2.2 Hz, H–7), and 6.87 (1H, dd, *J* = 2.2, 8.6 Hz, H–5)], 1,3,5−trisubstituted aromatic ring [δ_H 6.96 (1H, t, *J* = 2.0 Hz, H–4'), 6.90 (1H, t, *J* = 2.0 Hz, H–6'), and 6.39 (1H, t, *J* = 2.0 Hz, H–2')], an aromatic proton [δ_H 6.93 (1H, s, H−3)] and two ether groups [δ_H 3.88 (3H, s, 6–OCH_3) and 3.86 (3H, s, 3'–OCH_3)] conjugated with 7 additional quaternary carbons from 1D NMR spectra suggested that compound **16** was morusalfuran E (Ha et al., 2016). The HMBC correlations δ_H 3.88 (6–OCH_3)/δ_C 158.23 (C–6) and δ_H 3.86 (3'–OCH_3)/δ_C 161.28 (C–3') confirm position of the ether groups.

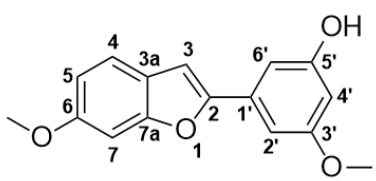

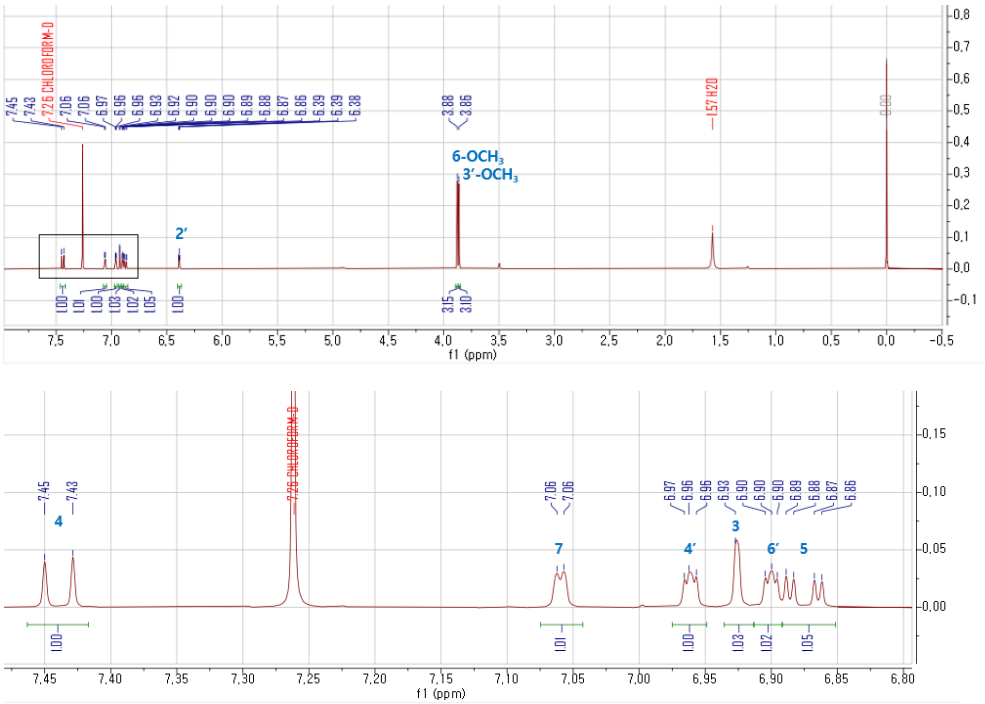

Figure 56. ^{1}H NMR spectrum of compound **16** (recorded at 400 MHz, $CDCl_3$) and its zoomed spectrum between 6.80 – 7.50 ppm

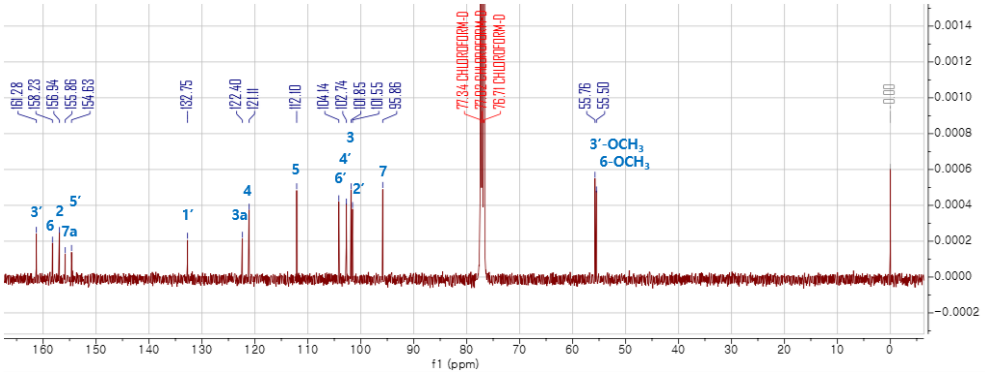

Figure 57. ^{13}C NMR spectrum of compound **16** (recorded at 100 MHz, $CDCl_3$)

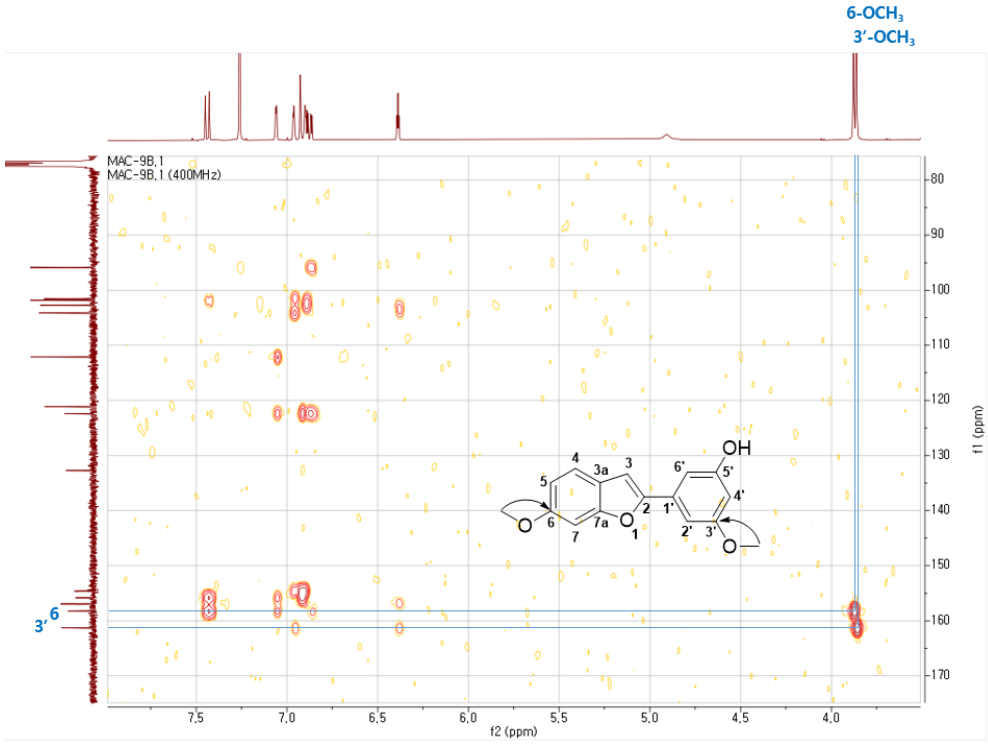

Figure 58. Key HMBC correlations of compound **16** in $CDCl_3$

3.3.17. Compound **17**

Compound **17** was isolated as light brown amorphous solid. The HRESIMS spectra presented deprotonated ion at *m/z* 323.1280 $[M-H]^-$ (calcd for $C_{20}H_{19}O_4$, 323.1283), indicating molecular formula $C_{20}H_{20}O_4$ with degree of unsaturation of 11. Four proton signals from ^1H NMR spectrum [δ_H 6.86 (1H, s, H–3), 7.42 (1H, d, J = 8.5 Hz, H–4), 6.87 (1H, d, J = 8.5 Hz, H–5), and 7.04 (1H, d, J = 2.5 Hz, H–7)] was comparably similar to **16**, indicating that the key skeleton of **17** is benzofuran. Other proton signals including *meta*–positioned aromatic protons [δ_H 6.88 (1H, s, H–2') and 6.88 (1H, s, H–6')], one ether group [δ_H 3.87 (3H, s, 6–OCH_3)], and a prenyl moiety [δ_H 3.45 (2H, d, J = 7.1 Hz, H–1''), 5.29 (1H, t, J = 7.1, 7.1 Hz, H–2''), 1.85 (3H, s, H–4''), and 1.78 (3H, s, H–5'')] coupled with 20 carbons from ^{13}C NMR spectrum led to finding that compound **17** is 3',5'–dihydroxy–6–methoxy–4'–prenyl–2–arylbenzofuran, also known as sanggenofuran B from another literature (Shi et al., 2007). This hypothesis was confirmed by HMBC correlations from δ_H 3.87 (6–OCH_3) to δ_C 158.1 (C–6) for the ether group, and from δ_H 3.45 (H–1'') to δ_C 113.7 (C–4'), δ_C 155.3 (C–3') and δ_C 158.3 (C–5') for prenyl group.

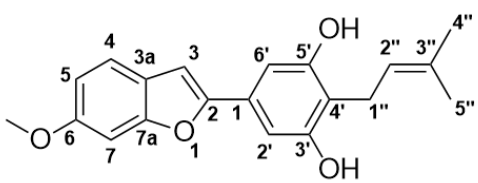

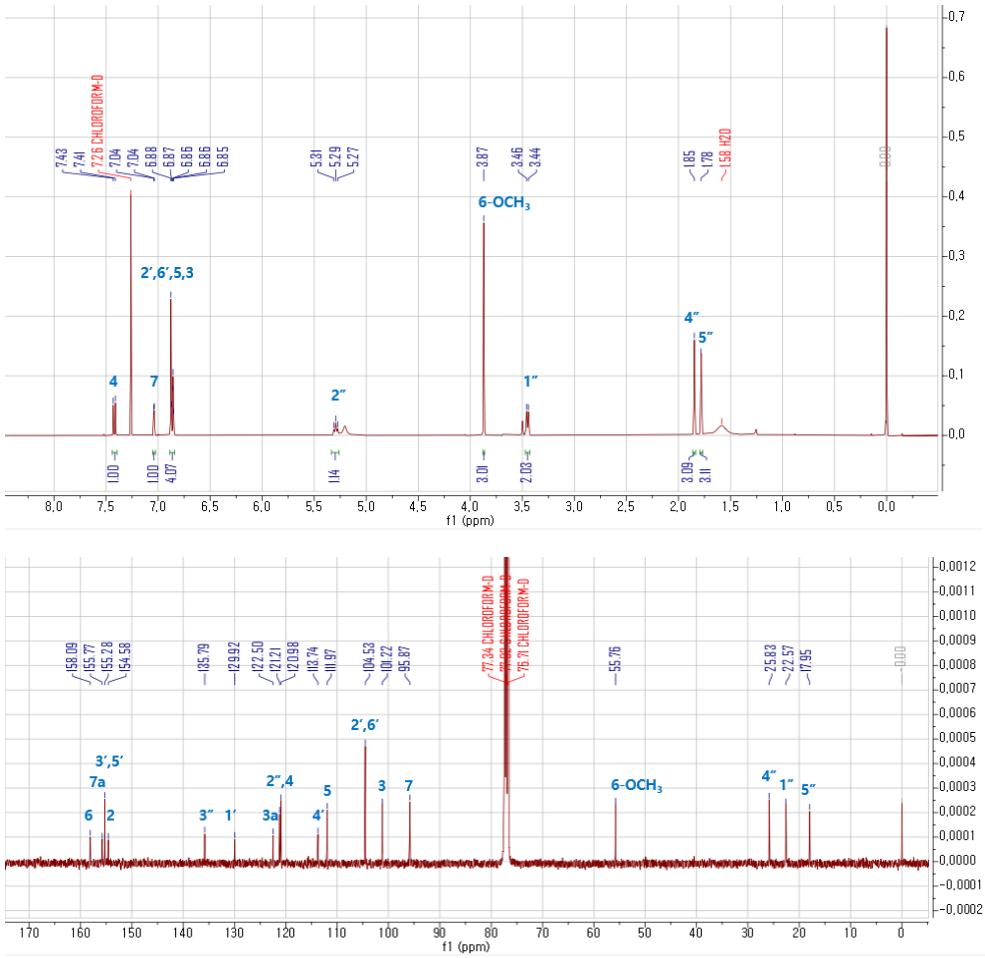

Figure 59. ^{1}H and ^{13}C NMR spectra of compound **17** (recorded at 400/100 MHz, $CDCl_3$)

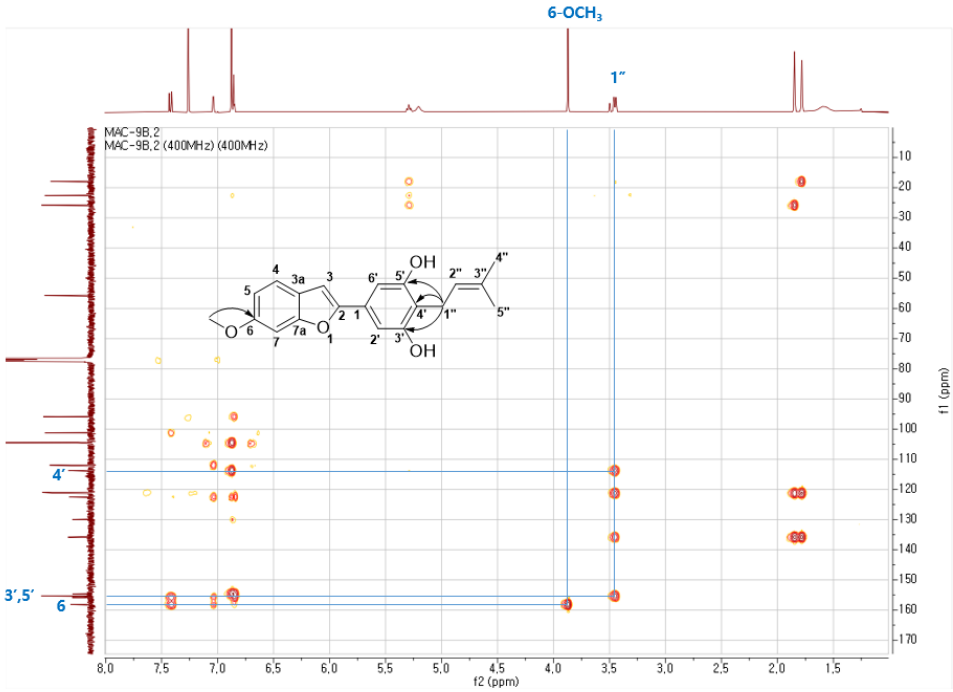

Figure 60. Key HMBC correlations of compound **17** in $CDCl_3$

3.3.18. Compound **18**

Compound **18** was obtained as white amorphous solid. Its molecular formula, $C_{14}H_{10}O_4$, was determined by HRESIMS, with results of *m/z* 241.0513 $[M - H]^-$ (calcd for $C_{14}H_9O_4$, 241.0506). In ^1H NMR spectrum, main structure of benzofuran [δ_H 6.91 (1H, *br* s, H–3), 7.35 (1H, d, *J* = 8.4 Hz, H–4), 6.73 (1H, dd, *J* = 2.1, 8.4 Hz, H–5), and 6.89 (1H, d, *J* = 2.1 Hz, H–7)] and 1,3,5−trisubstituted aromatic ring [δ_H 6.75 (2H, d, *J* = 2.2 Hz, H–2', H–6') and 6.24 (1H, t, *J* = 2.2, 2.2 Hz, H–4')] were revealed. The ^{13}C NMR confirms that the structure contains 14 carbons. Overall, the structure was decided as 5−(6−hydroxybenzofuran−2−yl)benzene−1,3−diol after comparing to other literature, which has common name moracin M (Basnet et al., 1993).

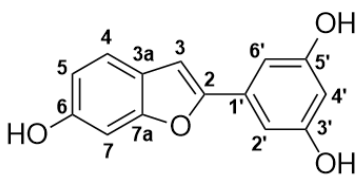

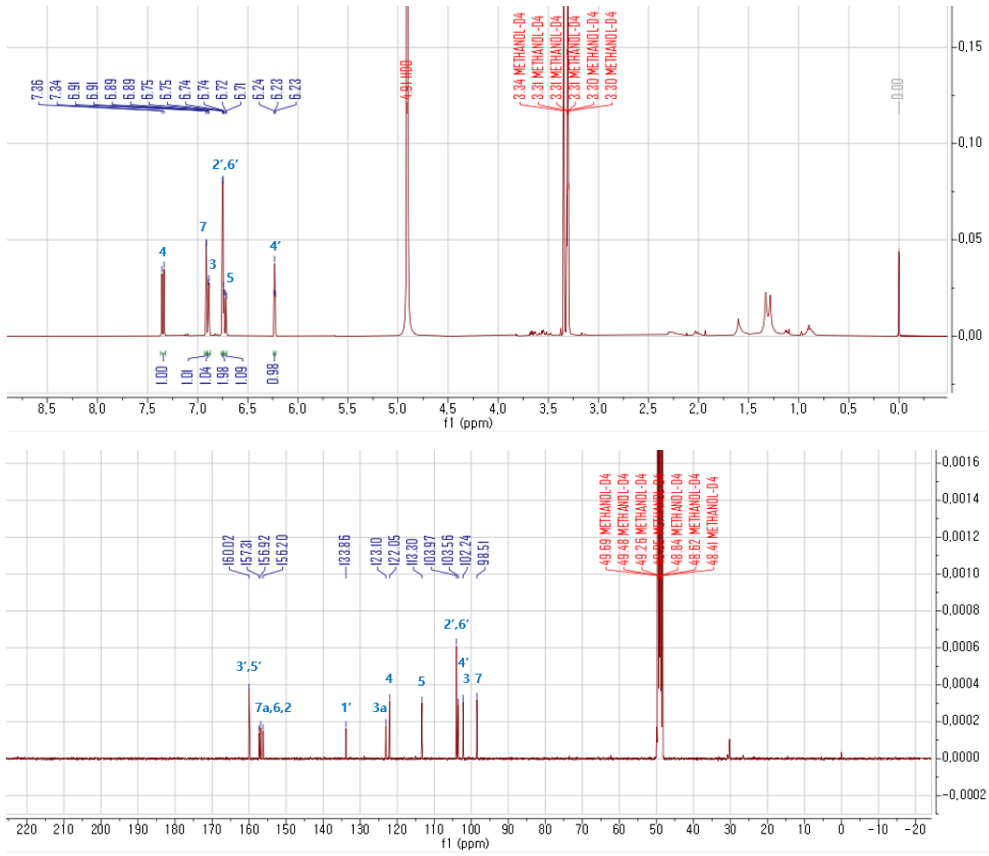

Figure 61. ^{1}H and ^{13}C NMR spectra of compound **18** (recorded at 400/100 MHz, MeOD−d_4)

3.3.19. Compound **19**

Compound **19** was obtained as light brown amorphous solid with its molecular formula determined as $C_{16}H_{14}O_5$ based on HRESIMS analysis (*m/z* 285.0758 $[M - H]^-$ (calcd for $C_{16}H_{13}O_4$, 285.0768)). In ^1H NMR spectrum, benzofuran skeleton [δ_H 6.95 (1H, s, H–3), 7.14 (1H, s, H–4), and 6.92 (1H, s, H–7)] and 1,3,5−trisubstituted aromatic ring [δ_H 6.85 (2H, d, overlaid, H–2', H–6') and 6.33 (1H, t, *J* = 2.2, 2.2 Hz, H–4')] were identified as **18**. The ^{13}C NMR confirmed presence of 16 carbons. Overall, the structure of compound **19** was decided as 2−(3−Hydroxy−5−methoxyphenyl)−6−methoxy−5−benzofuranol, also known as moracin B (Li HX, 2018; Zhang L et al., 2016).

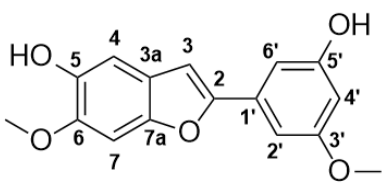

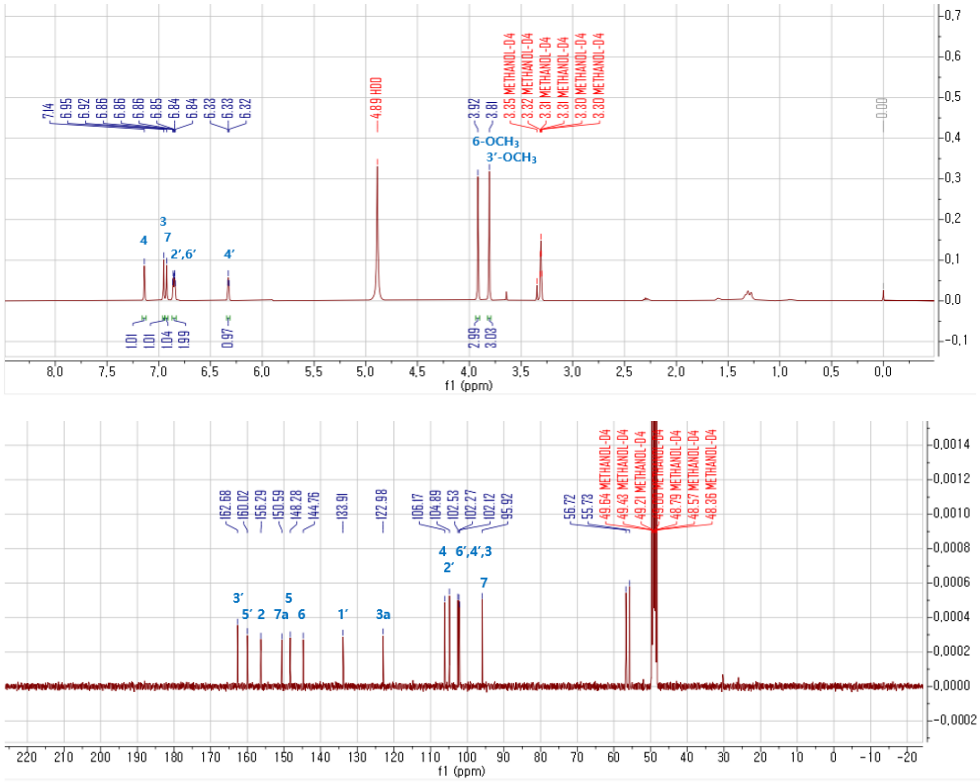

Figure 62. ^{1}H and ^{13}C NMR spectra of compound **19** (recorded at 400/100 MHz, MeOD−d_4)

3.3.20. Compound **20**

Compound **20** was isolated as colorless amorphous solid where molecular formula was determined as $C_{10}H_8O_4$ based on HRESIMS results (*m/z* 191.0344 $[M - H]^-$ (calcd for $C_{10}H_7O_4$, 191.0344)). Likewise with **18** and **19**, benzofuran skeleton [δ_H 7.16 (1H, d, *J* = 8.3 Hz, H-4), 6.72 (1H, d, *J* = 8.3 Hz, H-5), and 6.89 (1H, s, H-3)] and 1,3,5-trisubstituted aromatic ring [δ_H 6.78 (2H, d, *J* = 2.2 Hz, H-2', H-6') and 6.24 (1H, t, *J* = 2.2, 2.2 Hz, H-4')] were identified from ^{1}H NMR spectrum, as well as prenyl group [δ_H 3.59 (2H, d, *J* = 7.3 Hz, H-1''), 5.41 (1H, t, *J* = 7.3, 7.3 Hz, H-2''), 1.89 (3H, s, H-4''), and 1.69 (3H, s, H-5'')]. The ^{13}C NMR spectrum confirmed presence of 10 carbons. Compared with ^{1}H and ^{13}C NMR data from another resource, compound **20** was identified as 5-(6-Hyroxy-7-(3-methylbut-2-enyl)benzofuran-2-yl)benzene-1,3-diol, also known as moracin S (Kapche, et al., 2009; Masagalli et al., 2021).

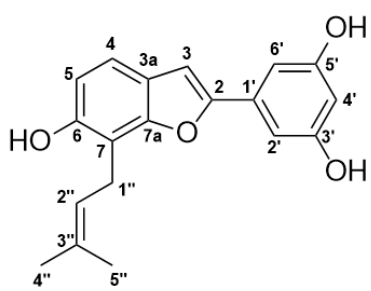

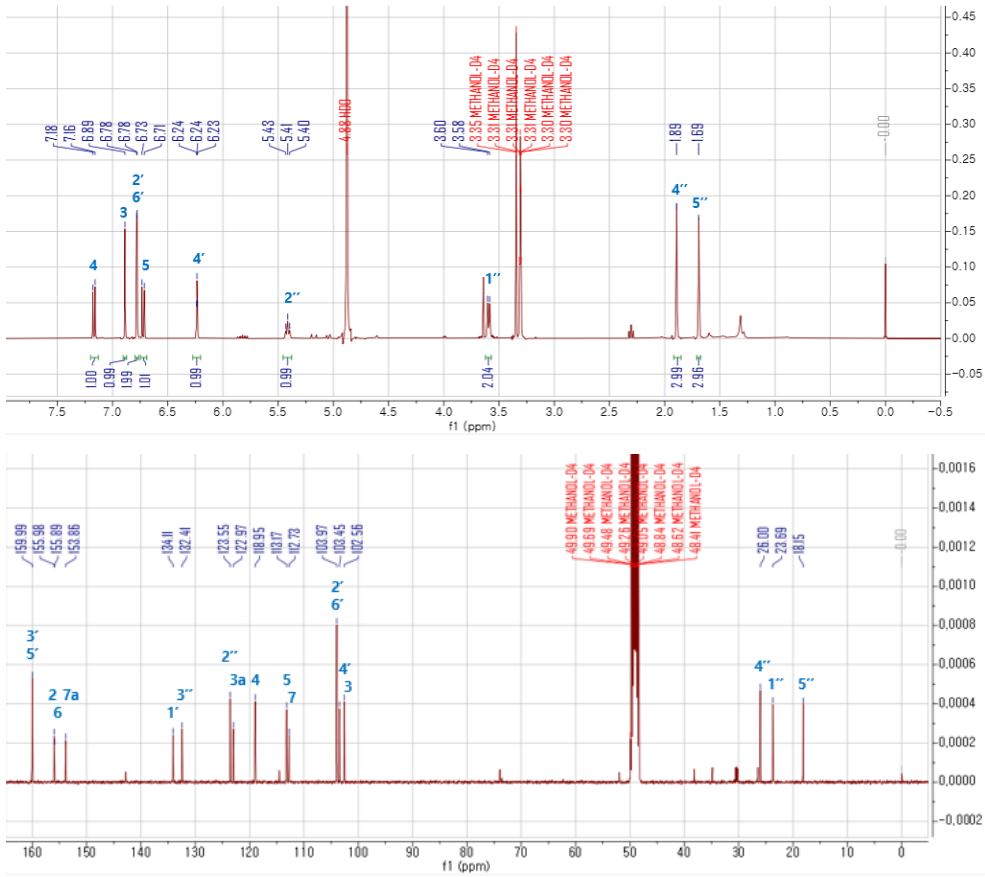

Figure 63. ^{1}H and ^{13}C NMR spectra of compound **20** (recorded at 400/100 MHz, MeOD−d_4)

Chapter 4. Conclusion

In conclusion, chloroform fraction of methanol extract of *Morus alba* showed highest PCSK9 inhibitory effect, leading to further isolation of 6 fractions MAC-6, MAC-7, MAC-8, MAC-9, MAC-14 and MAC-15 which also showed the most favorable results.

As a result, 20 single compounds were obtained including 6 new flavanones which are sanggenol W (**1**), morusalnol D-F (**2**, **3**, **4**) and Neovanone A-B (**5**, **6**). It was noticeable that cycloaltilisin 7 (**10**) was also isolated from *Morus alba* for the first time. Other known compounds include abyssinoflavanone V (**7**), sanggenol O-P (**8**, **11**), cyclomorusin (**9**), morachalcone A (**12**), betulinic acid (**13**), scopoletin (**14**), umbelliferone (**15**), morusalfuran E (**16**), sanggenofuran B (**17**), and moracin M, B and S (**18-20**).

Part 2
Application of molecular networking to network pharmacology

Chapter 1. Introduction

1.1. Study Background

1.1.1. Classic drug discovery process and its limitations

Drug discovery is long, costly marathon starting from development of lead compound to launch of new drug. The whole drug discovery process can take up to more than 10−15 years with budget over 1−2 billion dollars (Sun et al., 2022). Out of 10 thousand chemical compounds extracted from library, only 11.83% of drugs tested for Phase I of clinical trials are approved for market (Schaduangrat et al., 2020). Forum on Neuroscience and Nervous System Disorders et al. also highlighted several disadvantages for traditional drug discovery process such as unknown biological mechanisms for certain disorders, high degree of uncertainty of success of a new drug after long and costly experiments, and limitation of representing human model with animal trials.

Despite such limitations, many pharmaceutical companies attempt their best effort to develop new medications due to continuous increase in total pharmaceutical revenues as indicated by exceed in 1 trillion US dollars worldwide in 2014 (González Peña et al., 2021). Considering annual growth rate at 5.8% of the market

(González Peña et al., 2021), drug development industry, although regarded high risk high return, is still promising.

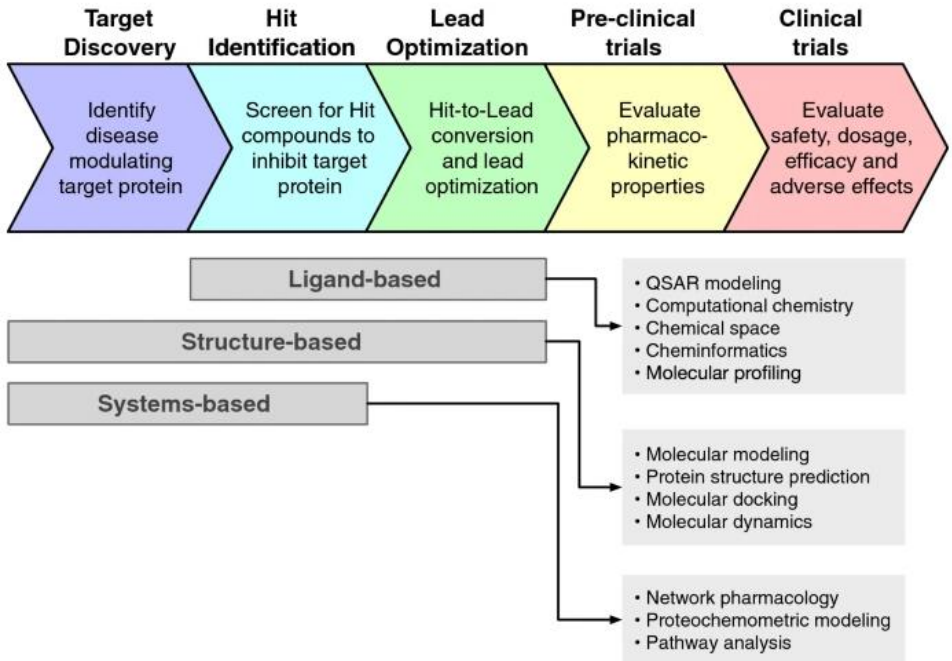

Figure 64. Summary of drug discovery process (Schaduangrat et al., 2020)

1.1.2. Network pharmacology and molecular networking

With rapid enhancement of information technology starting end of the 20th century, the network pharmacology is newly suggested paradigm that aim to understand drug interaction with multiple targets and their related diseases (Hopkins, 2008). Based on the fact that chemical compounds normally bind to multiple targets, the network pharmacology escapes from traditional one-drug/one-target/one-disease approach to overcome challenges associated with safety, efficacy and sustainability, and thereby discovering new drug lead from existing drug molecules experimented from various therapeutic conditions to give results of unbiased

investigation (Chandran et al., 2017). The *Morus alba* has also been subjected for network pharmacology, particularly for leaves (Li, 2021; Oh, 2021).

In addition, molecular networking is also another useful source that identify compounds based on tandem mass (MS/MS) spectra of small molecules in specific fraction (Aron, 2020). It is normally aided by Global Natural Products Social (GNPS; https://gnps.ucsd.edu) platform for visualization of clusters of molecules with predicted molecules (Wang et al., 2016).

1.2. Purpose of research

The aim of part 2 of this study is to investigate how molecular networking could be applied to network pharmacology. For such investigations, two computer-based experiments have been performed. The first task was to analyze and predict molecules available from molecular networking, and incorporating the compounds to network pharmacology process to forecast proportion of cholesterol-related diseases. The second mission was to identify key skeletons of compounds that are associated with cholesterol-related diseases using network pharmacology, then predicting active fraction that contains such skeletons using molecular networking.

Chapter 2. Experimental section

2.1. Molecular networking

Six fractions obtained after partition were prepared as sample to obtain MS/MS spectra at concentration shown in Table 7 below. Measurement and analysis of the MS^2 spectra were performed using MassLynx 4.1 software (Waters Co., USA) at Dongguk University.

Table 7. Concentration of each fraction prior to MS^2 spectra measurement

Fraction	Code	Concentration (mg/mL)
Crude MeOH extract	MAT	2.0
Hexane	MAH	1.0
Chloroform	MAC	1.0
Ethyl acetate	MAE	1.0
n-Butanol	MAB	1.0
Residue (water)	MAW	1.0

Tandem mass (MS/MS) spectra of small molecules from the six fractions were analyzed by Global Natural Products Social (GNPS; https://gnps.ucsd.edu) platform. For all networks, entered values for each option were set as shown in Table 8. Minimum Peak Intensity was set at 1.0 to remove trace of impurities.

Table 8. Values entered for each option on GNPS

Advanced network options	Value
Min Pairs Cos	0.65
Minimum Matched Fragment Ions	6
Minimum Cluster Size	1
Advanced filtering options	**Value**
Minimum Peak Intensity	1.0

Visualization of the molecular mass clusters was achieved by Cytoscape v.3.9.1 (Shannon et al., 2003). Colors for the nodes were differentiated based on their fractions (MAT−pink, MAH−blue, MAC−green, MAE−orange, MAB−yellow, MAW−black). Presence of compounds were predicted based on molecular mass, fragmentation pattern and neighboring single compounds identified by the GNPS platform.

2.2. Network pharmacology

2.2.1. Extraction of nodes

Network pharmacology involved extraction of multiple nodes following three simple steps. Firstly, compounds associated with *Morus alba* were identified by NPASS (Zeng et al., 2018), and their targets were extracted to retain compound to target (C−T) nodes. Secondly, target to target (T−T) nodes were mined from STRING (Szklarczyk et al., 2019) to identify interacting targets. Textmining was excluded from active interaction sources because the score is based on extraction of keywords from abstracts of scientific literature, and hence, indicating risk of extracting results with low reliability. The minimum required interaction score was set at above 0.900 which was defined as the highest confidence by the database. Finally, target to disease (T−D) nodes were obtained from both Uniprot (UniProt Consortium, 2021) and OMIM (OMIM, 1966). For reverse pathway, cholesterol diseases and their related targets were pulled from cholesterol metabolism pathway (04979N) recorded in KEGG Pathway and gene ontology (Kanehisa and Goto, 2000) under '5.4 Digestive system'.

2.2.2. Visualization of the network

After completion of extraction, the nodes were organized into two Excel files. The first file contained all connections between two nodes (C−T; T−T; T−D) which were arranged under node 1 and node 2 in alphabetical order for identification and removal of duplicate data. Its purpose is to form cluster and networks based on the connections between the nodes. The file was imported by the Cytoscape program through File → Import → Network from File.

For the second file, all nodes and their classification (compound, target, disease) were recorded under node and CTD header respectively. This file was created so that nodes from same classification are displayed with same color. The file was imported through File → Import → Table from File.

For better visualization, background color was changed to blue (Layout Tools → Style → Network → Background Paint). Color of nodes based on their classification was differed using green (R102−G255−B0) for compounds, orange (R255−G204−B51) for diseases and purple (R153−G0−B204) for targets (Layout Tools → Style → Node → Fill Color). The complex set of clusters were divided based on their classification through Menu → Layout → Attribute Circle Layout → CTD.

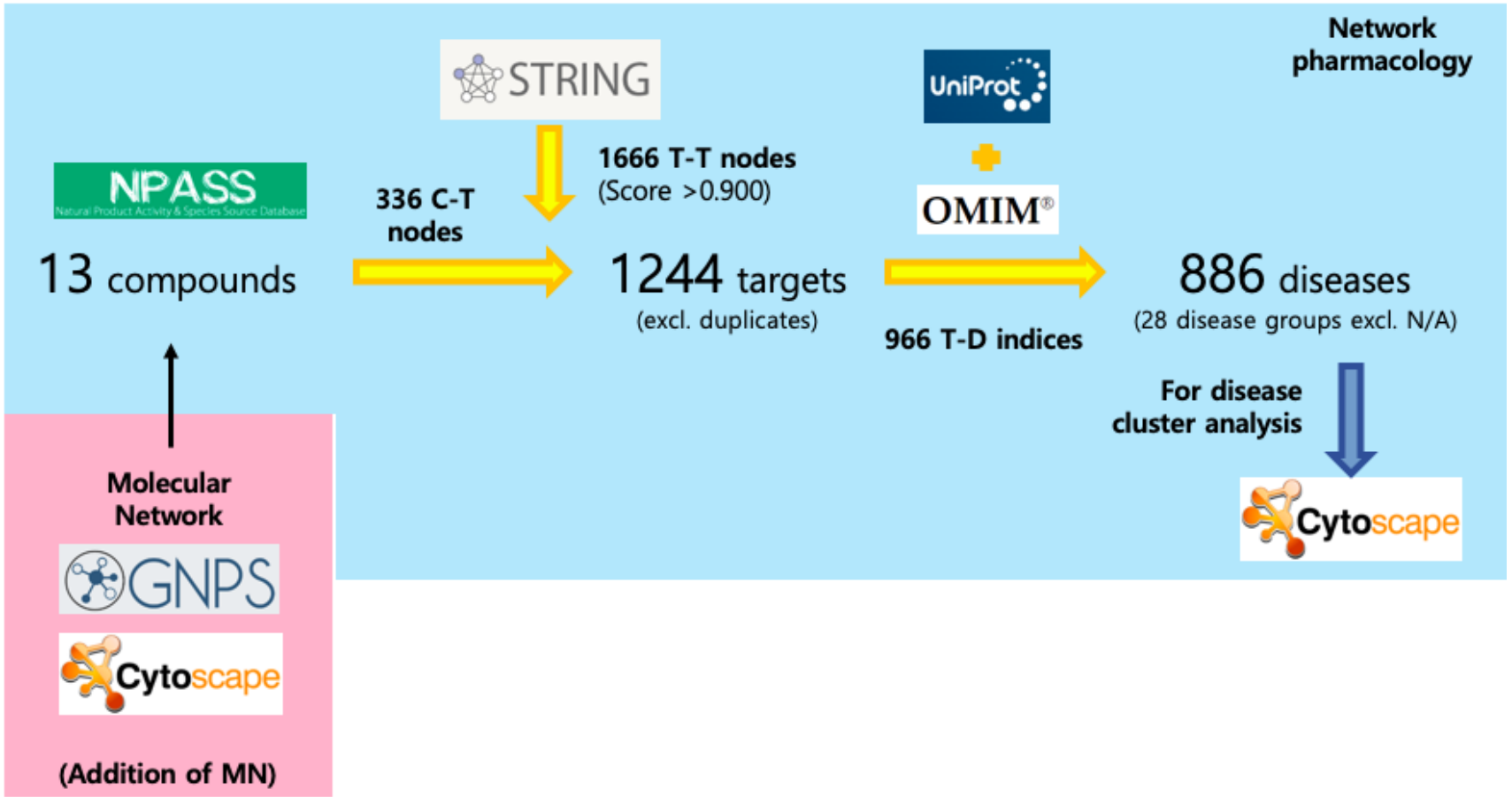

Scheme 2. Method for network pharmacology (C−T−D)

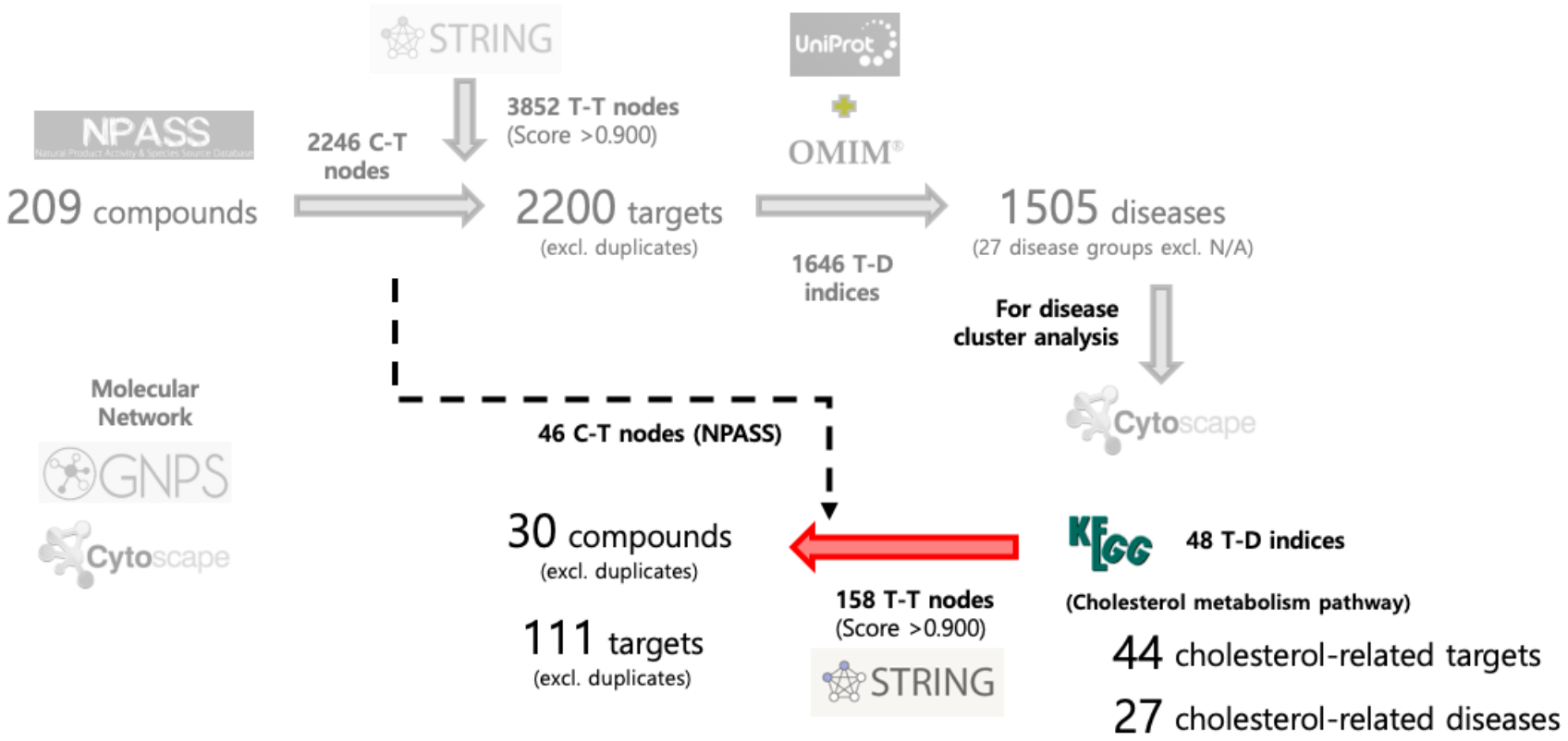

Scheme 3. Method for network pharmacology (D−T−C)

Chapter 3. Results

3.1. Prediction of plant-related diseases

From the network, a few individual single compounds, such as umbelliferone, isoquercetin, hydroxypalmitic acid, trans-resveratrol and kuwanon C, and several clusters were identified.

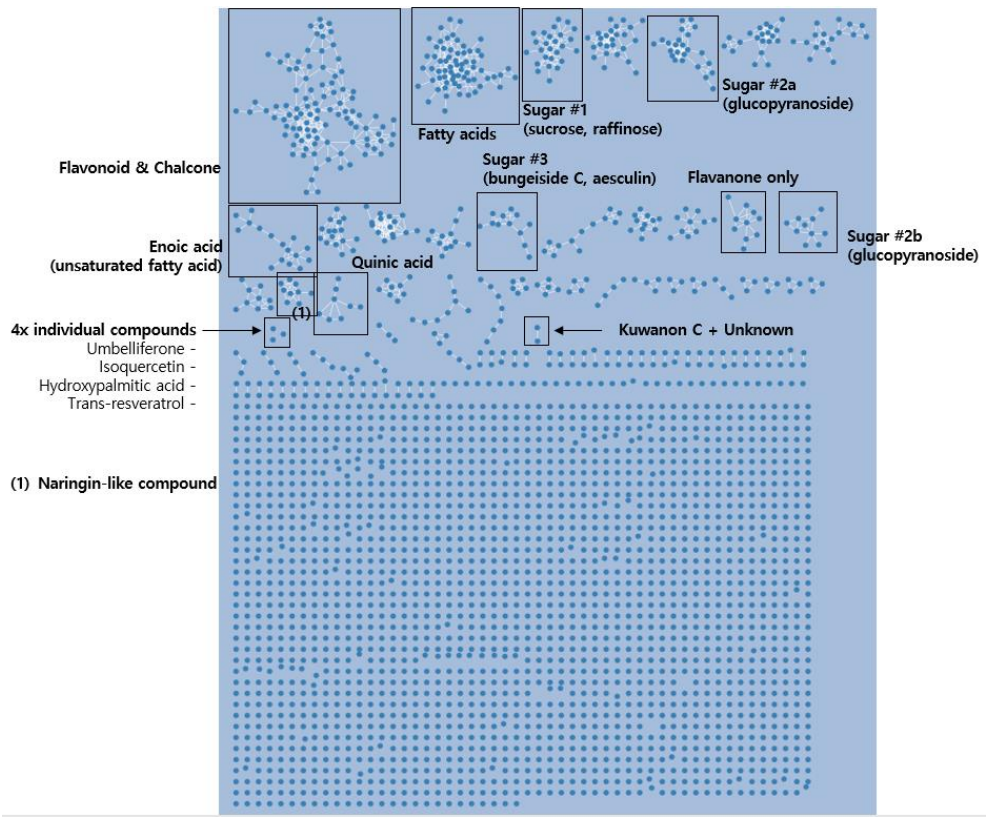

Figure 65. Overview of molecular networking

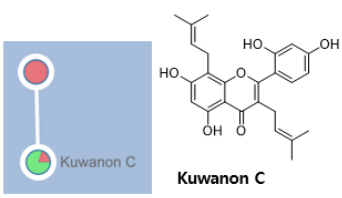

Figure 66. Kuwanon C identified from molecular networking

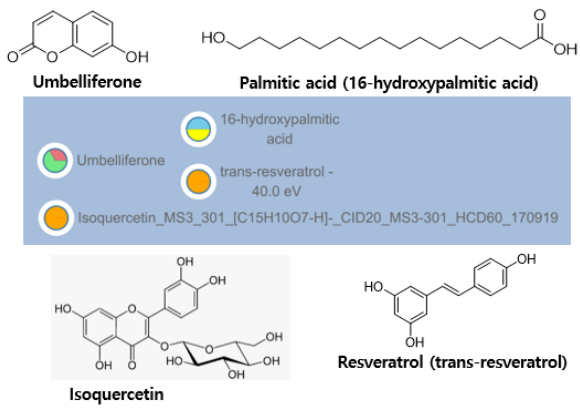

Figure 67. Individual compounds identified from molecular networking

The first key cluster (Figure 68) included morin, homobutein and epigallocatechin gallate, which are flavonoid and chalcone skeletons. From the cluster, sanggenol P, kuwanon E and G, and leachianone G were predicted based on their molecular mass.

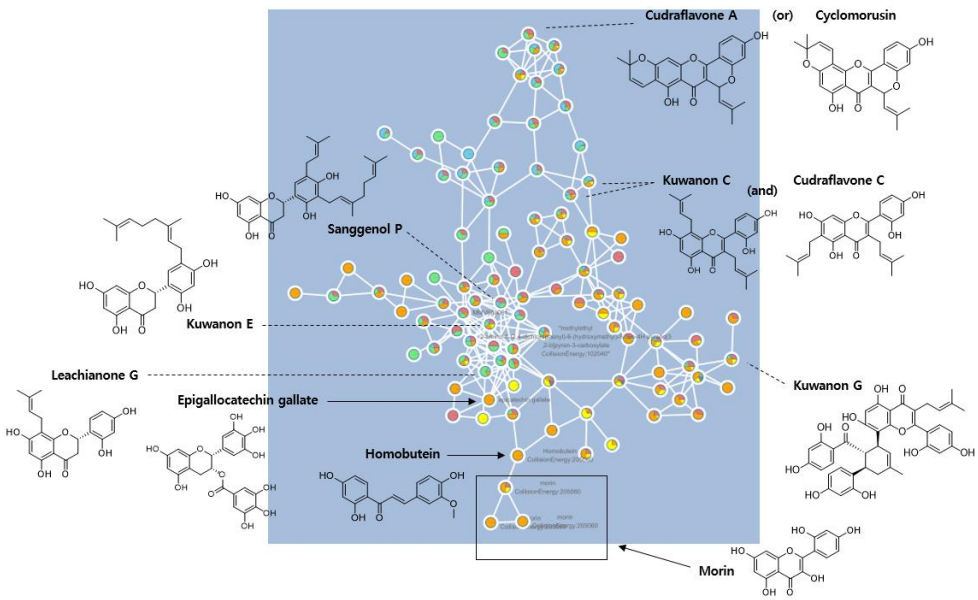

Figure 68. Key cluster 1 (flavonoid and chalcone)

The second cluster (Figure 69) was solely flavanone base, indicating presence of cycloaltilisin 7 and abyssinoflavone V which were isolated from chloroform fraction as in Part 1.

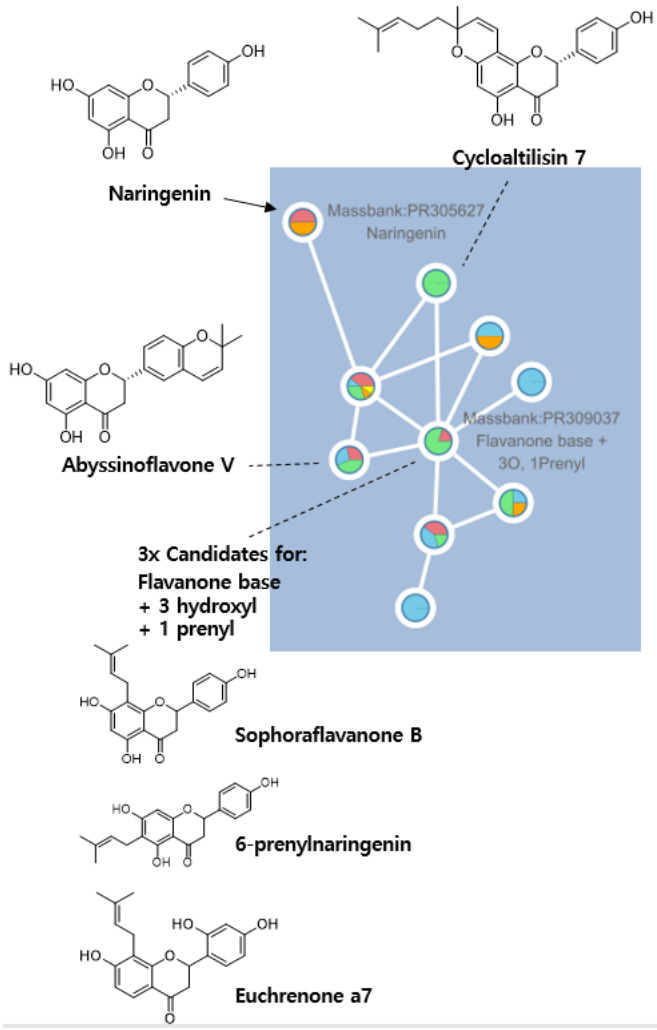

Figure 69. Key cluster 2 (flavanone-only)

The third, fourth, and fifth clusters (Figure 70-72) were quinic acid-related, simple sugar, and sugar moiety respectively based on identification of chlorogenic acid, caffeoyl quinic acid, sucrose, raffinose, bungeiside C and aesculin by GNPS.

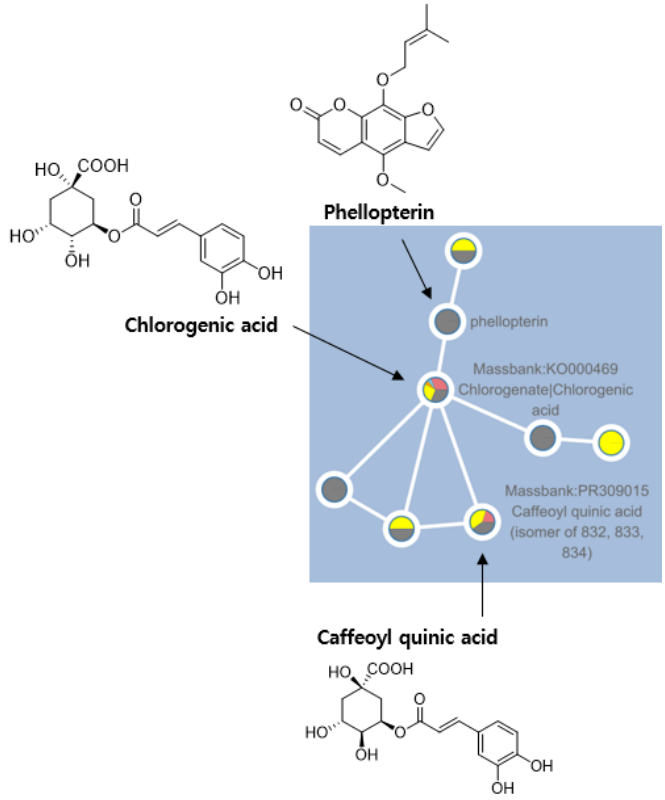

Figure 70. Key cluster 3 (quinic acid-related)

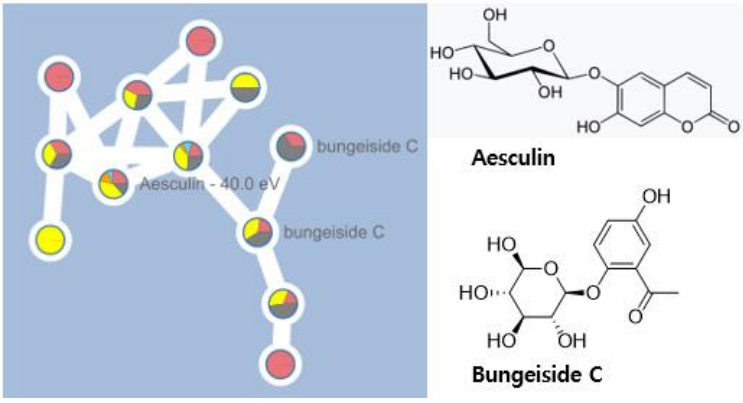

Figure 71. Key cluster 4 (simple sugar)

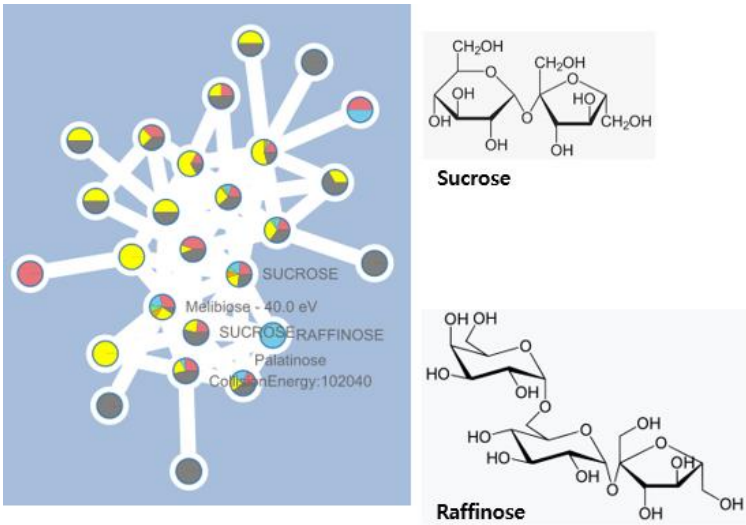

Figure 72. Key cluster 5 (sugar containing)

Overall, 13 compounds (caffeoyl quinic acid, chlorogenic acid, chlorogenic acid methyl ester, cyclomorusin, epigallocatechin gallate, isoquercetin, kuwanon C and E, morin, naringin, palmitic acid, resveratrol, and umbelliferone) identified or predicted from molecular networking were integrated into network pharmacology. Total of 336 C-T nodes, 1666 T-T nodes, and 966 T-D indices were incorporated to form network pharmacology (Figure 73).

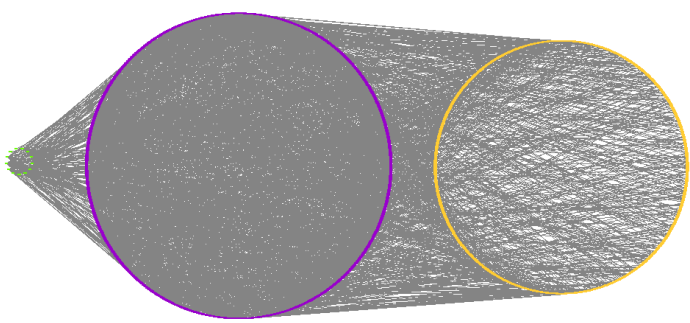

Figure 73. CTD clusters from C-T-D network (compound, green; target, purple; disease; orange) (13 compounds, 1244 targets, 886 diseases)

The diseases were then categorized into 28 groups excluding those that were classified as not applicable. As a result, 13 cholesterol-related diseases, distributed among four disease groups (Table 9), were identified from the network, which accounts for approximately 1.5% of all diseases.

1. ApoA-I and apoC-III deficiency, combined
2. Bile acid synthesis defect, congenital, 6
3. Cholestasis of pregnancy, intrahepatic 3
4. Cholestasis, benign recurrent intrahepatic, 2
5. Cholestasis, progressive familial intrahepatic, 2
6. Cholestasis, progressive familial intrahepatic, 3
7. Cholestasis, progressive familial intrahepatic, 5
8. HMG-CoA lyase deficiency
9. Hyperapobetalipoproteinemia
10. Hypercholesterolemia, familial, due to LDLR defect, modifier of
11. Hypercholesterolemia, familial, modifier of
12. Hypoalphalipoproteinemia, primary, 2, with or without corneal clouding
13. Sea-blue histiocyte disease

Next, network pharmacology was also performed using original 209 compounds identified by NPASS website regardless of molecular networking in order to examine the accountability of addition of the molecular networking process to network pharmacology (Figure 74). 2246 C-T nodes, 3852 T-T nodes, and 1646 T-D indices were extracted.

Table 9. Identified disease groups and their proportion (MN-incorporated network pharmacology)

Disease group	No.	%
Neurology	126	14.22
Cancer	101	11.40
Genetic	100	11.29
Endocrine	59	6.66
Immunity	52	5.87
Metabolic disorder *	50	5.64
Cardiovascular *****	48	5.42
Musculoskeletal	44	4.97
Blood-related disorder	41	4.63
Multi-systemic *	37	4.18
Eyes	30	3.39
Dermatology	26	2.93
Neurodevelopmental disorder	19	2.14
Liver disorder ******	16	1.81
Developmental delay	13	1.47
Infection	12	1.35
Renal	12	1.35
Respiratory	12	1.35
Diabetes	10	1.13
Ear	8	0.90
Gastrointestinal	6	0.68
Sexual and Reproductive	6	0.68
Cell	4	0.45
Mental disorder	4	0.45
Oral and Dental	4	0.45
Rheumatology	2	0.23
Addiction	1	0.11
Pain	1	0.11
Not Applicable (N/A)	42	4.74

*: Number of cholesterol-related diseases identified from network pharmacology

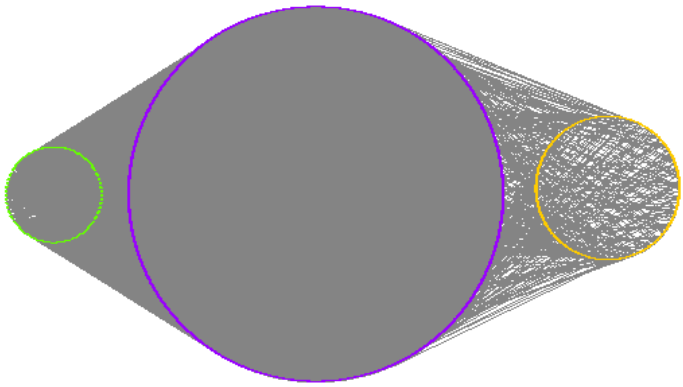

Figure 74. CTD clusters from D-T-C network (compound, green; target, purple; disease; orange) (209 compounds, 2200 targets, 1505 diseases)

The diseases were then categorized into 28 groups excluding N/A (Table 10). As a result, 18 cholesterol-related diseases were identified from the network, which is approximately 1.2% of all diseases showing very similar value to that of molecular network-added clusters.

1. ApoA-I and apoC-III deficiency, combined
2. Bile acid synthesis defect, congenital, 2
3. Bile acid synthesis defect, congenital, 6
4. Cerebrotendinous xanthomatosis
5. Cholestasis of pregnancy, intrahepatic 3
6. Cholestasis, benign recurrent intrahepatic, 2
7. Cholestasis, progressive familial intrahepatic, 2
8. Cholestasis, progressive familial intrahepatic, 3
9. Cholestasis, progressive familial intrahepatic, 5
10. Combined hyperlipidemia, familial
11. HMG-CoA lyase deficiency
12. Hyperapobetalipoproteinemia
13. Hypercholesterolemia, familial, due to LDLR defect, modifier of
14. Hypercholesterolemia, familial, modifier of
15. Hypoalphalipoproteinemia, primary, 1
16. Hypoalphalipoproteinemia, primary, 2, with or without corneal clouding
17. Sea-blue histiocyte disease
18. Tangier disease

This approves hypothesis that smaller sample of data obtained from molecular networking could be used in network pharmacology to predict plant-related diseases.

Table 10. Identified disease groups and their proportion (MN-independent network pharmacology)

Disease group	No.	%
Neurology	211	14.02
Genetic *	166	11.03
Cancer	129	8.57
Blood-related disorder *	104	6.91
Endocrine	98	6.51
Metabolic disorder *	90	5.98
Immunity	84	5.58
Cardiovascular *******	82	5.45
Musculoskeletal	78	5.18
Multi-systemic *	64	4.25
Eyes	52	3.46
Dermatology	43	2.86
Neurodevelopmental disorder	34	2.26
Diabetes	23	1.53
Respiratory	23	1.53
Renal	22	1.46
Developmental delay	20	1.33
Infection	19	1.26
Sexual and Reproductive	19	1.26
Liver disorder *******	18	1.20
Gastrointestinal	15	1.00
Ear	14	0.93
Cell	9	0.60
Mental disorder	6	0.40
Oral and Dental	4	0.27
Rheumatology	4	0.27
Pain	3	0.20
Addiction	2	0.13
Not Applicable (N/A)	69	4.58

*: Number of cholesterol-related diseases identified from network pharmacology

3.2. Prediction of active fraction based on key skeleton

Key compounds were identified from both C−T−D and D−T−C networks. For the D−T−C network, 48 T−D indices were identified from 44 cholesterol−related targets and 27 cholesterol−related diseases listed in cholesterol metabolism pathway (Figure 75) from KEGG Pathway and GO website (Kanehisa and Goto, 2000).

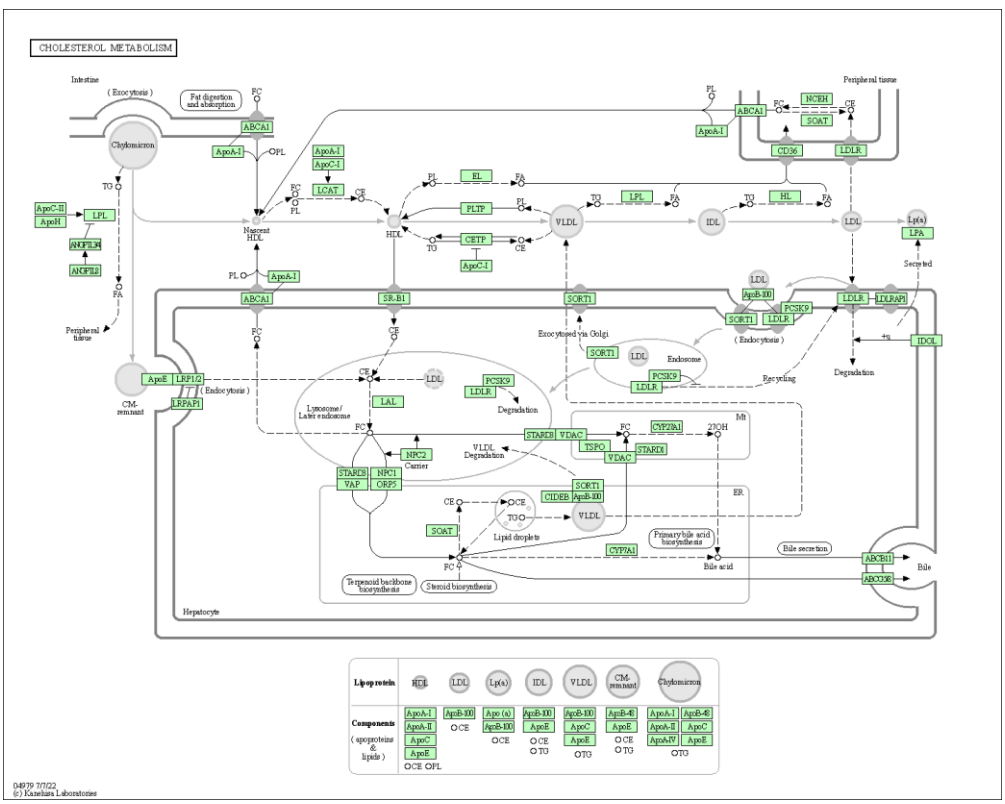

Figure 75. Cholesterol metabolism pathway (Kanehisa and Goto, 2000)

To identify disease−specific compounds, the reversed method for C−T−D network in Clause 3.1 was applied (Scheme 3), extracting 158 T−T nodes from STRING and 46 C−T nodes from NPASS.

Overall, the network contained 30 compounds, 111 targets and 27 diseases. The extracted 30 key compounds from D−T−C

network were then combined with 14 key compounds from C-T-D network that were directly related to the 18 cholesterol-related diseases from KEGG Pathway and GO website. Exploring the key compounds, 16 out of 35 duplicate-removed key compounds were found to be either flavanol-derivative or phenolic acid-derivative, both accounting for approximately 45.7% altogether (Table 11). As a result, conjecture was established that flavonols and phenolic acids are key skeletons that target cholesterol-related targets.

The claim is supported by a review (Adorni, 2020) that combined several studies regarding naturally occurring PCSK9 inhibitors, and it stated that compounds such as flavonols (e.g. kaempferol, quercetin) and phenolic acids (e.g. coumaric acid) are likely to reduce cholesterol.

Table 11. Key compounds identified from both C-T-D and D-T-C network

Key compounds	Base structure
Adenine[2]	Amino acid
Ascorbate[2] (Vitamin C)	Vitamin
Astragalin[1]	Flavonol (+glycoside)
Betulinic acid[1,2]	Triterpenoid
Caffeic acid[2]	Phenolic acid
Chlorogenic acid[2]	Phenolic acid
Chlorogenic acid methyl ester[2]	Phenolic acid
Cinnamic acid[2]	Phenolic acid
Coumaric acid[2]	Phenolic acid
Duvoglustat[2]	Alkaloid
Ellagic acid[1]	Polyphenol
Epigallocatechin gallate[1,2]	Flavan-3-ol
Eugenol[2]	Arylbenzene
Ferulic acid[2]	Phenolic acid

Gallic acid[2]	Phenolic acid
Guaiacol[2]	Monomethoxybenzene
Hyperoside[1]	Flavonol (+glycoside)
Isoquercetin[1]	Flavonol
Kaempferol[1,2]	Flavonol
Linoleic acid[1,2]	Long chain fatty acid (unsaturated)
Luteolin[2]	Flavone
Metacresol[2]	Methylphenol
Methyl (9*Z*,12*Z*)−octadeca−9,12−dienoate[2]	Long chain fatty acid (unsaturated)
Methyl salicylate[2]	Benzoic ester
Moracin M[2]	Benzofuran
Morin[2]	Flavonol
Myricetin[2]	Flavonol
Oleanolic acid[1,2]	Triterpenoid
Palmitic acid[1,2]	Long chain fatty acid (saturated)
Quercetin[1,2]	Flavonol
Resveratrol[1,2]	Stilbene
Riboflavin[1,2] (Vitamin B12)	Vitamin
Rutin[1]	Flavonol (+glycoside)
Taxifolin[2]	Flavonol
Umbelliferone[2]	Coumarin

[1]: From C−T−D network

[2]: From D−T−C network

Based on molecular networking results which was already gained in Clause 3.1, key skeletons were identified in specific fractions (Table 12). For instance, higher proportion of green (MAC) and orange (MAE) nodes were recognized for flavonoid, indicating that flavonoids should be isolated from chloroform and ethyl acetate fractions.

Table 12. Key skeletons and their respective fractions

Key skeleton	Fractions				
	MAH	MAC	MAE	MAB	MAW
Flavonoids		V	V		
Fatty acids			V		
Phenolic acids				V	V
Sugar moiety				V	V

The claim was supported by results obtained from Part 1 as flavonoids, including flavanones, were dominant skeleton isolated from chloroform fraction. Therefore, in accordance to results, chloroform and EA fractions need to be isolated to obtain flavonols, while butanol and water fractions need to be separated to obtain phenolic acids. Hence, molecular networking could be applied as a guide to predict active fraction prior to separation of compounds.

Chapter 4. Conclusion

In conclusion, molecular networking could be applied to network pharmacology to predict plant-related diseases. The molecular networking could assist prediction of compounds available from the fraction, which could then allow formation of network pharmacology clusters to identify diseases related to plant of interest. It was found that cholesterol-related diseases alone took part of approximately 1.2 to 1.5 percent of all diseases.

Prediction of active fractions that contain key skeletons was also guaranteed after interpretation of molecular networking to network pharmacology. The result stated that key skeletons that are associated with cholesterol metabolism are flavonol and phenolic acid derivatives, which were approximately 45.7% of all key compounds identified from the network pharmacology. The molecular networking suggested that Flavonol should be isolated from chloroform and ethyl acetate fraction, while phenolic acid derviatives should be attained from butanol and water fractions.

BIBLIOGRAPHY

Adorni MP, Zimetti F, Lupo MG, Ruscica M, Ferri N. Naturally Occurring PCSK9 Inhibitors. Nutrients. 2020;12(5).

American Heart Association (AHA). Prevention and Treatment of High Cholesterol (Hyperlipidemia): American Heart Association; 2022 [cited 2022 Dec 12]. Available from: https://www.heart.org/en/health-topics/cholesterol/prevention-and-treatment-of-high-cholesterol-hyperlipidemia.

Aron AT, Gentry EC, McPhail KL, Nothias L-F, Nothias-Esposito M, Bouslimani A, et al. Reproducible molecular networking of untargeted mass spectrometry data using GNPS. Nature Protocols. 2020;15(6):1954-91.

Barberá O, Marco JA, Sanz JF, Sánchez-Parareda J. 3-Methoxyflavones and coumarins from Artemisia incanescens. Phytochemistry. 1986;25(10):2357-60.

Basnet P, Kadota S, Terashima S, ShimizuM, Namba T. Two new 2-arylbenzofuran derivatives from hypoglycemic activity-bearing fractions of Morus insignis. Chem Pharm Bull (Tokyo). 1993;41(7):1238-43.

Bokotey, S., Kövári-Rádkai, M., Podányi, B., Ritz, I., Hanusz, M., & Bátori, S. (2002). STUDIES ON SYNTHESIS OF 3(2H)-BENZOFURANONE DERIVATIVES. Synthetic Communications, 32(15), 2325-2343. https://doi.org/10.1081/SCC-120006003

Carta F, Vullo D, Maresca A, Scozzafava A, Supuran CT. Mono-/dihydroxybenzoic acid esters and phenol pyridinium derivatives as inhibitors of the mammalian carbonic anhydrase isoforms I, II, VII, IX, XII and XIV. Bioorganic & Medicinal

Chemistry. 2013;21(6):1564-9.

Centers for Disease Control and Prevention. LDL and HDL Cholesterol and Triglycerides: Centers for Disease Control and Prevention; 2022 [updated October 24, 2022; cited December 19, 2022]. Available from: https://www.cdc.gov/cholesterol/ldl_hdl.htm.

Choi Y-J, Lee SJ, Kim HI, Lee HJ, Kang SJ, Kim TY, et al. Platycodin D enhances LDLR expression and LDL uptake via down-regulation of IDOL mRNA in hepatic cells. Scientific Reports. 2020;10(1):19834.

Cui L, Ndinteh DT, Na M, Thuong PT, Silike-Muruumu J, Njamen D, et al. Isoprenylated Flavonoids from the Stem Bark of Erythrina abyssinica. Journal of Natural Products. 2007;70(6):1039-42.

El-Beshbishy HA, Singab ANB, Sinkkonen J, Pihlaja K. Hypolipidemic and antioxidant effects of Morus alba L. (Egyptian mulberry) root bark fractions supplementation in cholesterol-fed rats. Life Sciences. 2006;78(23):2724-33.

Eo HJ, Park JH, Park GH, Lee MH, Lee JR, Koo JS, et al. Anti-inflammatory and anti-cancer activity of mulberry (Morus alba L.) root bark. BMC Complementary and Alternative Medicine. 2014;14(1):200.

Forum on Neuroscience and Nervous System Disorders, Board on Health Sciences Policy, Institute of Medicine. Improving and Accelerating Therapeutic Development for Nervous System Disorders: Workshop Summary. Washington (DC): National Academies Press (US); 2014 [cited 2022 Dec 6]. Available from: https://www.ncbi.nlm.nih.gov/books/NBK195047/.

Go GW, Mani A. Low-density lipoprotein receptor (LDLR) family orchestrates cholesterol homeostasis. Yale J Biol Med.

2012;85(1):19-28.

González Peña OI, López Zavala M, Cabral Ruelas H. Pharmaceuticals Market, Consumption Trends and Disease Incidence Are Not Driving the Pharmaceutical Research on Water and Wastewater. Int J Environ Res Public Health. 2021;18(5).

Guo Y-Q, Tang G-H, Lou L-L, Li W, Zhang B, Liu B, et al. Prenylated flavonoids as potent phosphodiesterase-4 inhibitors from Morus alba: Isolation, modification, and structure-activity relationship study. European Journal of Medicinal Chemistry. 2018;144:758-66.

Ha MT, Shrestha S, Tran TH, Kim JA, Woo MH, Choi JS, et al. Inhibition of PTP1B by farnesylated 2-arylbenzofurans isolated from Morus alba root bark: unraveling the mechanism of inhibition based on in vitro and in silico studies. Archives of pharmacal research. 2020;43(9):961-75.

Ha MT, Tran MH, Ah KJ, Jo K-J, Kim J, Kim WD, et al. Potential pancreatic lipase inhibitory activity of phenolic constituents from the root bark of Morus alba L. Bioorganic & Medicinal Chemistry Letters. 2016;26(12):2788-94.

Hopkins AL. Network pharmacology: the next paradigm in drug discovery. Nature Chemical Biology. 2008;4(11):682-90.

Ichimaru M, Moriyasu M, Nishiyama Y, Kato A, Mathenge SG, Juma FD, et al. Structural Elucidation of New Flavanones Isolated from Erythrina abyssinica. Journal of Natural Products. 1996;59(12):1113-6.

Jung J-W, Ko W-M, Park J-H, Seo K-H, Oh E-J, Lee D-Y, et al. Isoprenylated flavonoids from the root bark of Morus alba and their hepatoprotective and neuroprotective activities. Archives of Pharmacal Research. 2015;38(11):2066-75.

Kanehisa M, Goto S. KEGG: kyoto encyclopedia of genes and genomes. Nucleic Acids Res. 2000;28(1):27-30.

Kapche GDWF, Fozing CD, Donfack JH, Fotso GW, Amadou D, Tchana AN, et al. Prenylated arylbenzofuran derivatives from Morus mesozygia with antioxidant activity. Phytochemistry. 2009;70(2):216-21.

Lagace TA. PCSK9 and LDLR degradation: regulatory mechanisms in circulation and in cells. Curr Opin Lipidol. 2014;25(5):387-93.

Lee IS and Yoon CR. Research for the table of contents in Donguibogam. Journal of Korean Medical classics. 2005;18(3):136-71.

Li HX, Park JU, Su XD, Kim KT, Kang JS, Kim YR, et al. Identification of Anti-Melanogenesis Constituents from Morus alba L. Leaves. Molecules. 2018;23(10):2559.

Li M, Wu X, Wang X, Shen T, Ren D. Two novel compounds from the root bark of Morus alba L. Natural Product Research. 2018;32(1):36-42.

Li R, Wang C, Chen Y, Li N, Wang Q, Zhang M, et al. A combined network pharmacology and molecular biology approach to investigate the active ingredients and potential mechanisms of mulberry (Morus alba L.) leaf on obesity. Phytomedicine. 2021;92:153714.

Lin CK, Tseng CK, Chen KH, Wu SH, Liaw CC, Lee JC. Betulinic acid exerts anti-hepatitis C virus activity via the suppression of NF-κB- and MAPK-ERK1/2-mediated COX-2 expression. British journal of pharmacology. 2015;172(18):4481-92.

Masagalli JN, BasavanaGowda MK, Chae H-S, Choi WJ.

Synthesis of Moracin C and Its Derivatives with a 2-arylbenzofuran Motif and Evaluation of Their PCSK9 Inhibitory Effects in HepG2 Cells. Molecules. 2021;26(5):1327.

Meisel JW, Hu CT, Hamilton AD. Heterofunctionalized Cavitands by Macrocyclization of Sequence-Defined Foldamers. Organic Letters. 2019;21(19):7763-7.

Oh KK, Adnan M, Cho DH. Network Pharmacology Study on Morus alba L. Leaves: Pivotal Functions of Bioactives on RAS Signaling Pathway and Its Associated Target Proteins against Gout. International journal of molecular sciences. 2021;22(17).

OMIM (Online Mendelian Inheritance in Man): McKusick-Nathans Institute of Genetic Medicine, Johns Hopkins University (Baltimore, MD); 1966 [Available from: https://omim.org/]

Patil AD, Freyer AJ, Killmer L, Offen P, Taylor PB, Votta BJ, et al. A New Dimeric Dihydrochalcone and a New Prenylated Flavone from the Bud Covers of Artocarpus altilis: Potent Inhibitors of Cathepsin K. Journal of Natural Products. 2002;65(4):624-7.

Pel P, Chae H-S, Nhoek P, Kim Y-M, Chin Y-W. Chemical Constituents with Proprotein Convertase Subtilisin/Kexin Type 9 mRNA Expression Inhibitory Activity from Dried Immature Morus alba Fruits. Journal of Agricultural and Food Chemistry. 2017;65(26):5316-21.

Romano JJ, Casillas E. A short synthesis of morachalcone A. Tetrahedron Letters. 2005;46(13):2323-6.

Roth Gregory A.; Mensah George A.; Johnson Catherine O.; Addolorato G.; Ammirati E.; Baddour Larry M, et al. Global Burden of Cardiovascular Diseases and Risk Factors, 1990-2019. Journal of the American College of Cardiology. 2020. 76(25), 2982-3021.

Schaduangrat N, Lampa S, Simeon S, Gleeson MP, Spjuth O,

Nantasenamat C. Towards reproducible computational drug discovery. Journal of Cheminformatics. 2020;12(1):9.

Seong SH, Ha MT, Min BS, Jung HA, Choi JS. Moracin derivatives from Morus Radix as dual BACE1 and cholinesterase inhibitors with antioxidant and anti-glycation capacities. Life Sciences. 2018;210:20-8.

Seong SH, Ali MY, Jung HA, Choi JS. Umbelliferone derivatives exert neuroprotective effects by inhibiting monoamine oxidase A, self-amyloid β aggregation, and lipid peroxidation. Bioorganic Chemistry. 2019;92:103293.

Shannon P, Markiel A, Ozier O, Baliga NS, Wang JT, Ramage D, et al. Cytoscape: a software environment for integrated models of biomolecular interaction networks. Genome Res. 2003;13(11):2498-504.

Shi Y-Q, Nomura T, Fukai T. A new 2-arylbenzofuran from the root bark of Chinese Morus cathayana. Fitoterapia. 2007;78(7):617-8.

Sichaem J, Musa V, Dao T-B-N, Nguyen CH, Tran T-N, Nguyen N-H, et al. Chemical Constituents of the Leaves of Artocarpus integer. Chemistry of Natural Compounds. 2022;58(3):538-40.

Slade D, Ferreira D, Marais JPJ. Circular dichroism, a powerful tool for the assessment of absolute configuration of flavonoids. Phytochemistry. 2005;66(18):2177-215.

Stone KR. Morus alba: U.S. Department of Agriculture, Forest Service, Rocky Mountain Research Station, Fire Sciences Laboratory (Producer); 2009 [cited December 21, 2022]. Available from: https://www.fs.usda.gov/database/feis/plants/tree/moralb/all.html.

Sun D, Gao W, Hu H, Zhou S. Why 90% of clinical drug development fails and how to improve it? Acta Pharmaceutica Sinica B. 2022;12(7):3049-62.

Szklarczyk D, Gable AL, Lyon D, Junge A, Wyder S, Huerta-Cepas J, et al. STRING v11: protein-protein association networks with increased coverage, supporting functional discovery in genome-wide experimental datasets. Nucleic Acids Research. 2019;47(D1):D607-D13.

The Uniprot Consortium. UniProt: the universal protein knowledgebase in 2021. Nucleic Acids Res. 2021;49(D1):D480-d9.

Wang M, Carver JJ, Phelan VV, Sanchez LM, Garg N, Peng Y, et al. Sharing and community curation of mass spectrometry data with Global Natural Products Social Molecular Networking. Nat Biotechnol. 2016;34(8):828-37.

Wei B-L, Weng J-R, Chiu P-H, Hung C-F, Wang J-P, Lin C-N. Antiinflammatory Flavonoids from Artocarpus heterophyllus and Artocarpus communis. Journal of Agricultural and Food Chemistry. 2005;53(10):3867-71.

Wouters K, Shiri-Sverdlov R, Gorp PJv, Bilsen Mv, Hofker MH. Understanding hyperlipidemia and atherosclerosis: lessons from genetically modified apoe and ldlr mice. Clinical Chemistry and Laboratory Medicine (CCLM). 2005;43(5):470-9.

Wu L, Xiong W, Hu J-W, Li X-H, Fu J-P, Si C-L, et al. Chemical Constituents of Xylem of Sophora japonica Roots. Chemistry of Natural Compounds. 2018;54(3):610-2.

Zhang L, Tao G, Chen J, Zheng Z-P. Characterization of a New Flavone and Tyrosinase Inhibition Constituents from the Twigs of *Morus alba* L. Molecules. 2016;21(9):1130.

Zhang Y, Ma KL, Ruan XZ, Liu BC. Dysregulation of the

Low-Density Lipoprotein Receptor Pathway Is Involved in Lipid Disorder-Mediated Organ Injury. International journal of biological sciences. 2016;12(5):569-79.

Zhang X, Wu G, Gao W, Ding J, Huang X, Liu M, et al. Synergistic Photo-Copper-Catalyzed Hydroxylation of (Hetero)aryl Halides with Molecular Oxygen. Organic Letters. 2018;20(3):708-11.

Zeng X, Zhang P, He W, Qin C, Chen S, Tao L, et al. NPASS: natural product activity and species source database for natural product research, discovery and tool development. Nucleic Acids Res. 2018;46(D1):D1217-d22.

국문 초록

New flavanones isolated from root bark of *Morus alba*, and use of Molecular networking in Network pharmacology

WON Hongic

Pharmacognosy

The Graduate School of Pharmacy

Seoul National University

Morus alba L. (Moraceae)는 상백피로도 잘 알려져 있는 식물이며, 대한민국, 일본, 중국, 태국, 캄보디아 등 아시아 대륙에 걸쳐 분포한다. 전통적으로 상백피 뿌리 추출물은 심장보호, 진통제, 항산화, 고지혈증 등으로도 쓰였다. 최근에 심혈관 질병이 갈수록 늘어나고 있고 2019년 기준 전 세계적으로 높은 사망 원인 중 하나로 심혈관 질병이 지목된 바, 콜레스테롤을 낮춰주는 화합물 발견은 미래 전망이 밝다고 볼 수 있다. 잘 알려진 심혈관 질병의 이유로는 혈청 속 높은 저밀도 지단백질 콜레스테롤 (LDL-C)이 꼽히며, 이는 PCSK9으로 인해 분해되는 저밀도 지단백질 수용체 'LDLR'을 조정한다. 따라서, 심혈관 질병을 이겨내기 위해선 PCSK9 억제 효과를 나타내는 화합물 발견이 중요하다.

첫 번째 파트에서는 PCSK9 억제 효과를 보인 분획에서 분리된 20종의 화합물 구조를 동정하였고, 이는 천연물에서 새롭게 발견된 6종의 플라바논을 포함한다. *M. alba*의 뿌리 껍질 부위의 메탄올 추출물을 다양한 column chromatography 방법을 동원해 분리하였다. 분리된 20

종의 화합물은 1D 및 2D NMR spectroscopy와 HRESIMS 등을 포함한 여러가지 이화학적 및 분광학적 방법을 통해 화학구조를 결정하였고, 여러 참조 문헌들도 부분구조 확인을 위해 적극적으로 참고하였다.

두 번째 파트에선 네트워크 약리학에 Molecular networking을 활용함으로서 콜레스테롤 관련 질병들 유추하는 것과 확인된 화합물 골격 구조를 통해 활성화된 분획을 예측하는 것에 대해 탐구하였다. 다양한 구조 예측은 GNPS를 동원한 molecular network를 통해 이루어졌고, 화합물-수용체-질환 연결고리는 다양한 네트워크 약리학 관련 데이터베이스들을 통해 완성되었다.

주요어: *Morus alba*, flavanone, network pharmacology, molecular network
학 번: 2021-28287